

7. SITES 1110–1113¹

Shipboard Scientific Party²

SITES 1110 THROUGH 1113

Site 1110

Hole 1110A (APC):

9°43.599'S, 151°34.511'E; 3246.4 mbsl
0–9.5 mbsf cored; 9.5 m recovered (100%)

Hole 1110B (APC/XCB):

9°43.609'S, 151°34.509'E; 3246.3 mbsl
0–22.3 mbsf cored; 5.37 m recovered (24%)

Hole 1110C (RCB):

9°43.599'S, 151°34.498'E; 3245.8 mbsl
0–15.0 mbsf drilled; no cores taken

Hole 1110D (RCB):

9°43.588'S, 151°34.526'E; 3245.8 mbsl
0–22.7 mbsf drilled; 22.7–28.7 mbsf cored;
0.10 m recovered (2%)

Site 1111

Hole 1111A (RCB):

9°43.059'S, 151°34.533'E; 3200.7 mbsl
0–173.7 mbsf cored; 15.19 m recovered (9%)

Site 1112

Hole 1112A (RCB):

9°44.749'S, 151°36.721'E; 3046.7 mbsl
0–122.4 mbsf cored; 5.85 m recovered (5%)

Hole 1112B (RCB):

9°44.746'S, 151°36.714'E; 3046.6 mbsl

¹Examples of how to reference the whole or part of this volume.
²Shipboard Scientific Party addresses.

0–126.1 mbsf drilled without coring; 126.1–164.6 mbsf cored;
1.19 m recovered (3%)

Site 1113

Hole 1113A (RCB):

9°45.449'S, 151°36.737'E; 2915.6 mbsl

0–25.2 mbsf cored; 0.44 m recovered (2%)

Sites 1110 through 1113 were drilled in various locations near the foot of Moresby Seamount in an attempt to find a viable alternate location to our primary Site 1108. With the hydrocarbon safety restriction of 485 mbsf, the depth reached at Site 1108, we sought to intercept the Moresby low-angle normal fault in other locations or at shallower depths. We first tried two locations ~6 km west-northwest of Site 1108, near the rift basin depocenter located due north of Moresby Seamount. We then tried two other locations updip of Site 1108, all without success.

At Site 1110, where the fault may be 400–450 mbsf, multiple holes were unable to penetrate below ~29 mbsf because of talus beneath ~9 m of surficial calcareous clay, late Pleistocene in age (<0.22 Ma). The pebbles and cobbles of the talus include mica schists, amphibolites, and rare granite porphyry.

Moving 1 km north, at Site 1111, we cored a single hole through ~154 m of Pleistocene deposits (<1.02 Ma): talus pebbles and cobbles in calcareous ooze, clay, and silty clay with lesser nannofossil-rich silt, sand, and gravel. The talus includes metasediments (mica schist and gneiss) and variably metamorphosed igneous rocks, both basic (dolerite, metadolerite, and lamprophyre) and acidic (granite porphyry). Coring was stopped at 174 mbsf in large metamorphic cobbles. Based on temperatures measured at the mudline and at 136 mbsf, the thermal gradient is $95^{\circ}\text{C}\cdot\text{km}^{-1}$, similar to that encountered at Site 1108, and the heat flow is $86\text{ mW}\cdot\text{m}^{-2}$.

Site 1112 is 1.5 km west of, and updip from, Site 1108, where the depth to the fault is ~450 mbsf. Another thick pile of talus deposits in Pleistocene (<1.75 Ma) sediments, including silty clay with occasional ash, required two RCB holes to reach 165 mbsf. The recovery consisted of pebbles only, mostly of metadolerite and epidosite, but also minor andesite, granite porphyry, mica schist, and sandstone.

After offsetting 1.3 km south, we attempted a “bare rock” spud at the base of the slope of Moresby Seamount where the fault crops out (Site 1113), but there was enough talus to make the hole unstable and repeatedly refill, and it was abandoned at 25 mbsf in mica schist and epidosite pebbles and cobbles.

Most of the metamorphic rocks recovered from the talus of Moresby Seamount have igneous protoliths. In addition, mica schists and gneisses record an early tectono-metamorphic stage characterized by the development of a foliation under epidote-amphibolite to amphibolite facies conditions. A later retrograde metamorphism in the greenschist facies affected all protoliths. This later stage was coeval to brittle extensional deformation and extensive hydrothermal alteration, probably during the normal faulting of Moresby Seamount and the subsequent unroofing of its basement.

OPERATIONS

Transit to Site 1110 (ACE-10A)

Because we had left a positioning beacon at Site 1108, we traveled to that site during the transit from Site 1109 to Site 1110 (ACE-10A). Once arriving at Site 1108 we signaled the beacon to release and lowered the thrusters. The beacon was successfully recovered at 0245 hr on 4 July 1998. While the ship moved the final 3.3 nmi (6.1 km) to Site 1110 in dynamic positioning mode, we assembled the advanced hydraulic piston corer/extended core barrel (APC/XCB) coring assembly and began to run the assembly in the hole.

Hole 1110A

At 0600 hr on 4 July 1998 the positioning beacon for Site 1110 was deployed. The pipe was lowered the remaining distance to the seafloor, and Hole 1110A was spudded at 0945 hr. Core 1H was taken with the bit at 3243.9 meters below sea level (mbsl) and recovered 7.03 m; therefore, the seafloor was calculated to be at 3246.4 mbsl (Tables T1, T2). Core 2H failed to fully stroke and recovered 2.5 m of sand and gravel. We terminated this hole at a total depth of 9.5 mbsf, and Hole 1110A ended at 1100 hr when the pipe was pulled clear of the mudline.

Hole 1110B

Without offsetting the ship, we spudded Hole 1110B at 1130 hr on 4 July 1998. Core 1H was taken with the bit at 3241.9 mbsl and recovered 5.08 m; therefore, the seafloor was calculated to be at 3246.3 mbsl. We then switched to XCB coring. Core 3X took ~2.5 hr to cut and was recovered with the soft formation XCB cutting structure destroyed. High and erratic torque, slow rate of penetration (ROP), and very low recovery were enough to convince us that the XCB system was not well suited to the formation. Coring was terminated at a total depth of 22.3 mbsf, the drill string was recovered, and Hole 1110B was ended at 2330 hr on 4 July when the bit cleared the rig floor.

Hole 1110C

After assembling a rotary core barrel (RCB) bottom-hole assembly (BHA), we tripped the pipe back to the seafloor. The ship was offset 30 m on a course of 280°, and we spudded Hole 1110C at 0545 hr on 5 July 1998. A seafloor depth of 3245.8 mbsl was determined by tagging the seafloor with the drilling assembly. Repeated attempts were made to drill ahead with a center bit in place. After 7 hr of high torque, packing off, overpull, fill, and extremely slow penetration, it became painfully clear that a satisfactory hole was not going to be possible at this location. The hole was terminated after penetrating a mere 15.0 meters below seafloor (mbsf) without even one attempt to cut a core. Hole 1110C ended at 1300 hr on 5 July when the bit cleared the mudline.

Hole 1110D

The center bit was recovered, and a core barrel was deployed. The ship was offset 30 m north and 30 m east prior to spudding Hole 1110D at 1430 hr on 5 July 1998. The seafloor was tagged at 3245.8 mbsl, and

T1. Coring summaries, p. 66.

T2. Site 1110 coring summary by section, p. 70.

drilling (without coring) proceeded to a depth of 22.7 mbsf. A single core was cut to a depth of 28.7 mbsf before this hole was abandoned for the same reason as Hole 1110C. High torque, packing off, overpull, and generally poor hole conditions prevailed once again. The drill pipe was pulled clear of the seafloor at 1845 hr, officially ending Hole 1110D, and the core barrel was retrieved while we waited for the released positioning beacon to surface. Recovery for the 6.0-m interval cored was 0.16 m, or 2.7%.

Transit to Site 1111 (ACE-11A)

The positioning beacon was recovered aboard at 1945 hr and with the drill bit positioned three stands above the seafloor we moved the ship ~1 km north to Site 1111 (ACE-11A). A positioning beacon was deployed at 2030 hr on 5 July 1998 at the Site 1111 Global Positioning System (GPS) coordinates.

Hole 1111A

The drill string was tripped the remaining distance to the seafloor, and at 2230 hr on 5 July 1998 we spudded Hole 1111A (Table T3). The seafloor was determined to be at 3200.8 mbsl. The RCB coring continued through Core 18R to 173.7 mbsf. Drilling rates in the upper part of the hole were 5–10 min per core and recovery, with the exception of two isolated cores at 43%, was very low (1%–7%). A single temperature measurement was taken at 94 mbsf inside the drill pipe using the Davis-Villinger Temperature Probe (DVTP). Two additional measurements were taken using the DVTP with the probe pushed into the formation at 117.2 and 136.5 mbsf. A slow ROP (6.0 m/hr) and concerns over the potential for future instability of the hole led us to abandon the hole at 173.7 mbsf. The hole was displaced with 30 bbl of weighted mud, and the drill string was pulled clear of the mudline at 0335 hr on 7 July 1998. The beacon was released and the pipe trip continued to a depth of 2941 mbsl, where it was secured for the transit to the next site. The beacon was recovered at 0430 hr, ending Hole 1111A. Recovery for the hole was 15.19 m (8.7%).

Transit to Site 1112 (ACE-12A)

The ~2.6-nmi transit to Site 1112 (ACE-12A) took 3 hr, and the positioning beacon was deployed at 0730 hr on 7 July 1998.

Hole 1112A

After picking up the top drive we advanced the pipe the remaining distance to the seafloor. Hole 1112A was spudded at 0900 hr, and the seafloor depth was established to be 3046.7 mbsl (Table T4). The RCB coring continued through Core 11R to a depth of 101.8 mbsf. Although recovery was poor, the hole stability remained reasonably good until this point. At 0745 hr on 8 July, the hole packed off, preventing circulation, and the driller experienced high torque on the pipe. The pipe was pulled up to 39.0 mbsf and then reamed back to bottom. This wiper trip took ~1.25 hr and encountered 5.0 m of fill in the bottom of the hole. After the fill was washed out, the hole was advanced two more cores to 116.4 mbsf. The bit was encountering resistance at 105.0 mbsf; therefore, the pipe was pulled back up to 96.0 mbsf and then reamed back to

T3. Site 1111 coring summary by section, p. 71.

T4. Site 1112 coring summary by section, p. 73.

116.4 mbsf. At this point we swept the hole with a double sepiolite mud pill (total of 50 bbl) and circulated it out of the hole before recovering the wash barrel. Once again the bit began to take weight at 105.0 mbsf, and 2 hr more were spent pulling the pipe back to 96.0 mbsf then reaming back to 105.0 mbsf, where we circulated another 30-bbl sepiolite mud pill. Because there appeared to be a bad spot in the hole at 105 mbsf, we decided to pull the drill string back up the hole and change the spacing out of the drill string using a 20-ft knobby drilling joint. This was intended to enable us to drill past the trouble spot and make a connection without having to pull the pipe back above the bad spot. The hole packed off again during this process, and we ultimately had to pull the pipe to 77.0 mbsf before circulation could be restored. The bit was reamed down again and reached 116.4 mbsf after 7.0 m of fill was washed out. Another 30-bbl sepiolite mud pill was circulated, and we resumed coring with Core 14R. The hole was advanced to 122.4 mbsf where high pump pressure and top-drive stalling occurred with as little as 10,000 lb weight on bit (WOB). At this point, we decided that this hole was not salvageable; therefore, Core 14R was retrieved and we pulled out of the hole. Because this hole was never advanced beyond the unconsolidated “talus” material it was abandoned using no heavy mud or cement. The seafloor was cleared at 2330 hr on 8 July 1998, and the bit cleared the rig floor at 0430 hr on 9 July, officially ending Hole 1112A. Recovery for the hole was 5.85 m (4.8%).

Hole 1112B

After the RCB core bit was replaced with a new C-4 bit, the pipe was lowered back to the seafloor and a brief jet-in test was conducted in case a reentry cone was ultimately required at this site. The bit was advanced to a depth of 20 mbsf in ~50 min using up to 100 strokes per minute (spm). The pipe was pulled clear of the mudline in preparation for spudding Hole 1112B.

Hole 1112B was spudded at 1130 hr on 9 July 1998, and the seafloor was determined to be at 3046.7 mbsl. The hole was drilled to 87.0 mbsf with a wash barrel (Core 1W) in place; however, at that depth the driller experienced high torque on the pipe and up to 30,000 lb of overpull. After we worked on the pipe for 30 min, the hole appeared to be cleaned up and Core 1W was retrieved. We then continued drilling with a second wash barrel (Core 2W) to 126.1 mbsf. After Core 2W was recovered, we deployed a bit deplugger to ensure that the throat of the bit was unobstructed before initiating RCB coring. Cores 3R through 5R were then taken from 126.1 to 155.0 mbsf.

After the recovery of Core 5R, the hole again packed off and the top drive began to stall. The pipe was worked up and down the hole for the next 8.25 hr with overpulls of 20,000–40,000 lb. Several 30- to 50-bbl sepiolite pills were circulated and the bit was eventually able to reach back to bottom after 6 m of fill on the bottom was drilled out. Core 6R was then cut to 164.0 mbsf. Once again, the hole packed off and another 5.25 hr was spent fighting hole problems before we abandoned further attempts to deepen the hole. The pipe was pulled clear of the seafloor at 1400 hr on 11 July, ending Hole 1112B. Recovery for the hole was 1.19 m (3.1%).

Transit to Site 1113 (ACE-13A)

After raising the drill pipe to 2745 mbsl and recovering the positioning beacon, we began the DP transit to Site 1113 (ACE-13A). The positioning beacon was deployed at the GPS Site 1113 coordinates at 1645 hr on 11 July.

Hole 1113A

The vessel was positioned over the site as the drill pipe was lowered back to the seafloor. The top drive was picked up, and Hole 1113A was spudded at 2045 hr on 11 July 1998 (Table T5). The seafloor was tagged at a depth of 2915.6 mbsl, and we cut RCB Cores 1R and 2R to 20.2 mbsf. After making the drill pipe connection, but before cutting the next core, we found that 7 m of sediment had filled the bottom of the hole. The fill was washed out, and Core 3R was cut to 25.2 mbsf. We decided to terminate the hole because of the extremely slow ROP (0.8 m/hr) and poor hole conditions at such shallow subseafloor depths. The pipe was pulled clear of the seafloor at 1345 hr on 12 July, and the bit cleared the rig floor ending Hole 1113A at 2000 hr. Recovery for the hole was 0.44 m (1.7%).

LITHOSTRATIGRAPHY

Introduction

A minor amount of sediments, sedimentary rocks, and lithoclasts was recovered at Sites 1110, 1111, and 1112. No sediment was recovered at Site 1113. The different sediment types are recognized on the basis of sediment or rock type, grain size, sedimentary structures, color, compositions determined in smear slide and thin sections, bulk mineralogy (X-ray diffraction [XRD]), and calcium carbonate determinations. Details of the sediments are given first, followed by a brief interpretation, in the order of Site 1110, Site 1111, and then Site 1112. The very low recovery did not warrant presentation of lithologic logs as given for the other sites drilled during Leg 180. In addition, much of the recovery from Sites 1110, 1111, 1112, and 1113 consisted of angular fragments of igneous and metamorphic rocks interpreted as talus (see *“Igneous and Metamorphic Petrology,”* p. 11).

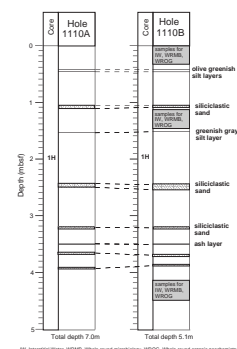
Site 1110

Quaternary, mainly fine-grained sediments, together with minor amounts of coarser grained sediment and isolated clasts of metamorphic and minor igneous rock, were recovered at Site 1110. The sediments are described below, whereas the metamorphic clasts are described separately (see also *“Igneous and Metamorphic Petrology,”* p. 11).

The uppermost few meters at Site 1110 were cored in Holes 180-1110A and 1110B. These two cores include a number of distinctive marker horizons, notably an individual very thin volcanic ash bed (~2 cm thick), siliciclastic sands, and greenish silt layers, which together allow a precise correlation between the three holes (Fig. F1; see also *“Composite Depths,”* p. 26), confirming that a complete succession was recovered.

T5. Site 1113 coring summary by section, p. 75.

F1. Correlation of successions in Core 180-1110A-1H with Core 180-1110B-1H, p. 28.



Lithostratigraphic Unit I

Description: calcareous ooze and clay, silty clay, sand; metamorphic and igneous rock clasts

Interval: Cores 180-1110A-1H and 2H; 180-1110B-1H through 3X; and 180-1110D-1W and 2R

Depth: 0–9.5 mbsf (Hole 1110A); 0.0–22.3 mbsf (Hole 1110B); and 0.0–28.7 mbsf (Hole 1110D)

Age: Quaternary

The sedimentary lithologies recovered are described below.

Nannofossil Ooze, Nannofossil Clay, and Foraminifer-Rich Ooze

Gray and olive gray, clay-rich nannofossil ooze and foraminiferal ooze dominate the upper part of the recovery in Cores 180-1110A-1H and 2H. In Core 180-1110B-1H, calcium-carbonate analyses indicate values from 27 to 41 wt% (see [“Organic Geochemistry,”](#) p. 22).

Very thin beds (<3 cm) of nannofossil-rich ooze exhibit sharp bases, normal grading, and diffuse tops (e.g., Fig. F2). Sulfide mottling is observed in places. Beneath this, Core 180-1110A-2H contains numerous structureless beds of greenish gray nannofossil ooze, up to several tens of centimeters thick (see also description of Section 180-1110B-1H-CC in [“Calcareous Nannofossils,”](#) p. 17).

In smear slides ([“Site 1110 Smear Slides,”](#) p. 11) the nannofossil ooze contains nannofossils, quartz, feldspar, biotite, accessory minerals, biogenic and inorganic calcite, together with planktonic foraminifers, radiolarians, and sponge spicules. Volcanic glass is seen in some, but not all samples. Also, radiolarians are sporadic. The XRD analysis of silty nannofossil clay indicates the presence of quartz, calcite, plagioclase, chlorite, amphibole, and illite (see Table T6).

Silty Clay

Silty clay, with or without abundant nannofossils, is present in Cores 180-1110A-1H and 2H. This lithology exists as four subtle color variants (i.e., greenish gray, dark gray, dark olive gray, and olive). Silty clay also predominates in Core 180-1110B-2X, where it contains numerous small shell fragments. One XRD analysis revealed the presence of calcite, quartz, chlorite, plagioclase, and amphibole (see Table T6). The calcium carbonate contents of samples from Core 180-1110A-2H are 9.2–35.4 wt%.

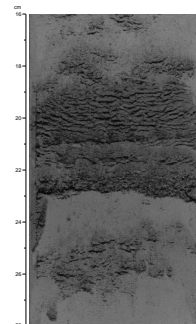
Silt

A thin bed of normal-graded volcanoclastic silt is present in interval 180-1110A-2H-1, 25–26 cm. Silt recovered in Section 180-1110A-1H-5 is volcanoclastic, with >70% colorless glass shards. In smear slides, the silt contains similar components as the fine-grained sand, described below, with the addition of clay, rare chloritic or glauconitic grains ([“Site 1110 Smear Slides,”](#) p. 11).

Sand

Very thin beds of normal-graded sandstone (<2.5 cm thick) were rarely recovered. Blue gray sand of siliciclastic origin was observed in Core 180-1110A-1H as a minor lithology. Compositionally, as seen in smear slides ([“Site 1110 Smear Slides,”](#) p. 11), the sand is dominated by metamorphic lithoclasts and planktonic foraminifers. In addition, quartz, plagioclase, mica, epidote, shell fragments, biotite, muscovite, rare igneous rock fragments, accessory minerals, biogenic and inorganic

F2. Nannofossil-rich clay sediment with volcanic glass, p. 29.



T6. XRD analyses of whole-rock samples, p. 76.

calcite, coccoliths, and sponge spicules are present. The XRD analysis confirmed the presence of chlorite and illite as the clay minerals present, in addition to quartz, plagioclase, and amphibole (Table T6).

Conglomerate

Gravel, mainly composed of metamorphic rock fragments (up to 1.8 cm in size), is present in Sections 180-1110A-2H-2 and 2H-CC. A single bed, graded from granules to coarse grains, then medium- and fine-grained sand, is present from 0 to 50 cm in Section 180-1110A-2H-2 (Fig. F3). Individual clasts are greenschist mylonite and pelitic schist with additional rare clasts of granite. Similar gravel is seen in Core 180-1110B-3X.

Volcanic Ash

A thin volcanic ash bed was identified in interval 180-1110B-1H-3, 51–53 cm. In addition, volcanic glass is widely disseminated throughout other sediment types.

Clasts

A number of isolated metamorphic clasts and rare igneous rocks were recovered in Cores 180-1110B-3X and 180-1110D-1W and 2R. These are mostly angular and up to 5 cm in size, although their size is probably an artifact of drilling. Clast types included epidiosites, greenschist metapelite, greenschist mylonite, and microgranite (see “[Igneous and Metamorphic Petrology](#),” p. 11).

Interpretation

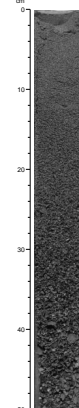
Based on paleontological evidence, the fine-grained sediments recovered from Site 1110 accumulated in deep water (see “[Biostratigraphy](#),” p. 17). The background sediment is represented by nannofossil- and foraminifer-rich ooze and clay, with a minor contribution from siliceous micro-organisms (radiolarians and sponge spicules). Rare thin beds consisting almost entirely of glass are interpreted as pyroclastic air-fall tuff. More commonly, volcanic glass is reworked through other lithologies.

Three types of gravity-flow deposits are recognized: (1) very thin, normal-graded beds of clay and silty clay, composed of mixed siliciclastic-derived sediments and volcanic ash. These are interpreted as hemipelagic sediment that was redeposited by low-density turbidity currents; (2) thin beds of graded sand composed of siliciclastic (metamorphic) grains and planktonic foraminifers, also interpreted as turbidity current deposits; and (3) granule conglomerate grading into sand, composed of metamorphic detritus and interpreted as high-density turbidity current deposits.

In addition, isolated angular clasts, as long as 7 cm, were recovered. These are mainly composed of green-colored schist of probable greenschist metamorphic grade, dark pelitic schist, and altered, but undeformed, granitic rock. The clasts were probably derived from mass-flow deposits.

In summary, Site 1110 records deep-water Quaternary sedimentation in a setting of extreme sediment instability, as shown by the abundance of turbidites and inferred mass-flow deposits. Metamorphic clasts are most likely to be talus deposits derived from the nearby Moresby Seamount.

F3. Graded conglomerate and sand, p. 30.



Site 1111

There was limited recovery of sediments and individual clasts of igneous, metamorphic, and rare sedimentary rocks at Site 1111.

There was no recovery from the seafloor to 10.1 mbsf (represented by Core 1R), and thereafter only minimal recovery in Cores 2R, 3R, 4R, 6R to 8R, 10R to 18R, and no recovery at all in Cores 5R and 9R. The hole reached 173 mbsf. Most of the material recovered consisted of clasts of metamorphic rock and minimal recovery of fine-, medium-, and coarse-grained sediment. Only in Core 8R was there any more substantial recovery.

Lithostratigraphic Unit I

Description: clay, silt, and sand, and clasts of mainly metamorphic rock

Interval: Cores 180-1111A-1R through 18R

Depth: 0–173.7 mbsf

Age: Pleistocene

The lithologies recovered are described below.

Nannofossil Clay

Nannofossil-bearing clay was recovered in Core 2R. The clay is green, massive, and contains planktonic foraminifers, sponge spicules, and calcareous fragments. Silty nannofossil clay and ooze were found, based on XRD analysis, to consist of plagioclase, quartz, calcite, chlorite, illite, and smectite(?) (Table T6).

Calcareous Clay

Very minor greenish gray calcareous clay with pebbles of epidote schist was recovered in Core 3R. Very minor, greenish brown clay with lamprophyre was recovered, in addition to discrete clasts of lamprophyre in Core 4R. The XRD data indicate that the calcareous clay contains only calcite and aragonite, whereas the silty clay additionally contains plagioclase and chlorite (Table T6).

Silty Clay

Dark greenish gray nannofossil-rich silty clay was recovered in Sections 8R-1 through 8R-3 and 8R-CC. A smear slide of the silty clay was found to contain quartz, feldspar, muscovite, clear volcanic glass, epidote, biogenic and inorganic carbonate grains, planktonic foraminifers, radiolarians, coccoliths, sponge spicules, and rare fine plant material (“Site 1111 Smear Slides,” p. 24).

Silt

Very minor nannofossil-rich silt was recovered in Core 6R, together with fragments of dolerite and metadolerite.

Sand

Very minor dark greenish gray silt and fine-grained sand were recovered in Core 7R. A small amount of dark greenish, coarse-grained sand was also observed, together with angular to subangular fragments of phyllite and gabbro. Blue gray, normal-graded, coarse- to fine-grained sand is present in interval 180-1111A-8R-1, 69.5–53.5 cm. In addition, a very thin bed of volcanoclastic sand is present in interval 180-1111A-8R-2, 124–125 cm.

A smear slide of fine-grained sand contains abundant metamorphic rock fragments, quartz, feldspar, muscovite, inorganic calcite, foraminifers, nannofossils, and sponge spicules, together with common pyrite, in both amorphous form and as isolated cubes ([“Site 1111 Smear Slides,”](#) p. 24).

Interpretation

The Pleistocene sediments recovered at Site 1111 record similar depositional processes to those at Site 1110 (see [“Site 1110,”](#) p. 6), as far as can be determined from the minimal recovery. The succession is inferred to contain abundant talus of mainly metamorphic rocks, intercalated with clay and silty clay, silt, and sand. Some of the sediments may also represent matrix to the talus. The sediment is mainly disturbed, and very few sedimentary structures indicative of a depositional process are preserved. Those that exist again suggest deposition by turbidity currents. In addition, the talus is interpreted as the product of mass flows derived from the adjacent margin of the Moresby Seamount.

Site 1112

Description: silty clay, nannofossil ooze, silty claystone, volcaniclastic sandstone, volcanic ash; igneous and metamorphic rock clasts

Interval: Cores 180-1112A-1R through 14R and 1112B-3R through 6R

Depth: 0–164.6 mbsf

Age: Pleistocene

At Site 1112 there was also only limited recovery of sediments including individual clasts of igneous, metamorphic, and rare sedimentary rocks. Minimal recovery from Cores 1R and 2R (0–20.5 mbsf) revealed nannofossil-rich silty clay with rare laminae and thin beds of coarse-grained siliciclastic sandstone. In the latter core, two thin beds of volcanic ash were observed. Cores 3R through 13R consist mainly of metamorphic rocks (greenschist metadolerite) and volcaniclastic sandstone with some silty claystone. The results of smear-slide analysis of the sediments and sedimentary rocks recovered from this site are described below and in [“Site 1112 Smear Slides,”](#) p. 30.

Silty Clay and Silty Clayey Nannofossil Ooze

Five smear slides were studied, which showed these sediments to be composed of grains of quartz, feldspar, biotite, rare basaltic and metamorphic rock fragments, clear volcanic glass, inorganic calcite, abundant coccoliths, planktonic foraminifers, rare siliceous sponge spicules, rare diatoms, and rare radiolarians.

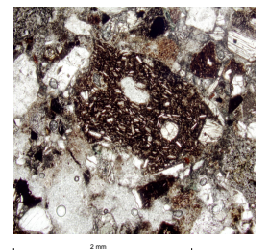
Volcanic Ash

Smear-slide analysis of the two beds of volcanic ash (silt clay) showed the higher of these (light gray) to be dominated by brown glass shards, whereas the lower (dark gray) was dominated by colorless glass shards.

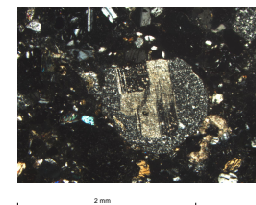
Volcaniclastic Sandstone

Two thin sections of the volcaniclastic sandstones were studied: (1) a coarse-grained volcaniclastic sandstone (Sample 180-1112A-9R-CC, 25–27 cm) consisting of abundant rounded to subrounded volcanic lithoclasts of mafic (basaltic and andesitic) and acidic origin (rhyolitic and dacitic), and minor devitrified glass (vitric) (Figs. [F4](#), [F5](#); [“Sites 1110–](#)

F4. Basalt clast with laths and phenocrysts, [p. 31](#).



F5. Coarse-grained sandstone, [p. 32](#).



1113 Thin Sections”). Also present are angular detrital grains of plagioclase, feldspar, biotite (chloritized), hornblende, and clinopyroxene; and (2) a medium-grained volcanoclastic sandstone (Sample 180-1112A-3R-1, 2–5 cm) composed of abundant rounded to subrounded lithoclasts of basaltic and andesitic fragments and angular detrital grains of plagioclase, feldspar, quartz, biotite, hornblende, and clinopyroxene (Fig. F6).

Silty Claystone

Examination of a single thin section of silty claystone (Sample 180-1112A-6R-1, 10–12 cm) showed this to be composed of detrital grains of feldspar, biotite, quartz, clinopyroxene, opaque minerals, and minor carbonaceous detritus set in a claystone matrix (“Sites 1110–1113 Thin Sections”).

Interpretation

The Pleistocene sediments recovered at Site 1112 record similar depositional processes to those at Sites 1110 and 1111 (see “Site 1110,” p. 6, and “Site 1111,” p. 9), as far as can be determined from the minimal recovery. The succession is inferred to contain abundant talus of mainly metamorphic rocks, intercalated with clay and silty clay, silt, and sand. The sediment is mainly disturbed, and very few sedimentary structures indicative of depositional process are preserved. Those that exist, again suggest deposition by turbidity currents. Of the two ash layers recovered, the clear volcanic glass is thought to represent an ash fallout whereas the brown basaltic glass is probably of submarine origin related to spreading of the Woodlark Basin.

IGNEOUS AND METAMORPHIC PETROLOGY

Introduction

The clasts from Sites 1110 through 1113 are highly heterogeneous in terms of mineralogy, consistent with the interpretation that the holes drilled here are located in talus fans from the Moresby Seamount. In hand specimen, the majority are massive to weakly foliated rocks ranging in color from dark gray to greenish, caused by the presence of increasing amounts of epidote. Some are banded, and veins, sometimes folded, are common. Thin-section examination suggests that most of these rocks were originally dolerites that have been subjected to varying degrees of veining, shearing, and hydrothermal alteration under greenschist facies conditions. We refer to them loosely as metadolerites, although the protolith is, in some cases, in doubt.

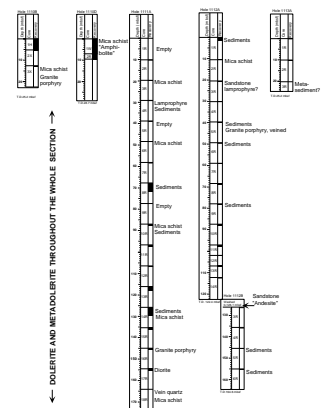
Other lithologies include small amounts of mica schist, which probably has a pelitic protolith, as well as lamprophyres, granite porphyries, sedimentary rocks (volcanogenic sandstones), and so forth. Figure F7 shows the total recovery from each section and notes where these diverse rock types occur. Small amounts of clay were also recovered, sometimes adhering to the clasts. Such clay is a likely matrix of the heterogeneous clasts described here.

Protoliths of the metamorphic rocks clearly include igneous acidic types (granites and porphyritic granites), basic rocks (mainly dolerites, as indicated by relict igneous textures visible in hand specimen, which resemble those seen in the relatively fresh dolerite at Site 1109), and

F6. Well-sorted medium-grained sandstone, p. 33.



F7. Recovery log of Sites 1110–1113 with distribution of rock types, p. 34.



sedimentary rocks, as inferred by the presence of abundant micaceous minerals in schists. The following is a detailed description of the various rock types and textures within the unit referred to as heterogeneous talus at each of the sites. Because all the sites apparently sampled the same unit—talus from the seamount—we consider them together here. Similar material from Site 1108 has already been briefly described in the Site 1108 chapter (see “[Lithostratigraphy](#),” p. 6, in the “Site 1108” chapter). In addition, we give more detail on the Site 1108 material in the following sections.

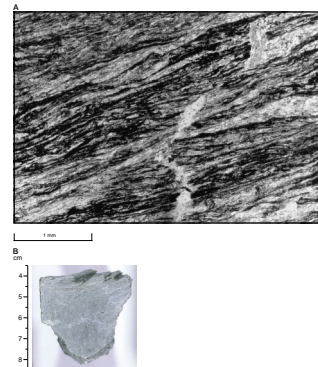
Metasedimentary Rocks

A number of fine-grained mica schist clasts were recovered from 0 to 20 mbsf in Holes 1110B and 1110D, 1111A, and 1112B, whose distribution is shown in Figure F7. They consist of primary muscovite, quartz, and plagioclase with secondary chlorite, calcite, epidote, zoisite, clay minerals, iron oxide, and trace amounts of pyrite. Ductile structures, which range from lepidoblastic to mylonitic, including foliation planes and asymmetric tails around plagioclase and quartz porphyroclasts with quartz and chlorite in pressure shadows, are indicative of shear. The temperature conditions prevailing during the evolution of the mica schists is inferred to have ranged between 300°C (quartz shows evidence of recrystallization) and 500°C (plagioclase shows evidence of brittle deformation) (Rubie, 1983). The general aspect of these clasts in thin section shows a foliation plane (Fig. F8A), whereas some samples show subsequent folding of the foliation plane (Fig. F8B). This deformation is thought to have occurred early in the metamorphic evolution, before the retrograde metamorphic evolution under greenschist facies conditions, because calcite and epidote grains are not ductilely deformed.

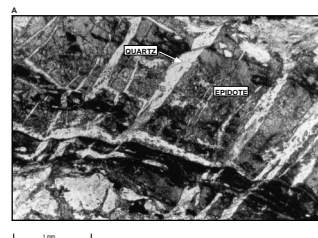
As deformation proceeded, the epidote-rich layers were boudinaged (Fig. F9A), and fractures filled with quartz and calcite oriented perpendicular to the foliation were created. This indicates that brittle deformation occurred at a late stage of the metamorphic evolution (see also Fig. F10). Shearing is also associated with this late tectono-metamorphic stage because asymmetric pressure shadows with quartz and calcite fibers around pyrite grains occur (Fig. F11). Pyrite, chlorite, epidote, and quartz are indicative of hydrothermal alteration.

Some rocks were classified as carbonate or epidote schist according to the development of an assemblage characteristic of greenschist facies metamorphism, probably associated with strong hydrothermal alteration. Some may also have been dolerites, judging from the large amounts of epidote. It was not possible to deduce the protolith of some of the rocks with greater mylonitization. The highly schistose foliation in both hand-specimen and thin-section examination shows high contents of mica and epidote (Fig. F9B), suggesting that in some examples the primary composition was pelitic and a metasedimentary origin is likely. Fine-grained mylonites of feldspathic composition, apparently metamorphosed under greenschist facies conditions, were recovered at Site 1108, located to the east of Sites 1112 and 1113, and compositionally banded rocks of uncertain origin were found at the other talus sites. Primary mineralogy of these gneissic to mylonitic rocks is almost completely obliterated, but probably consisted largely of quartz and plagioclase (Figs. F12A, F12B). Well-developed foliation planes are crosscut perpendicularly by fractures filled with quartz, calcite, and plagioclase,

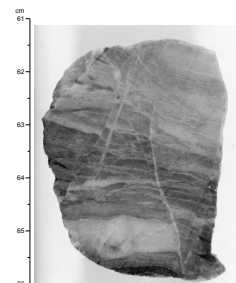
F8. Thin-section view of epidote-mica schist, p. 35.



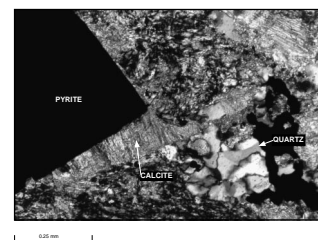
F9. Hand specimen and thin-section view of deformed metadolerite, p. 36.



F10. Foliated epidote-quartz schist cut by fractures, p. 38.



F11. Pyrite grain with calcite and quartz in mica schist, p. 39.



which indicate late brittle deformation. Shear is indicated by chlorite sigmoidal trails surrounding lenses of quartz.

Acid to Intermediate Igneous Rocks

Pebbles of granite porphyry (phenocrysts of plagioclase in a fine-grained quartz groundmass) were recovered at depths ranging from 20 to 150 mbsf in Holes 1108B, 1110B, 1111A, and 1112A. The precise locations of these samples are as follows: Samples 180-1108B-3R-CC, 4–5 cm; 180-1108B-13R-CC, 0–5 cm; 180-1110B-3X-1, (Piece 3, 17–23 cm); 180-1111A-16R-CC (Piece 4, 16–20 cm); and 180-1112B-1W-1, 12–17 cm. Analysis of one of these porphyries is shown in Table T7 and T8 (Analysis 6), confirming its granitic composition (69% SiO₂). The ferromagnesian minerals (Fig. F13) are green hornblende and/or biotite occurring as phenocrysts. From their mineralogy (dominantly feldspar with lesser amount of ferromagnesian), these samples appear to have calc-alkaline to alkaline affinities and the chemistry of the analyzed example is not particularly rich in Zr, but highly enriched in Sr and Ba, which tends to confirm this inference.

Sample 180-1108B-13R-CC, 0–5 cm, contains deep green pleochroic amphibole. Some samples show both ductile and brittle deformation indicated respectively by undulose extinction within plagioclase phenocrysts and by the presence of veins filled with calcite and pyrite. Additional alteration products include chlorite, sericite, quartz, calcite, and iron oxide in all samples. Although these samples have been classified as granitic in composition, the groundmass is too fine to be resolved under the microscope, and the amount of quartz cannot be estimated without a chemical analysis. We assume that the analyses in Tables T7 and T8 are representative, but, in fact, other samples may be more intermediate in composition.

Two pebbles recovered from Hole 1112A (Sample 180-1112A-5R-1, Pieces 5 and 6, 20–36 cm) were identified in hand specimen as porphyries. They appear to be cut by numerous parallel fractures filled with quartz, but were not examined in thin section. All these porphyry types probably occur as dikes on Moresby Seamount.

One holocrystalline quartz trachyte pebble containing alkali feldspar was recovered at interval 180-1108B-47R-1, 45–46 cm, but it has not been studied further.

One pebble of vein quartz was recovered in Hole 1111A (interval 180-1111A-18R-1, 33–43 cm). It consists of 95% quartz with 5% calcite precipitated in veins. Undulose extinction and recrystallization at the margins of the quartz grains is indicative of ductile deformation, whereas calcite veins are indicative of brittle deformation.

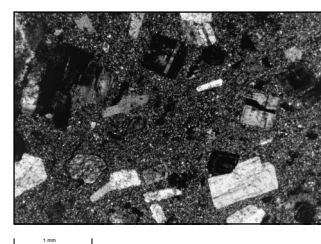
One medium-grained granitic gneiss was recovered during Leg 180 (Sample 180-1108B-8R-CC, Piece 3) (see “Lithostratigraphic Unit II,” p. 8, in the “Site 1108” chapter). It has a lepidoblastic texture and consists primarily of feldspar, quartz, and biotite elongated in the foliation plane. Accessory minerals include sphene and zircon. Very slight chlorite and sericite alteration is seen in thin section.

A volcanic or hypabyssal rock with microphenocrysts of clinopyroxene set in a groundmass of flow-oriented (trachytoid) amphibole prisms and felsic mesostasis was recovered from the deepest part of Site 1112 (Core 180-1112B-1W). This rock has been provisionally named “andesite,” but the relatively high alkali content, especially K₂O (Tables T7, T8; Analysis 5), suggests that it may be related to the shoshonitic rocks

F12. High-temperature structures in mica schist and gneiss, p. 40.



F13. Feldspar porphyry in quartzofeldspathic matrix, p. 42.



T7. Moresby Seamount talus major element analyses, p. 77.

T8. Moresby Seamount talus trace element analyses, p. 78.

of nearby Woodlark Island (Ashley and Flood, 1981), as is the “lamprophyre” discussed in “[Other Basic Igneous Rocks](#),” p. 15.

Basic Igneous Rocks

The basic igneous clasts at Sites 1110–1113 are mainly metadolerite that shows various degrees of alteration to greenschist facies assemblages.

We use the term “dolerite” to refer to clasts where the original mineralogy and texture is sufficiently well preserved to allow an easy recognition of the original protolith, whereas rocks that are so changed as to have lost this texture and mineralogy because of deformation and new mineral growth, are called metadolerites, providing the composition is appropriate.

In general, dolerites were recovered in the deeper levels of the holes from 30 to ~170 mbsf. Between ~35 and 95 mbsf, the metadolerite seems to prevail. Below ~95 mbsf, metadolerite forms the main lithology recovered in Hole 1111A, whereas dolerite forms the main lithology recovered in Hole 1112B. These dolerite clasts are mixed with a few clasts of other lithologies (lamprophyre, porphyries, vein quartz, etc.) as shown in Figure [F7](#).

Dolerite

Dolerite clasts were recovered in the deeper levels of Holes 1111A, 1112A, and 1112B. This dolerite is medium grained, generally granular, although occasionally ophitic, and relatively unaltered. It is similar to the small portion of the dolerite recovered at Site 1109 (see “[Igneous and Metamorphic Petrology](#),” p. 35, in the “Site 1109” chapter) that also had a granular texture rather than the typical ophitic texture. An example of a moderately altered dolerite with ophitic texture is shown in Figure [F14](#). At Site 1109 the dolerite contains similar proportions of plagioclase and clinopyroxene, with rare opaque minerals and green alteration products that appear to be replacing olivine or interstitial glass. Feldspar shows various degrees of sericitization.

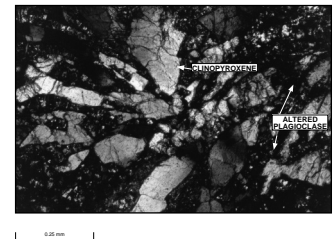
Many of the dolerite clasts are cut by veins filled with angular rock and mineral fragments in an opaque groundmass of highly milled material, which is unresolvable by optical methods. There is no fabric to these bodies, and clasts make up about 30% of them. They, therefore, fall under the term “cataclasite.” The cataclastic veins displace an earlier generation of quartz veins (Fig. [F15](#)) and probably formed late in the history of the rock. Similar material occurs abundantly at Site 1117 and is depicted in Figure [F5](#), p. 17, in the “Site 1117” chapter.

Similar pebbles of dolerite with altered feldspars and sporadic epidote, probably representing incipient greenschist facies metamorphism, were recovered in Hole 1108B (e.g., interval 180-1108B-47R-CC, 1–3 cm; an analysis of this rock is given in Table [T4](#), p. 126, in the “Site 1114” chapter).

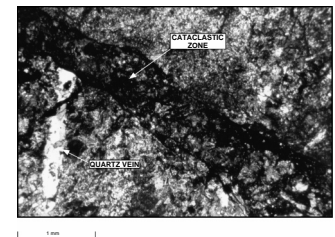
Metadolerite

A pebble of amphibole-plagioclase rock was recovered in Hole 1110D in the wash core (Core 180-1110D-1W) (Fig. [F16](#)). Mineralogy of this rock includes primary amphibole (green hornblende prisms), plagioclase, clinopyroxene, and quartz with secondary biotite (replacing amphibole) and sericite (replacing plagioclase). It may be interpreted as

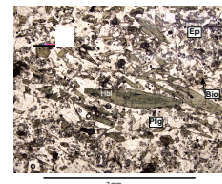
F14. Metadolerite showing the original ophitic texture, Site 1114, p. 43.



F15. Cataclastic zone across metadolerite and quartz vein, p. 44.



F16. Amphibole-plagioclase-rich rock, p. 45.



an amphibolite, but the slightly porphyritic character and the lack of any obvious planar or linear structures in thin section lead us to think that it may be a hornblende-rich igneous rock, perhaps of lamprophyric affinities. Limited deformation of thin biotite flakes is not thought to be significant in this context.

Metadolerites from Hole 1111A are fine grained, with lepidoblastic to mylonitic texture, and consist of plagioclase, amphibole (tremolite?), quartz, and iron oxide with secondary epidote, chlorite, quartz, calcite, and clay. These rocks have been ductilely deformed, leading to the formation of a foliation plane, which was subsequently folded. The latest metamorphism in the greenschist facies is static because both chlorite and epidote are fibrous and nonoriented. Late brittle deformation is indicated by the presence of fractures filled with quartz, calcite, chlorite, and iron oxide, although some fractures are reworked (Fig. F8A) and must belong to an earlier phase of brittle deformation.

Epidote-rich pebbles were recovered together with the dolerite from several holes. The rocks can be described mostly as epidosite or metadolerite because of the abundance of epidote alteration throughout previous dolerite rocks. These rocks are similar to those described earlier, but are more altered, showing pervasive hydrothermal alteration and veins filled with calcite, quartz, epidote, and pyrite, indicating brittle deformation. It is possible that these rocks represent areas of more intense alteration proximal to veins in the dolerite that have channeled hydrothermal fluid flow.

The question of the extent of chemical alteration during the transition from dolerite to metadolerite and ultimately to epidosite is addressed in the chapter on Site 1114 (see “[Igneous and Metamorphic Petrology](#),” p. 16, in the “Site 1114” chapter).

Other Basic Igneous Rocks

A pebble associated with the metadolerites and given the field term “lamprophyre” was recovered in Core 180-1111A-4R at about 29 mbsf. One pebble of diorite was recovered from near the base of the same hole at about 155 mbsf.

The lamprophyre has a few percent euhedral clinopyroxene phenocrysts and pseudomorphs after olivine phenocrysts, which may have made up about 10% of the rock originally. The groundmass is fresh with a panidiomorphic texture (i.e., euhedral ferromagnesian minerals in a felsic mesostasis). It consists of about 25% clinopyroxene and 35% amphibole needles. The felsic mesostasis could not be identified. Chemically, the rock is quite unlike the dolerites recovered at other sites (e.g., Site 1109), as shown in Tables T7 and T8. This difference is not likely to be caused by alteration because the rock is rather fresh, apart from the replacement of olivine. Most marked are the very high contents of K, Sr, and Ba, which suggest affinities to the shoshonitic rocks of the area. No completely satisfactory equivalent could be found from the “high-K” suite of Woodlark Island (Ashley and Flood, 1981), but this does not rule out the comparison, because such rocks, which are often highly porphyritic, show considerable variability. In particular, we note that the Site 1111 sample has about twice the K_2O content of any from Woodlark Island, which suggests that it is distinct. However, the very elevated Sr and Ba contents can be matched. In many ways, it resembles the subrecent Madilogo volcano near Port Moresby (Blake, 1976), an analysis of which is given for comparative purposes in Tables T7 and T8. This small volcano is probably an outlier of the Papuan

high-K province. We tentatively conclude that this rock is a representative of the widespread shoshonitic (also called the “high-K” suite) activity of the Papuan Peninsula and adjacent islands but cannot suggest a more localized provenance.

Basalt was a major constituent of the clasts recovered from the upper part of Hole 1108B, largely present in Cores 180-1108B-2R through 8R, although a few came from below this, perhaps having fallen from higher levels of the hole. Primary mineralogy consists of microphenocrysts of plagioclase and olivine within a glassy groundmass. Well-preserved quench textures, such as lanterns and swallow tails, are visible in thin section (Fig. F17). These glassy groundmasses vary from tachylitic (fresh but opaque and glassy) to pilotaxitic (glassy, containing aligned feldspar needles) to variolitic (devitrified glass with a spherulitic structure). One sample had complexly zoned plagioclase xenoliths (Fig. F18). The majority of basalts recovered are fresh and generally sparsely vesicular, which implies recent submarine extrusive origin within relatively shallow water (<500 m; see Lackschewitz et al., 1994; Fisher and Schmincke, 1984), although several factors affect the vesicularity. If this interpretation is correct, it is surprising because the only source of basalt known at the present time is at the nearby spreading center, which is everywhere deeper than 2000 m (Taylor et al., 1995). One basalt pebble was crystalline with vesicles filled with epidote and chlorite, and clearly has a completely different provenance. The basalts recovered in Hole 1108B were not found at Sites 1110 through 1113.

Clasts in Volcanogenic Sandstones

These are described under “Lithostratigraphy,” p. 6, in the “Site 1108” chapter. An abundance of types are recognized, including serpentinized ultramafics (with chromite grains), volcanics with plagioclase and/or hornblende phenocrysts, and metamorphic rocks. One rock had a remarkable, complexly zoned plagioclase clast with a great many narrow oscillatory zones (Fig. F19), a type commonly found in andesites, which suggests that these lithic clasts, at least in part, are of calc-alkaline affinities (e.g., MacKenzie et al., 1982).

Interpretation

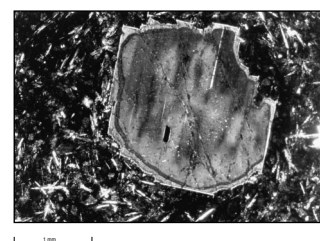
Most of the metamorphic rocks recovered at Site 1108 and Sites 1110–1113 were originally igneous, and some relict igneous textures are preserved. They are thought to be similar to the relatively fresh dolerite recovered at Site 1109, although we do not suggest that they belong to this body. There are occasional mica schists and gneisses, the former preferentially in the upper part of the holes. Both the mica schists and gneisses deposited as talus seem to record at least two tectonic and metamorphic stages, including the development of an early foliation plane followed by folding of the foliation, possibly prior to massive retrogression into lower greenschist facies conditions and extensive hydrothermal alteration.

Rocks deposited at Sites 1110 through 1113 come from a variety of sources, and it is likely that metamorphic, igneous, and sedimentary rocks are talus deposits from nearby Moresby Seamount. Metasedimentary rocks are most abundant from 0 to 20 mbsf. A mixture of igneous, metamorphic, and sedimentary rocks occurs from 20 to ~90 mbsf. The basic igneous rocks are most abundant from 90 mbsf to the bottoms of Holes 1111A and 1112B. The distribution observed in the talus deposits

F17. Swallowtail of quench plagioclase microlite in basalt, p. 46.



F18. Plagioclase xenocryst in glassy basalt pebble, p. 47.



F19. Oscillatory zoning in plagioclase clast in volcanoclastic sandstone, p. 48.



may indicate that the igneous basic rocks (dolerite and metadolerite) were the first talus deposits (Fig. F8). They most likely came from the top of the seamount, where in situ dolerite was recovered at Site 1114, when extensional tectonics started. As extension proceeded, deeper crustal levels of the basement were uplifted by normal faulting, unroofing the metamorphic rocks. Clasts of mica schist were subsequently shed as talus to the upper parts of the holes at Sites 1108 and 1110 through 1113.

The presence of numerous dolerite clasts suggests that the upper parts of Moresby Seamount (at least its northern flank) are composed largely of dolerite and metadolerite variably deformed and altered. The mixture of relatively fresh and altered material (e.g., epidiosites) suggests that the protolith is traversed by zones, perhaps originally faults, which have channelled hydrothermal fluid flow, with consequent wall rock reaction.

Talus material at Site 1108 is more variable than at the other sites discussed here, reflecting that the site is further away from the slope of Moresby Seamount and has received material from other sources, including recent submarine basalts, probably from the nearby Woodlark spreading center tip. The submarine basalts may have been transported from the active spreading tip, which lies only a short distance to the east, but the mode of transport is obscure.

We think that most of the rocks described above are present on Moresby Seamount. Experience gained from the holes drilled in largely sedimentary successions nearby show that rafting of pebbles must be a very rare event. Perhaps the more exotic igneous types are present as dikes cutting the dolerites and metadolerites, which apparently make up the bulk of Moresby Seamount.

BIOSTRATIGRAPHY

Introduction

We made biostratigraphic assignments to core-catcher samples in Holes 1110A, 1110B, 1111A, 1112A, and 1112B using calcareous nanofossils and planktonic foraminifers (Fig. F20). Estimates of paleobathymetry for these samples were made using benthic foraminiferal assemblages.

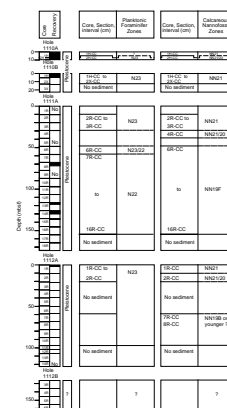
Calcareous Nannofossils

Abundance and Preservation

Sample 180-1110A-1H-CC contains abundant, well-preserved nanofossils. Few and well-preserved nanofossils occur in Sample 180-1110A-2H-CC. Samples 180-1110B-1H-CC and 2X-CC contain abundant, well-preserved nanofossils. Core 180-1110B-3X has no sediments.

There was no recovery of sediment in Cores 180-1111A-1R, 5R, 9R, 17R, and 18R. Samples 180-1111A-2R-CC to 4R-CC contain abundant, well-preserved nanofossils. Nannofossils in Samples 180-1111A-6R-CC and 7R-CC are common and well preserved. Nannofossils in Samples 180-1111A-8R-CC to 16R-CC are common to abundant, with preservation ranging from poor to good (mostly moderate). Reworking (and

F20. Planktonic foraminifer and calcareous nannofossil zones, p. 49.



some possible contamination from higher in the hole) is common throughout the samples.

Cores 180-1112A-3R to 6R, 11R to 14R, and 180-1113A-1R to 3R have no sediments. Samples 180-1112A-9R-CC and 10R-CC and 180-1112B-3R-CC through 6R-CC are barren of nannofossils. Samples 180-1112A-1R-CC and 2R-CC yield abundant and well-preserved nannofossils. Samples 180-1112A-7R-CC and 8R-CC contain rare and poorly preserved nannofossils.

Zonation

Cores 180-1110A-1H and 180-1110B-1H to 2X are placed in nannofossil Zone NN21, based on the presence of *Emiliana huxleyi*. Sample 180-1110A-2H-CC contains no *Pseudoemiliana lacunosa* and rare *E. huxleyi*, indicating Zone NN21–20.

Emiliana huxleyi is present in Samples 180-1111A-2R-CC and 3R-CC, indicating Zone NN21. Sample 180-1111A-4R-CC contains *E. huxleyi*, but also *Pseudoemiliana lacunosa*, which is probably reworked. The sample is assigned to Zones NN21–NN20 because of the mixed assemblage. We assign Samples 180-1111A-6R-CC to 16R-CC to Subzone NN19F, based on the presence of *Pseudoemiliana lacunosa* and *Gephyrocapsa omega*.

Core 180-1112A-1R is in the nannofossil Zone NN21, based on the common occurrence of *Emiliana huxleyi*. Sample 180-1112A-2R-CC contains rare *E. huxleyi*, indicating Zone NN21–NN20. We found five and one specimens of *Gephyrocapsa oceanica* in Samples 180-1112A-7R-CC and 8R-CC, respectively, which indicates Subzone NN19B or younger.

Planktonic Foraminifers

Sample 180-1110A-1H-CC, 11–14 cm, is a volcanic ash layer that contains only very small planktonic foraminifers of non-age-diagnostic species. Sample 180-1110A-1H-1, 91–93 cm, which contained well-preserved planktonic foraminifers, including *Bolliella calida* and *Bolliella adamsi*, was assigned to Zone N23. Sample 180-1110A-2H-CC was size sorted toward the large-size foraminifers and contained abundant phylite grains. It contains *Globorotalia truncatulinoides* and may belong to either Zone N22 or N23. Samples 180-1110B-1H-CC and 2X-CC contained abundant, well-preserved planktonic foraminifers. These samples were assigned to Zone N23, given the presence of *Bolliella adamsi* and *B. calida*, which marks the base of the zone.

Planktonic foraminifers were abundant and had moderate to good preservation in the core catchers of Samples 180-1111A-2R, 3R, 7R, 11R to 15R, and the bottom of Core 16R, as well as in Samples 180-1111A-13R-1, 91–93 cm, and 15R-1, 51–53 cm. Specimens were common and had moderate preservation in Sample 180-1111A-8R-CC. Specimens were few to rare and poorly preserved in Samples 180-1111A-4R-CC, 6R-CC, and 10R-CC. There was no recovery of sediments in Cores 1R, 5R, 9R, 17R, and 18R.

Samples 180-1111A-2R-CC and 3R-CC are assigned Zone N23, based on the presence of *Bolliella adamsi* and *B. calida*. Sample 180-1111A-6R-CC contained only a few planktonic foraminifers, among them *Globorotalia truncatulinoides* and pink *G. ruber* (which was present from Samples 180-1111A-6R-CC through 14R-CC). This sample might fall in either Zone N23 or N22. Samples 180-1111A-7R-CC and 10R-CC through 16R-

CC contained *Globorotalia truncatulinoides* without *G. tosaensis*, and *Pulleniatina* was dextrally coiled, indicating the upper part of Zone N22 (<0.65 Ma). A single occurrence of *Globorotalia tosaensis* in Sample 180-1111A-8R-CC was considered to be reworked.

Planktonic foraminifers were abundant and well preserved in Samples 180-1112A-1R-CC and 2R-CC. Core-catcher samples in Hole 1112B were barren of foraminifers. Samples 180-1112A-1R-CC and 2R-CC are assigned to Zone N23. Both samples contained *Bolliella calida*, marker for the zone. In addition, Sample 180-1112A-2R-CC contained pink specimens of *Globigerinoides ruber*, indicating an age no younger than 120 ka.

Benthic Foraminifers

A lower bathyal (2000–4000 m) assemblage of benthic foraminifers is present in Samples 180-1110A-2H-CC, 180-1110B-1H-CC, and 2X-CC, consistent with the present water depth of the site of ~3200 m. The diverse assemblage consists of such species as *Bolivinellina seminuda*, *Chilostomella oolina*, *Fontbotia wuellerstorfi*, *Gavelinopsis praegeri*, *Globocassidulina moluccensis*, *G. subglobosa*, *Melonis affinis*, *Oridorsalis umbonatus*, *Parrelloides bradyi*, *Pseudoparrella exigua*, *Quinqueloculina venusta*, and *Triloculina tricarinata* auct.

The benthic foraminiferal assemblages of Hole 1111A were consistent with the lower bathyal depth of the site (~3200 m) and contained such species as *Favocassidulina favus*, *Fontbotia wuellerstorfi*, *Hoeglundina elegans*, *Oridorsalis umbonatus*, *Parrelloides bradyi*, *Pullenia bulloides*, and *Uvigerina bradyana*. Only occasional specimens of shallow-water origin were incorporated into these assemblages. However, in Sample 180-1111A-13R-1, 0–1 cm (a winnowed, coarse sand that was sampled in a temperature probe), specimens of large shallow-water benthic species outnumbered the in situ assemblage of large benthic specimens. These reefal inhabitants included *Amphistegina bicirculata*, *A. lessonii*, *A. radiata*, *Calcarina spengleri*, *Gypsina vesicularis*, *Heterostegina depressa*, *Marginopora vertebralis*, *Planorbulinella larvata*, and *Schlumbergerella floresiana*, along with various alcyonarian spicules, bryozoans, calcareous algae, echinoid plates and spines, mollusks, and otoliths.

A surface sample (Sample 180-1112A-1R-1, 0–1 cm) at Site 1112, which is located at a water depth of 3047 m, contained an assemblage of small benthic specimens, including the species *Fijinionion schwageri*, *Melonis affinis*, *M. pompilioides*, *Pullenia bulloides*, *P. quinqueloba*, *Quinqueloculina venusta*, and *Saccamina* sp. In Samples 180-1112A-1R-CC and 2R-CC, the lower bathyal (>2000 m) assemblage of benthic foraminifers included the species *Favocassidulina favus*, *Fijinionion schwageri*, and *Fontbotia wuellerstorfi*.

PALEOMAGNETISM

The investigation of magnetic properties at Sites 1110, 1111, and 1112 included the measurement of (1) bulk susceptibility of whole core sections, (2) point susceptibility and remanent magnetization of archive half core sections, and (3) anisotropy of magnetic susceptibility and remanent magnetization of discrete samples. No magnetic properties were measured at Site 1113 because of poor recovery.

Magnetic Susceptibility

Magnetic susceptibility measurements were made on whole core sections as part of the multisensor track (MST) analysis (see “Physical Properties,” p. 22), and on half core sections as part of the archive multisensor track (AMST) analysis. The MST and AMST susceptibilities values (uncorrected for volume) at Sites 1110, 1111, and 1112 ranged between on the order of 10^{-4} and 10^{-3} SI (Figs. F21A, F21B).

Results of the measurements of magnetic susceptibility and its anisotropy (AMS) on discrete samples are listed in Table T9. Samples above ~8 mbsf at Holes 1110A, 1110B, and 1112A showed a relatively constant mean susceptibility of $\sim 4\text{--}5 \times 10^{-4}$ SI. At Hole 1111A, two samples at ~68–71 mbsf showed relatively higher susceptibilities ($\sim 4 \times 10^{-3}$ SI), whereas two at ~126–129 mbsf showed relatively lower susceptibilities ($\sim 1 \times 10^{-4}$ SI). The degree of anisotropy (P_j) values ranged between ~1.02 to 1.08, reflecting a low degree of anisotropy. The shape parameter (T) values of all samples except one were positive, which indicated predominantly oblate susceptibility ellipsoids. Limited data precluded defining a trend in the orientation of susceptibility axes from all samples. Two samples at ~68 and 71 mbsf from Hole 1111A showed a higher susceptibility and a greater degree of P_j than the other samples. These same two samples from Hole 1111A showed steep K_{\min} axes with subhorizontal K_{\max} axes.

Remanent Magnetization

Measurements of remanent magnetization were made on relatively undisturbed sections from archive-half cores and on discrete samples taken from working half core sections. Results are shown in Figure F22A, F22B, F22C, and F22D.

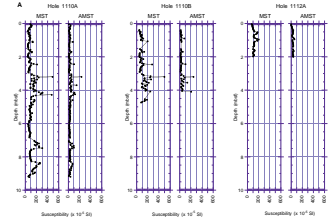
In Hole 1110A, intensity of remanent magnetization after AF demagnetization at 25 mT ranged from values on the order of 10^{-3} A·m⁻¹ to values on the order of 10^{-2} A·m⁻¹. In Hole 1110B, very low intensities on the order of 10^{-5} A·m⁻¹ occurred near the top of the recovered section, but values increased rapidly so that by 0.5 mbsf intensities were similar to those observed in Hole 1110A. Holes 1111A and 1112A showed intensity values similar to those observed at Site 1110.

The trends of intensity data (Fig. F22) compared with susceptibility data (Fig. F21) were not similar at any of the sites. The disagreement between the trends of remanent intensity and magnetic susceptibility suggests that the magnetic minerals that carry the remanent magnetization differ from those that dominate the magnetic susceptibility, at least for the intervals measured.

Demagnetization behavior of discrete samples from all sites generally showed two components of magnetization (Fig. F23). The soft component, which was removed by 5 or 10 mT alternating-field (AF) demagnetization, showed inclinations that were steep downward and probably represented an overprint acquired from the drill string.

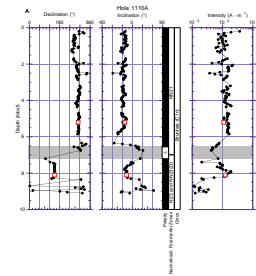
Seven out of 10 measured discrete samples yielded a characteristic remanent magnetization (ChRM) at demagnetization levels between ~15 and 25 mT. Three samples either showed a curved demagnetization trajectory, indicating a considerable overlap in the coercivity spectra of the soft and ChRM components, or a trajectory that did not decay toward the origin on vector demagnetization plots. The ChRM of the

F21. Susceptibility data from MST and AMST measurements, p. 50.

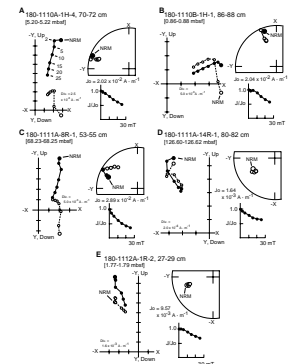


T9. Measurements of susceptibility and anisotropy, p. 79.

F22. Downhole plots of declination, inclination, and intensity, p. 52.



F23. Demagnetization behavior of samples from core sections, p. 56.



seven samples with stable demagnetization behavior showed inclinations between $\sim -20^\circ$ and -50° (Table T10).

Magnetostratigraphy

The polarity of the remanent magnetization after AF demagnetization at 25 mT for Site 1110 was determined primarily from the inclinations. Scatter within and between sections was relatively low except near the bottom of the hole where greater scatter was associated with coarse sands and pebbles. Directions were corroborated by discrete sample analysis (Fig. F22A, F22B). Only the Brunhes normal polarity chron (C1n) was recorded at this site, consistent with the paleontologic data.

Evidence for an excursion of the magnetic field during the Brunhes was indicated between ~ 6.5 and 7.2 mbsf in Hole 1110A (Fig. F22A), which may represent the Blake event (~ 0.128 Ma; Harland et al., 1990). Evidence of this event was not observed in Hole 1110B because recovery was limited to ~ 5 mbsf (Fig. F22B).

Data are shown for Holes 1111A and 1112A in Figure F22C and F22D.

INORGANIC GEOCHEMISTRY

The interstitial water (IW) sampling program at Sites 1110, 1111, 1112, and 1113 was limited because of extremely difficult coring conditions and concomitant poor core recovery. A total of eight IW samples was obtained from these sites. We collected four samples at Site 1110 from the first two sections of Core 180-1110B-1H, three from Site 1111, a single sample from the mudline core at Site 1112, and none from Site 1113.

Results and Discussion

The IW was analyzed for salinity, pH, alkalinity, major cations (Na^+ , K^+ , Ca^{2+} , Mg^{2+}) and anions (Cl^- , SO_4^{2-}), SiO_2 , NH_4^+ , Sr^{2+} , and Li^+ . Results of shipboard inorganic chemical analyses are presented in Table T11. No trend is evident in the IW constituents from Hole 1110B, except possibly for a depletion in Li^+ from seawater concentrations ($27 \mu\text{M}$) to a range of ~ 14.7 – $20.1 \mu\text{M}$, with the lowest value observed at 2.95 mbsf. Variations of other parameters are within analytical error.

The IW samples were recovered from deeper sediments (69–127 mbsf) at Site 1111, and significant deviations from seawater concentrations are observed. These include elevated alkalinities, slightly elevated Na^+ and Cl^- concentrations, an increasingly substantial SO_4^{2-} and Ca^{2+} depletion with depth, and variable but depleted Li^+ concentrations.

Insufficient data are available to permit a reliable interpretation of the results at Sites 1110 and 1112. Although only very limited data exist for IW from sediments at Site 1111, the increase in alkalinity and decrease in dissolved SO_4^{2-} with depth are consistent with bacterial decomposition of organic matter. The depleted Li^+ , Ca^{2+} , and Mg^{2+} concentrations also suggest diagenetic reactions, possibly involving biogenic silica and carbonates and alteration of volcanic minerals.

T10. Measurements of remanent magnetization, p. 80.

T11. Interstitial water geochemistry, p. 81.

ORGANIC GEOCHEMISTRY

At Sites 1110, 1111, and 1112, the shipboard organic geochemistry consisted of determinations of total organic carbon (TOC), inorganic carbon, total carbon, total nitrogen, and total sulfur in sediments, in addition to the routine hydrocarbon gas safety monitoring procedure. No samples were collected at Site 1113. The analytical techniques used are outlined in “Organic Geochemistry,” p. 25, in the “Explanatory Notes” chapter.

Volatile Hydrocarbons

Because of poor core recovery, very little data was collected at all of the sites. At Sites 1110 and 1112, methane concentrations were found to be low (<6 ppmv) at the surface, increasing to 35 ppmv by 69 mbsf at Site 1112 (Table T12; Fig. F24). Low methane concentrations (~3–32 ppmv) were generally found between 0 and 117 mbsf at Site 1111 (Table T12; Fig. F24) but showed a thousandfold increase between 117 and 127 mbsf. This correlates with the disappearance of sulfate in the pore waters at this depth (see Table T11 and “Inorganic Geochemistry,” p. 21) and is indicative of the start of bacterial methane production. No other hydrocarbon gases were detected at any of the sites.

CaCO₃, Sulfur, Organic Carbon, and Nitrogen

The CaCO₃ concentrations are given in Table T13. Organic carbon was found to be low at all the sites, and no nitrogen or sulfur was detected in any of the sediment samples (Table T13).

MICROBIOLOGY

Poor sample recovery severely limited the number of samples obtained at Sites 1110, 1111, 1112, and 1113 for microbiological analysis. Eight samples were obtained from these sites for shipboard microscopic determination of total bacterial populations: four from the surface core in Hole 1110B (0–4.5 mbsf), three from Hole 1111A (69.2, 117.2, and 127.3 mbsf) and one from Hole 1112A (1.5 mbsf). In addition, three whole-round samples were taken from the mudline core at Hole 1110B for shore-based experimentation. No samples were recovered for microbiological analysis from Site 1113.

Bacteria were present in all samples examined (Table T14; Fig. F25); their numbers decreased rapidly with increasing depth. Near-surface bacterial populations at Sites 1110 and 1112 are again similar to those at other sites with similar overlying water depths and near-surface organic carbon concentrations (see Table T11, p. 126, in the “Site 1108” chapter), and their distribution lies within the 95% prediction limits described by the model of Parkes et al. (1994) (Fig. F25).

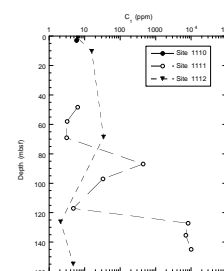
PHYSICAL PROPERTIES

Introduction

Four holes (Holes 1110A through 1110D) were drilled at Site 1110. Physical properties measurements were only conducted on APC cores

T12. Headspace gas in sediments, p. 82.

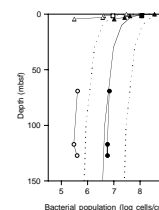
F24. C₁ profiles for Sites 1110, 1111, and 1112, p. 57.



T13. Calcium carbonate, carbon, nitrogen, and sulfur contents, p. 83.

T14. Bacterial populations and dividing and divided cells, p. 84.

F25. Bacterial populations and dividing and divided cells, p. 58.



from this site (Cores 180-1110A-1H and 2H and 180-1110B-1H) because of the very low recovery of hard rock in the XCB-cored interval and the fact that the recovered material consisted of clasts devoid of their matrix. At Site 1111, one hole (Hole 1111A) was drilled by RCB technique to a total depth of 173.7 mbsf. Again, physical properties measurements were limited by low core recovery. At Site 1112, total recovery was less than 1 m. Sparse physical properties data were collected, which are included in the data tables of this combined site summary. However, because there are so few data, Site 1112 is neither included in the figures nor discussed in the text. No physical properties measurements were made at Site 1113, again because of the low recovery.

Where applicable, measurements included MST readings (i.e., magnetic susceptibility, gamma-ray attenuation porosity evaluator [GRAPE] density, and natural gamma-ray count) and thermal conductivity measurements on unsplit cores, as well as index properties, PWS velocities, and sediment strength on split cores. Compilations of index property, velocity, thermal conductivity, and strength data are located in Tables T15, T16, and T17 (also in ASCII format in the TABLES directory).

Density and Porosity

All index properties data are summarized in Table T15. A full compilation of GRAPE data is presented with the MST measurement data set on the accompanying Lamont-Doherty Earth Observatory (LDEO) CD-ROM. Data from Site 1110 are limited, covering the interval from 0 to 9.5 mbsf. GRAPE bulk density increases from about 1.40 to 1.50 g·cm⁻³ at the seafloor to ~2.10 g·cm⁻³ at a depth of ~9 mbsf (Fig. F26). Measurements on discrete samples are generally consistent with the GRAPE data (Fig. F26). Grain density averages 2.70 g·cm⁻³ at Site 1110, which reflects the mineralogical composition of the predominantly calcareous clays, silty clays, and silts of lithostratigraphic Unit I (see “Lithostratigraphy,” p. 6). Grain density shows a maximum value of 2.85 g·cm⁻³ at ~9 m, where bulk density is also elevated. Porosity reflects bulk and grain density variations and decreases within the upper 10 mbsf from an initial value of 80% at the seafloor. A minimum value of 44% occurs at the depth of the highest bulk and grain densities (Fig. F26).

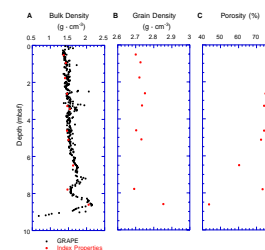
In Hole 1111A, GRAPE density decreases from values around 1.80 g·cm⁻³ at a depth of ~70 mbsf to 1.40 g·cm⁻³ on average at ~140 mbsf (Fig. F27). Unlike the GRAPE densities that show considerable scatter, bulk densities from the index properties range only from 1.55 to 1.70 g·cm⁻³ between 70 and 140 mbsf. The index property data should be less affected by core disturbance than the GRAPE densities and, as a result, should be considered more reliable. Grain densities from Site 1111 average 2.70 g·cm⁻³. Porosity ranges from 59% to 62% at 60 mbsf to between 65% and 68% at depths greater than 120 mbsf (Fig. F28). Interpretation of this porosity increase with depth should be conducted with caution because recovery was very limited.

Compressional Wave Velocity

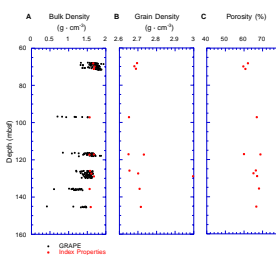
The *P*-wave velocity was measured using the *P*-wave logger (PWL) on the MST, the PWS1 and PWS2 insertion probe system, and the PWS3 contact probe system. Because of the poor quality of the PWL data, only

T15. Index properties measurements, p. 85.

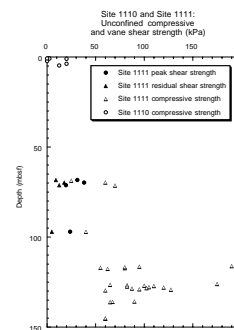
F26. Site 1110 bulk density, grain density, and porosity, p. 59.



F27. Site 1111 bulk density, grain density, and porosity, p. 60.



F28. Sites 1110, 1111 undrained shear and unconfined compressive strength, p. 61.



PWS1, PWS2, and PWS3 results will be discussed. All pertinent velocity data are listed in Table T16.

The PWS1 and PWS2 insertion probe system was used to measure the transverse and longitudinal (i.e., along the core axis) *P*-wave velocity in unconsolidated oozes and clays from Holes 1110A and 1110B. The velocities were consistent within these 10-m intervals, ranging between 1500 m·s⁻¹ and 1594 m·s⁻¹ (Table T16). In Hole 1111A, data collected from Cores 180-1111A-8R, 11R, and 13R through 16R show relatively constant velocities of 1450 m·s⁻¹ to 1605 m·s⁻¹ (at depths of 65–145 mbsf).

Thermal Conductivity

Thermal conductivity data presented in Table T17 were all obtained from unsplit cores recovered from Holes 1110A, 1110B, and 1111A. Three repeat measurements per interval were conducted (Table T17). Thermal conductivities of the uppermost sediments range between 0.8 and 1.0 W·m⁻¹·°C⁻¹, which is in agreement with results from similar sediments at previous locations (e.g., “Physical Properties,” p. 61, in the “Site 1109” chapter). Thermal conductivity values of 0.45 to 0.85 W·m⁻¹·°C⁻¹ were measured at depths between 70 and 150 mbsf of Hole 1111A. The lower end of this range is probably invalid data, reflecting void space and disaggregation of the core within the liner.

Shear Strength and Compressibility Measurements

Undrained shear strength and compressibility measurements were conducted on split cores from Sites 1110 and 1111 using the motorized miniature vane-shear device and the pocket penetrometer, respectively. The data from both sites are presented in Figure F28 and are listed in Table T18.

Both peak and residual undrained shear strength were measured in RCB cores from Site 1111. Failure of the semi-indurated clays and silts from 70 to 100 mbsf occurred at 20–40 kPa (Fig. F28). Residual strength values ranged from 5 to 20 kPa for the same depth interval. Below 100 mbsf, the sediment was too firm to insert the vane shear device into the split core.

Unconfined compressive strength ($2 S_u$) was measured at the very top of Site 1110 with results varying between almost zero kPa (in soupy intervals) and ~20 kPa. Below 70 mbsf in Hole 1111A, strength increases from 22 to 100 kPa at ~135 mbsf, but occasionally peaks to 180 kPa within the well-lithified silt layers. A gradual increase in strength with depth can be seen, although outliers exist and the data are limited (Fig. F28).

Magnetic Susceptibility

Magnetic susceptibility measurements (MSM) were routinely conducted as part of the MST measurement of sediment cores from Sites 1110 and 1111. The entire MSM data set is presented as part of the MST compilation in ASCII format on the accompanying LDEO CD-ROM.

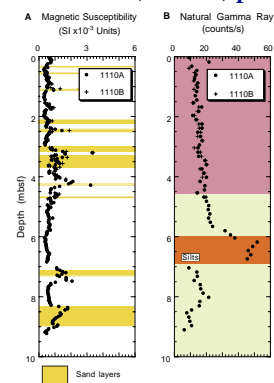
Similar to results from previous sites on Leg 180, (e.g., “Physical Properties,” p. 61, in the “Site 1109” chapter), some of the spikes in the susceptibility curve relate to the occurrence of relatively coarse grained sediment (Fig. F29). Within the nannofossil ooze (0–4.6 mbsf), thin

T16. Longitudinal and transverse velocities for cores, p. 86.

T17. Thermal conductivity in cores, p. 87.

T18. Shear and compressive strength data, p. 88.

F29. Bulk magnetic susceptibility for Holes 1110A, 1110B, p. 62.



(<2.5-cm-thick) sand layers exist as part of a series of fining-upward sequences (see “**Lithostratigraphy**,” p. 6). Many of these sand layers correspond to susceptibility spikes, highlighted in Figure F29A (Holes 1110A and 1110B).

Natural Gamma Ray

Natural gamma-ray (NGR) count was recorded from a small number of core sections at Sites 1110 and 1111. Insufficient information from Site 1111 precluded the recognition of any trends or relationships. The data from Holes 1110A and 1110B show minor scatter and range between 10 and 20 c/s (Fig. F29B). However, a broad NGR peak occurs at 5.7–6.9 mbsf and corresponds with a silt layer (see Fig. F29, orange/dark gray stipple, and “**Lithostratigraphy**,” p. 6; see also “**Core Descriptions**” content list for core photos). Further, the nannofossil ooze shows little NGR response (Fig. F29, pink/intermediate gray stipple), which is in contrast to the volcanoclastic sediments that appear below 4.5 mbsf (Fig. F29, yellow/light gray stipple). The full NGR data set can be found as part of the MST compilation in ASCII format on the accompanying LDEO CD-ROM.

IN SITU TEMPERATURE MEASUREMENTS

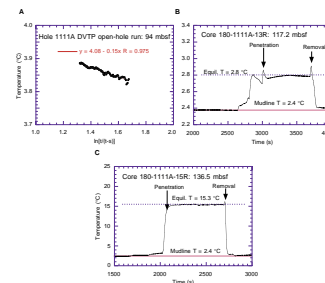
Of Sites 1110 through 1113, temperature measurements were made only at Site 1111. An open-hole temperature measurement was made within Hole 1111A using the Davis-Villinger Temperature Probe (DVTP) lowered on the wireline. The probe was held within the open hole at 91 mbsf for 20 min. In situ formation temperature measurements were obtained before taking Cores 180-1111A-13X and 15X using the DVTP at probe-tip depths of 117.2 and 136.5 mbsf, respectively. The measured mudline temperature was 2.4°C.

For the open-hole measurement at 91 mbsf, downhole equilibrium temperature was approximated by plotting temperature as a function of $\ln[t/(t-s)]$, where t is the total time elapsed since the drill bit penetrated that depth, and s is the total time elapsed between the initial penetration and the cessation of circulation (Fig. F30). The line was then extrapolated to infinite time (where $\ln[t/(t-s)] = 0$). Equilibrium formation temperatures for the in situ measurements were estimated using the CONEFIT program (see “**Explanatory Notes**” chapter). These estimates of equilibrium temperature used thermal conductivity of $0.9 \text{ W}\cdot\text{m}^{-1}\cdot\text{°C}^{-1}$, based on the available core data (see “**Physical Properties**,” p. 22).

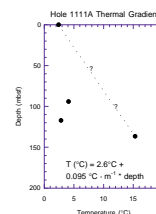
Resulting estimated temperatures are shown on Figure F31. Near-seafloor temperatures (4.0° and 2.8°C) were estimated at 94 and 117.2 mbsf, indicating movement of bottom water into the formation. It was not possible to verify whether bottom-water invasion was drilling induced or naturally occurring. Naturally occurring fluid flow requires a high permeability conduit to the seafloor, and it would need to be very recent for the high temperature difference (12.5°C) between 117.2 and 136.5 mbsf to be preserved. Calculations using one-dimensional thermal transport suggest that thermal conduction would significantly reduce this gradient in less than 100 yr.

With the assumption that the low temperatures at 94 and 117.2 mbsf are transient anomalies, we estimated the large-scale thermal gradient for Hole 1111A based on mudline temperature and the temperature at

F30. Temperature vs. $\ln[t/(t-s)]$ for DVTP measurements, Hole 1111A, p. 63.



F31. Temperatures as a function of depth and thermal gradient, Hole 1111A, p. 64.



136.5 mbsf (Fig. F31). The resulting thermal gradient is $0.095^{\circ}\text{C}\cdot\text{m}^{-1}$ ($95^{\circ}\text{C}\cdot\text{km}^{-1}$), similar to that at Site 1108. The computed heat flow is $86\text{ mW}\cdot\text{m}^{-2}$, using the measured thermal conductivity of $0.9\text{ W}\cdot\text{m}^{-1}\cdot^{\circ}\text{C}^{-1}$.

COMPOSITE DEPTHS

Introduction

We established composite depths based on the correlation between Cores 180-1110A-1H and 180-1110B-1H (Table T19). The correlation was made based on key beds and magnetic susceptibility curves (Fig. F32).

Correlation

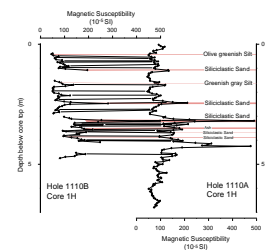
Sediments in Cores 180-1110A-1H and 180-1110B-1H have eight key sedimentary beds that enable visual correlation between the holes. The magnetic susceptibility curves are similar to each other, and 24 peaks (13 positive and 11 negative peaks) were used for correlation. Both sedimentary features and magnetic susceptibility allow a precise correlation (Fig. F32).

Composite Depths

Composite depth (Table T19) was established by the procedures described in “Composite Depths,” p. 79, of the “Site 1109” chapter. Based on our calculation, the top depth of Core 180-1110B-1H is 0.05 m deeper than the top of Core 180-1110A-1H.

T19. Correlative peaks of magnetic susceptibility, p. 89.

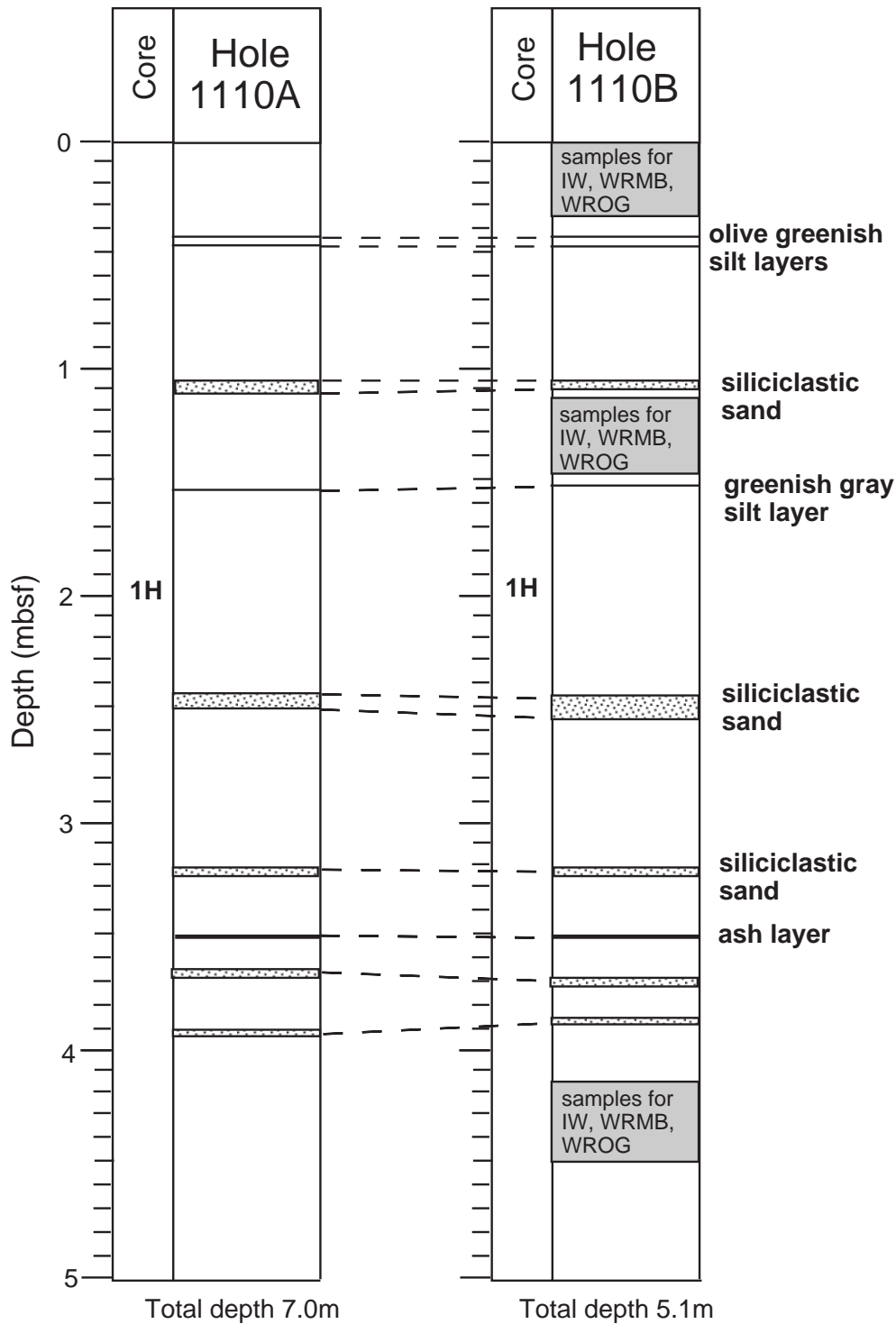
F32. Correlation of magnetic susceptibility, Cores 180-1110A-1H and 180-1110B-1H, p. 65.



REFERENCES

- Ashley, P.M., and Flood, R.H., 1981. Low-K tholeiites and high-K igneous rocks from Woodlark Island, Papua New Guinea. *J. Geol. Soc. Aust.*, 28:227–240.
- Berggren, W.A., Kent, D.V., Swisher, C.C., III, and Aubry, M.-P., 1995. A revised Cenozoic geochronology and chronostratigraphy. In Berggren, W.A., Kent, D.V., Aubry, M.-P., and Hardenbol, J. (Eds.), *Geochronology, Time Scales and Global Stratigraphic Correlation*. Spec. Publ.—Soc. Econ. Paleontol. Mineral. (Soc. Sediment. Geol.), 54:129–212.
- Blake, D.H., 1976. Madilogo, a late Quaternary volcano near Port Moresby, Papua New Guinea. In Johnson, R.W. (Ed.) *Volcanism in Australasia*: Amsterdam (Elsevier), 253–258.
- Fisher, R.F., and Schmincke, H.-U., 1984. *Pyroclastic Rocks*: New York (Springer Verlag), 400–407.
- Harland, W.B., Armstrong, R.L., Cox, A.V., Craig, L.E., Smith, A.G., and Smith, D.G., 1990. *A Geologic Time Scale 1989*: Cambridge (Cambridge Univ. Press).
- Jelinek, V., 1981. Characterization of the magnetic fabric of rocks. *Tectonophysics*, 79:63–67.
- Lackschewitz, K., Dehn, J., and Wallrabe-Adams, H.-J., 1994. Volcaniclastic sediments from mid-oceanic Kolbeinsey Ridge, north of Iceland: evidence for submarine volcanic fragmentation process. *Geology*, 22:975–978.
- MacKenzie, W.S., Donaldson, C.H., and Guilford, C., 1982. *Atlas of Igneous Rocks and their Textures*: Harlow, England (Longman).
- Parkes, R.J., Cragg, B.A., Bale, S.J., Getliff, J.M., Goodman, K., Rochelle, P.A., Fry, J.C., Weightman, A.J., and Harvey, S.M., 1994. A deep bacterial biosphere in Pacific Ocean sediments. *Nature*, 371:410–413.
- Rubie, D.C., 1983. Reaction-enhanced ductility: the role of solid-solid univariant reaction in deformation of the crust and mantle. *Tectonophysics*, 96:331–352.
- Taylor, B., Goodliffe, A., Martinez, F., and Hey, R., 1995. Continental rifting and initial sea-floor spreading in the Woodlark Basin. *Nature*, 374:534–537.

Figure F1. Correlation of the successions recovered in Core 180-1110A-1H with that in Core 180-1110B-1H. Note the excellent correlation. A correlation based on physical properties is included in "Composite Depths," p. 26.



IW=Interstitial Water, WRMB=Whole-round microbiology, WROG=Whole-round organic geochemistry

Figure F2. Nannofossil-rich clay representing the background sediment, with scattered nannofossils and volcanic glass. This is interbedded with very thin beds of nannofossil-rich silt and silty clay. The silt exhibits a sharp base and is normal graded with scattered foraminifers (interval 180-1110B-1H-3, 16-28 cm).

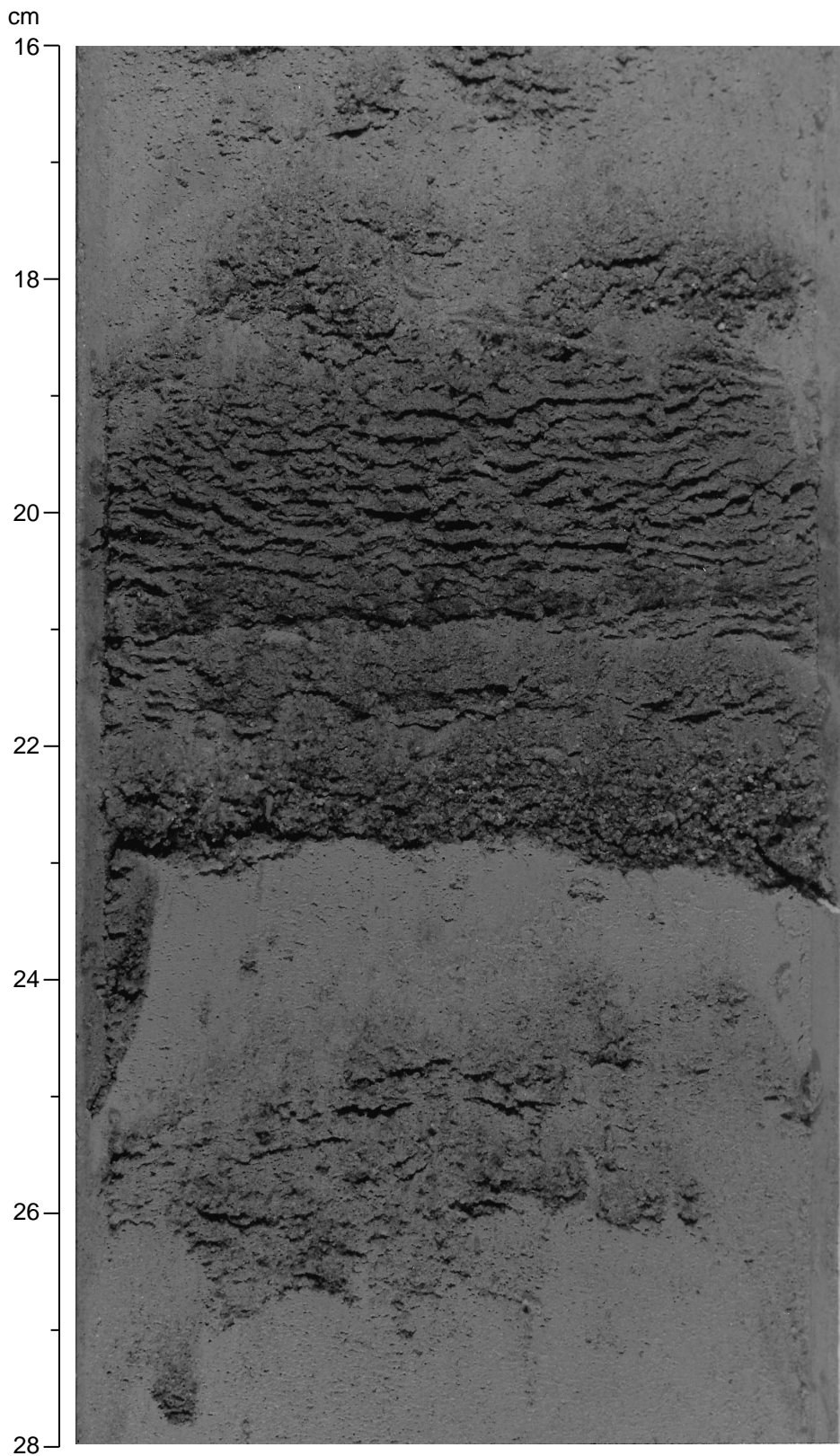


Figure F3. Graded conglomerate and sand. Granules grade upward into coarse-, medium-, then fine-grained sand. The composition is dominated by metamorphic rock fragments (interval 180-1110A-2H-2, 0-50 cm).

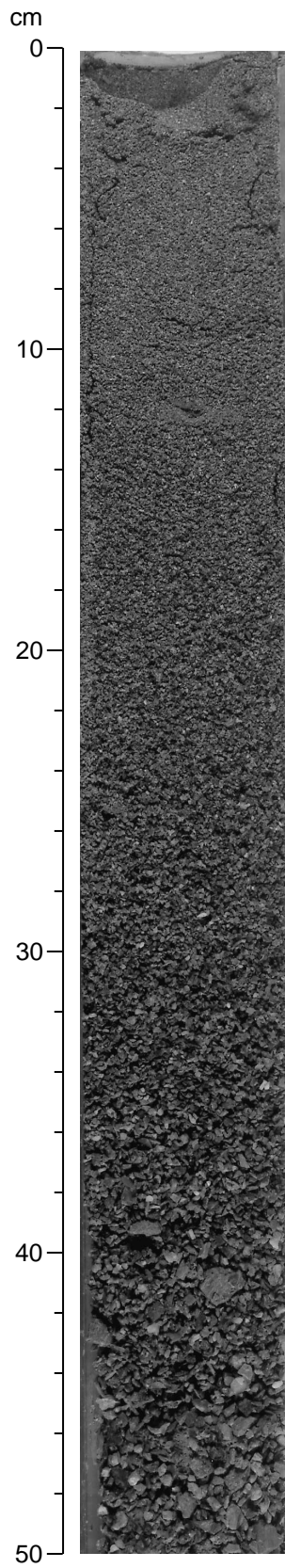
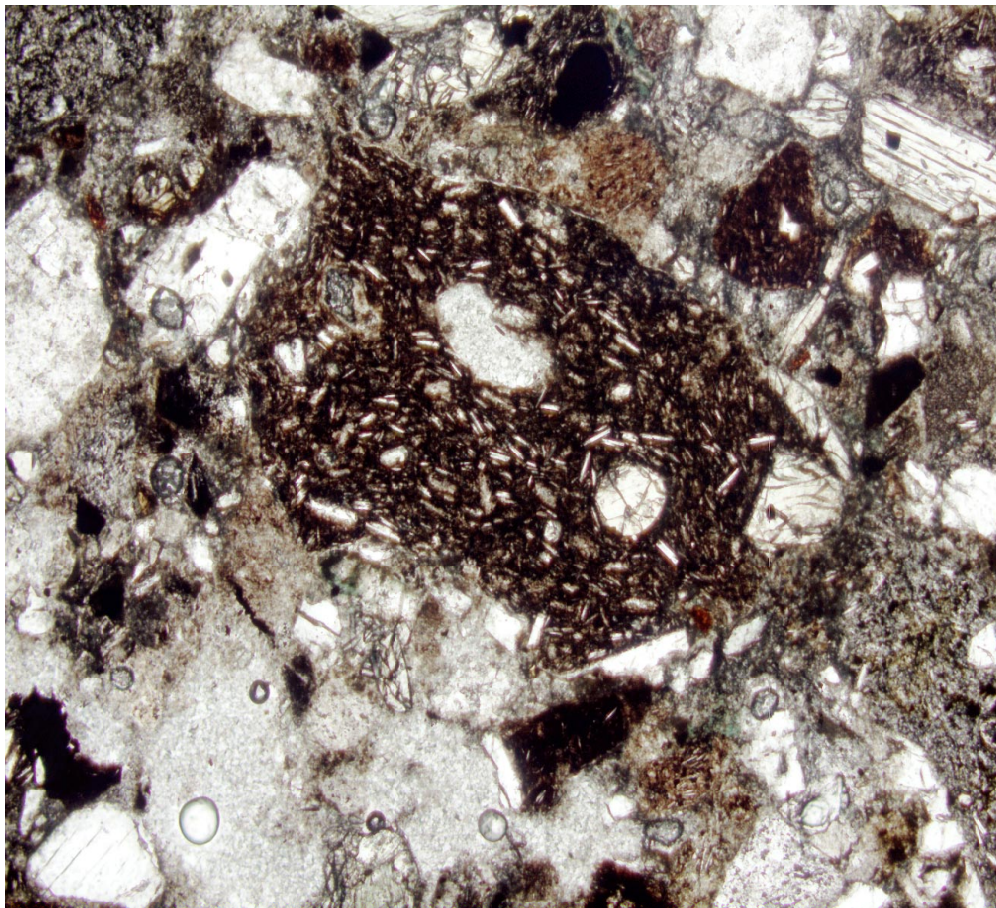
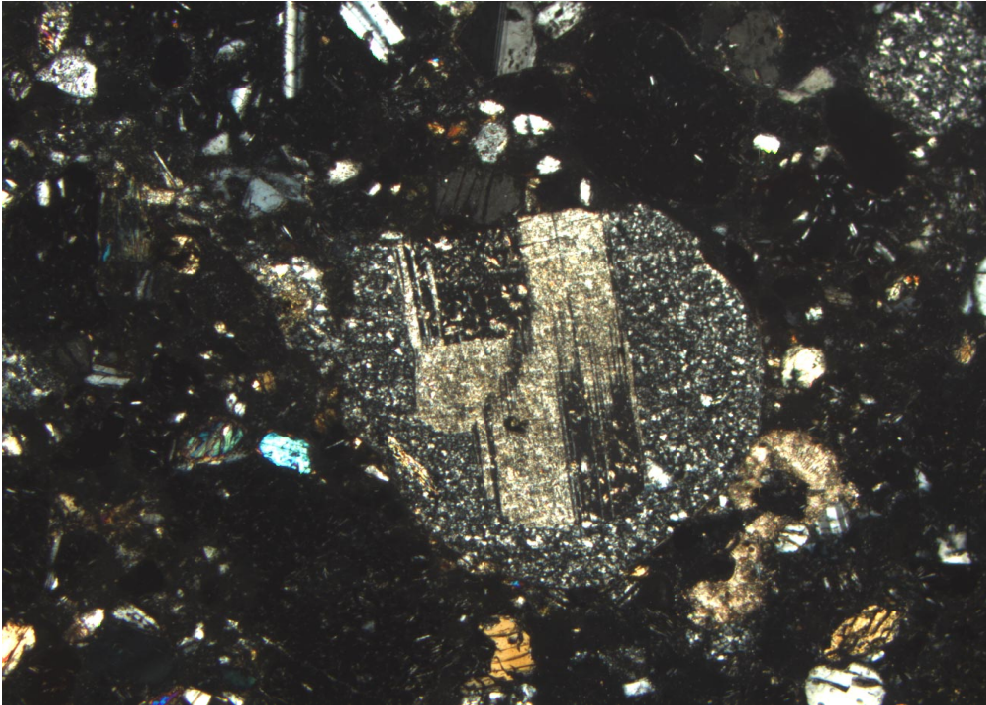


Figure F4. Digital photomicrograph (plane-polarized light) of a glassy basalt clast with plagioclase laths and clinopyroxene phenocrysts surrounded by angular detrital quartz and feldspar. Additional acidic grains are present near the margins of the field of view (interval 180-1112A-9R-CC, 25-27 cm).



2 mm

Figure F5. Digital photomicrograph (crossed nicols) of coarse-grained sandstone. Rounded lithoclast of feldspar-phyric acidic volcanic rock within small fragments of glassy basalt, detrital plagioclase, quartz, and pyroxene (interval 180-1112A-9R-CC, 25-27 cm).



2 mm

Figure F6. Digital photomicrograph (crossed nicols) of well-sorted medium-grained sandstone. Detrital grains of plagioclase, quartz, hornblende, clinopyroxene, and biotite; also basaltic and andesitic lithoclasts (interval 180-1112A-3R-1, 2-5 cm).



1 mm

Figure F7. Recovery log of Sites 1110-1113, showing the distribution of rock types, most of the recovered material falls loosely into the category of dolerite-metadolerite. T.D. = total depth.

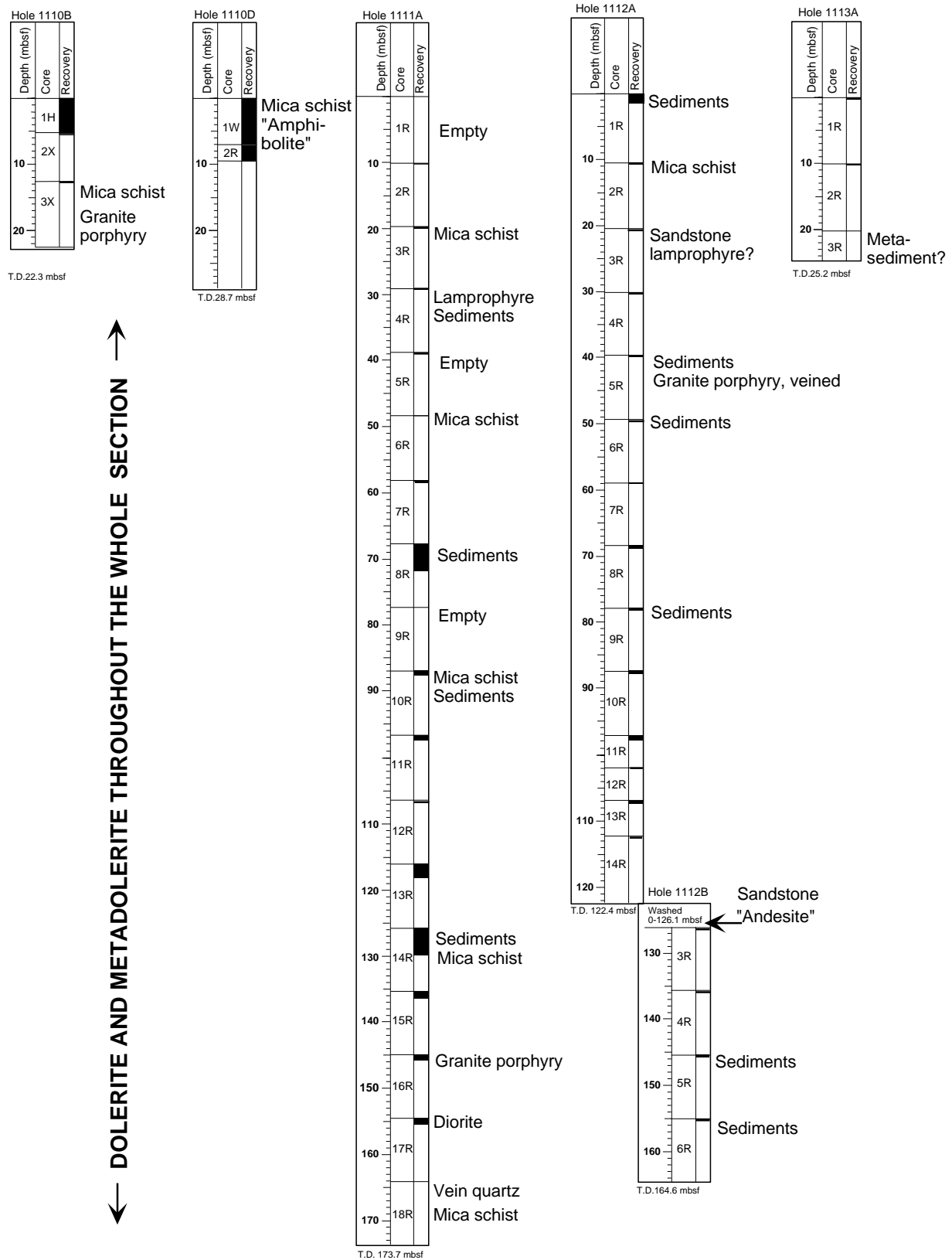


Figure F8. A. Thin-section view of an epidote-mica schist showing a thin quartz vein cutting the foliation at a steep angle, which has itself been folded (plane-polarized light; interval 180-1111A-18R-1, 76-78 cm). B. Hand specimen of a mica schist with folded foliation plane and cut by a thin, late-stage quartz vein that is folded (interval 180-1110B-3X-1, 3.5-8.5 cm).

A



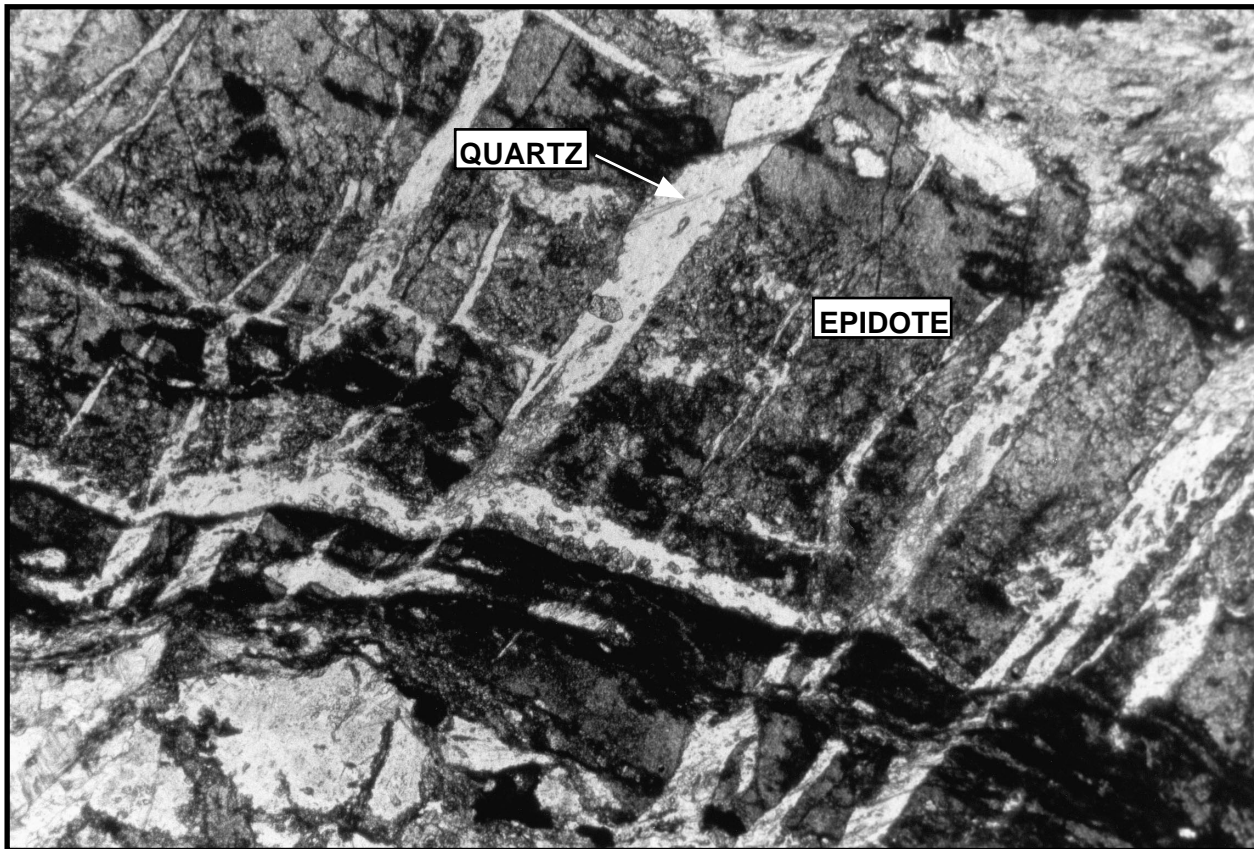
1 mm

B
cm



Figure F9. A. Boudinaged epidote layer in mica schist cut by veins filled with quartz oriented perpendicular to the foliation (plane-polarized light; interval 180-1110D-1W-1, 2-3 cm). (Continued on next page.)

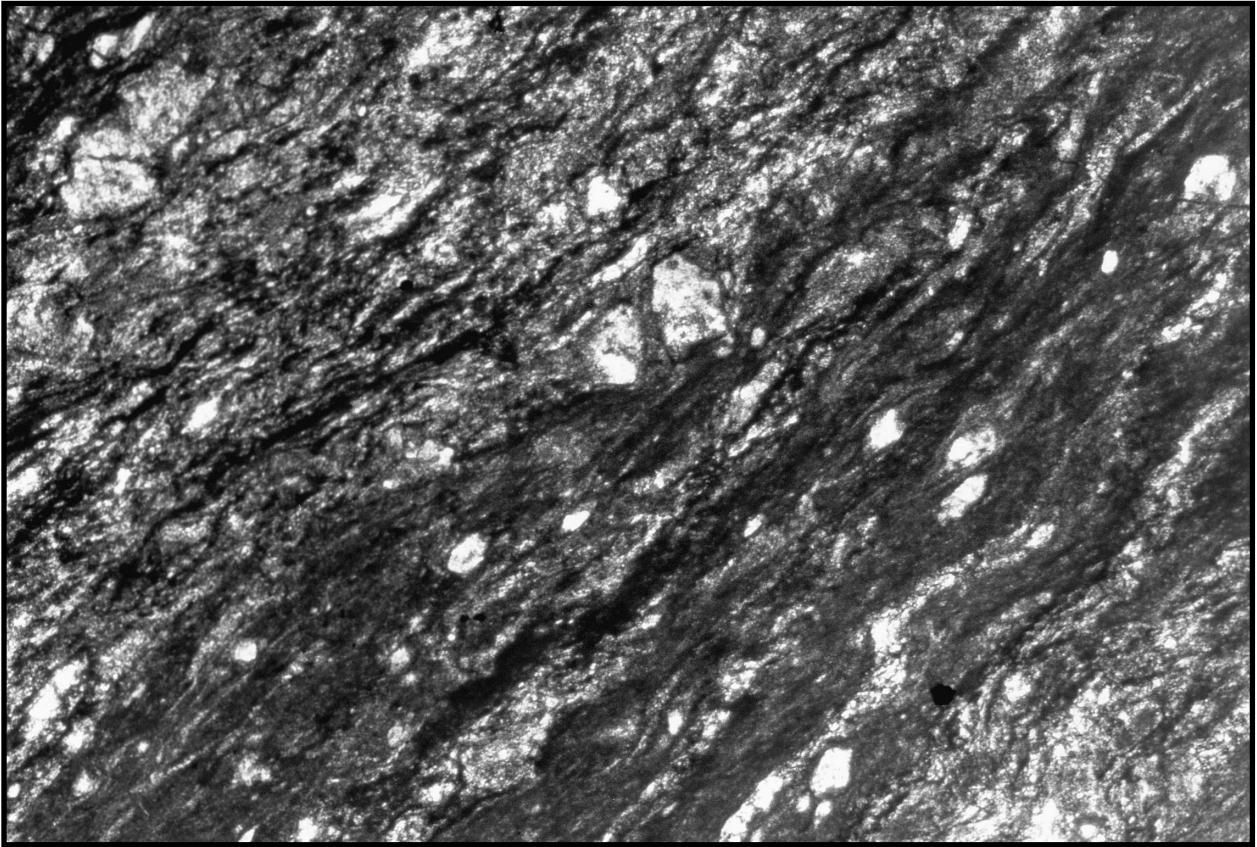
A



1 mm

Figure F9 (continued). B. Thin section of mylonitic metadolerite with porphyroclast relics of clinopyroxene (plane-polarized light; interval 180-1111A-16R-CC, 9-14 cm).

B



1 mm

Figure F10. Foliated epidote-quartz schist cut by late-stage fractures (interval 180-1111A-17R-1, 61-66 cm).

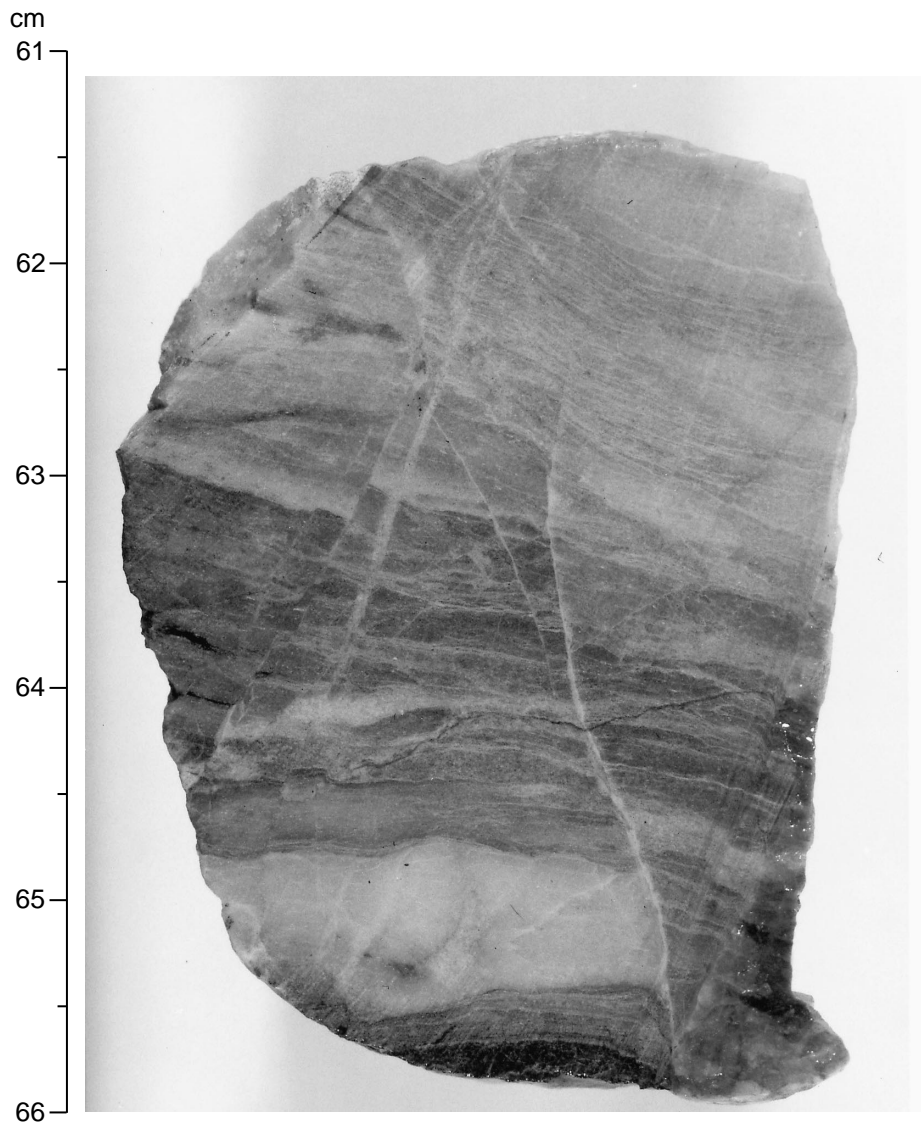


Figure F11. Euhedral pyrite grain with pressure shadow filled with fibrous calcite and quartz in calcareous mica schist (crossed polarizers; interval 180-1110B-3X-1, 5-10 cm).

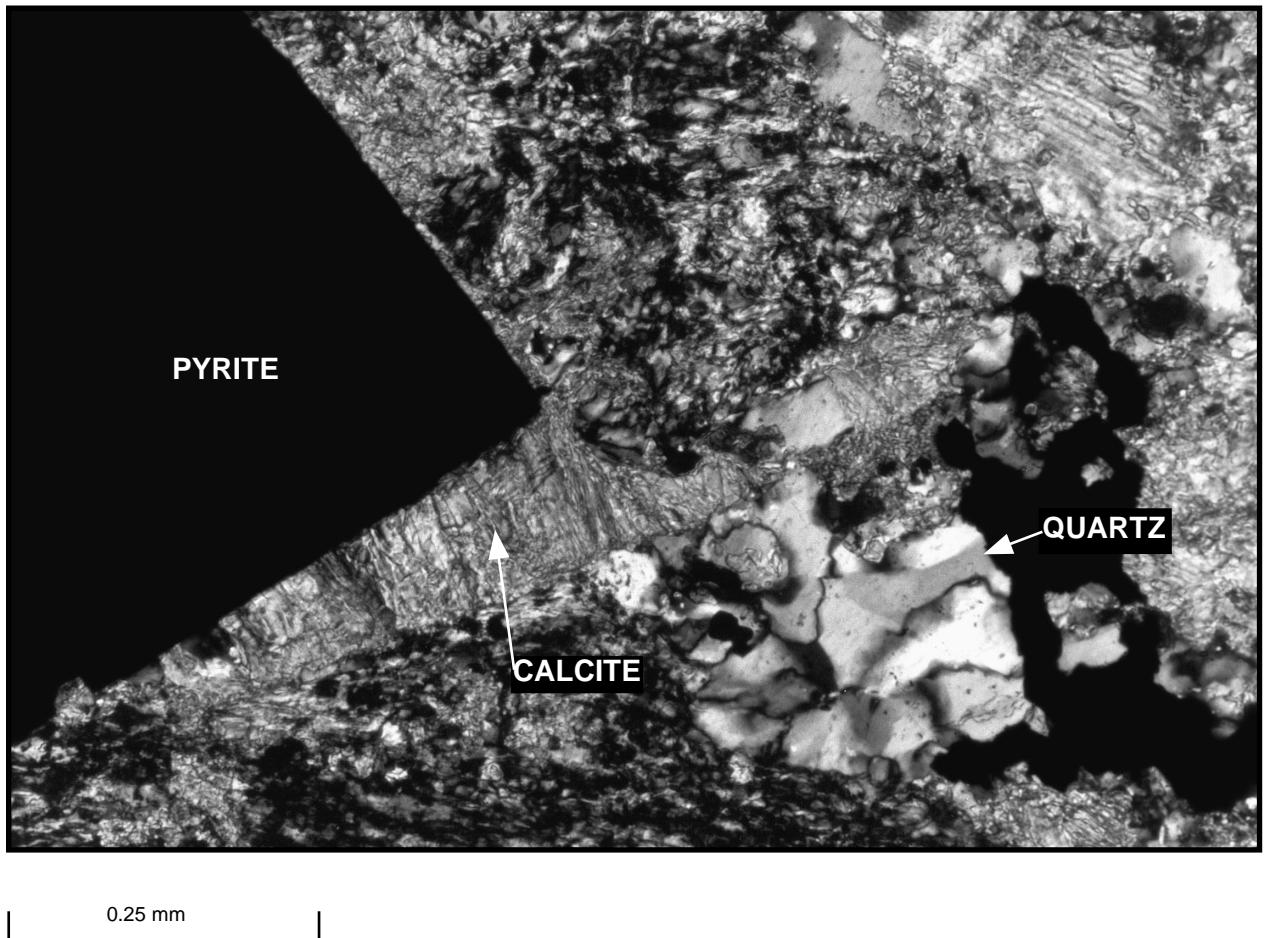


Figure F12. A. High-temperature foliation plane and shear band in mica schist (interval 180-1111A-18R-1, 86.5-95 cm). (Continued on next page.)

A cm

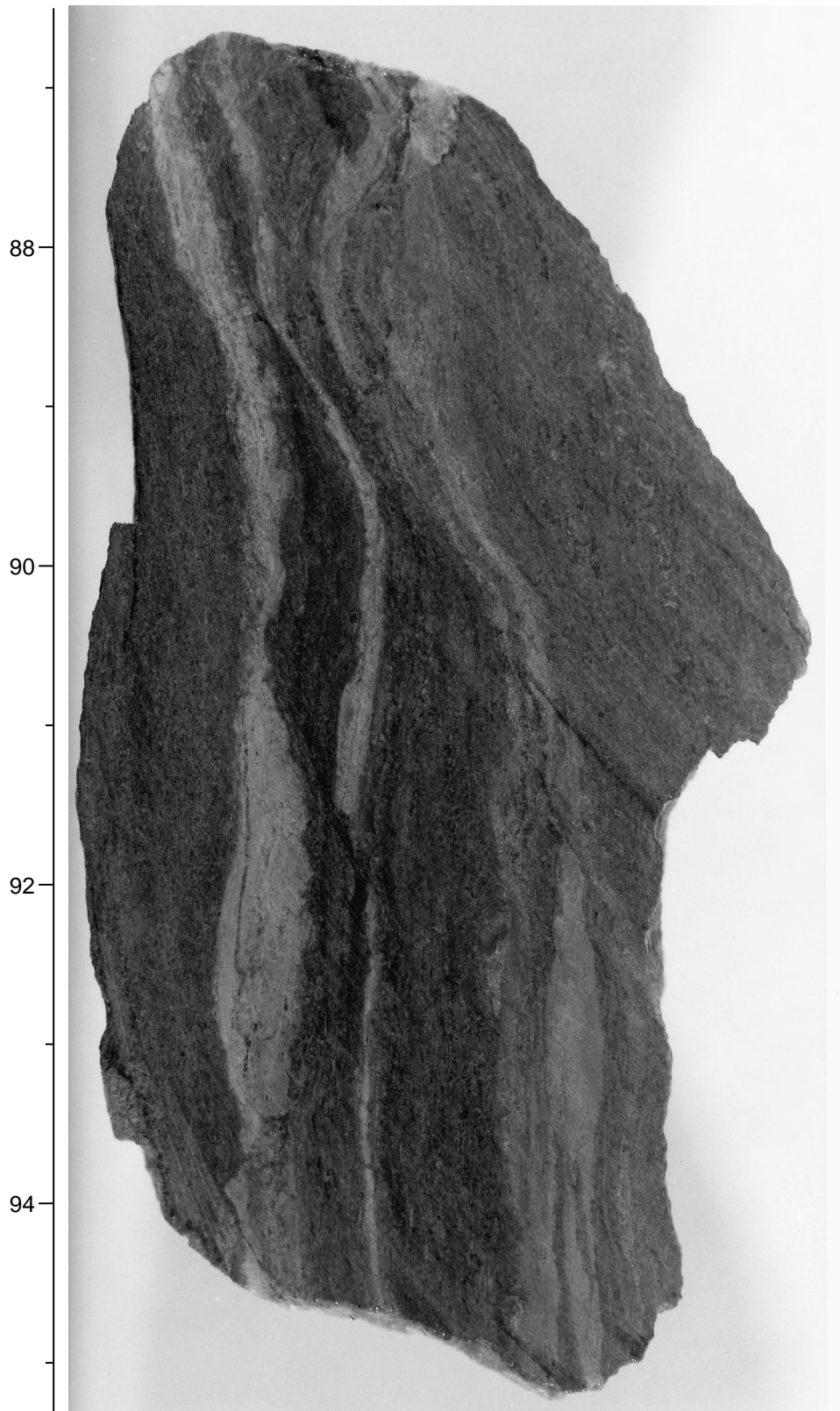
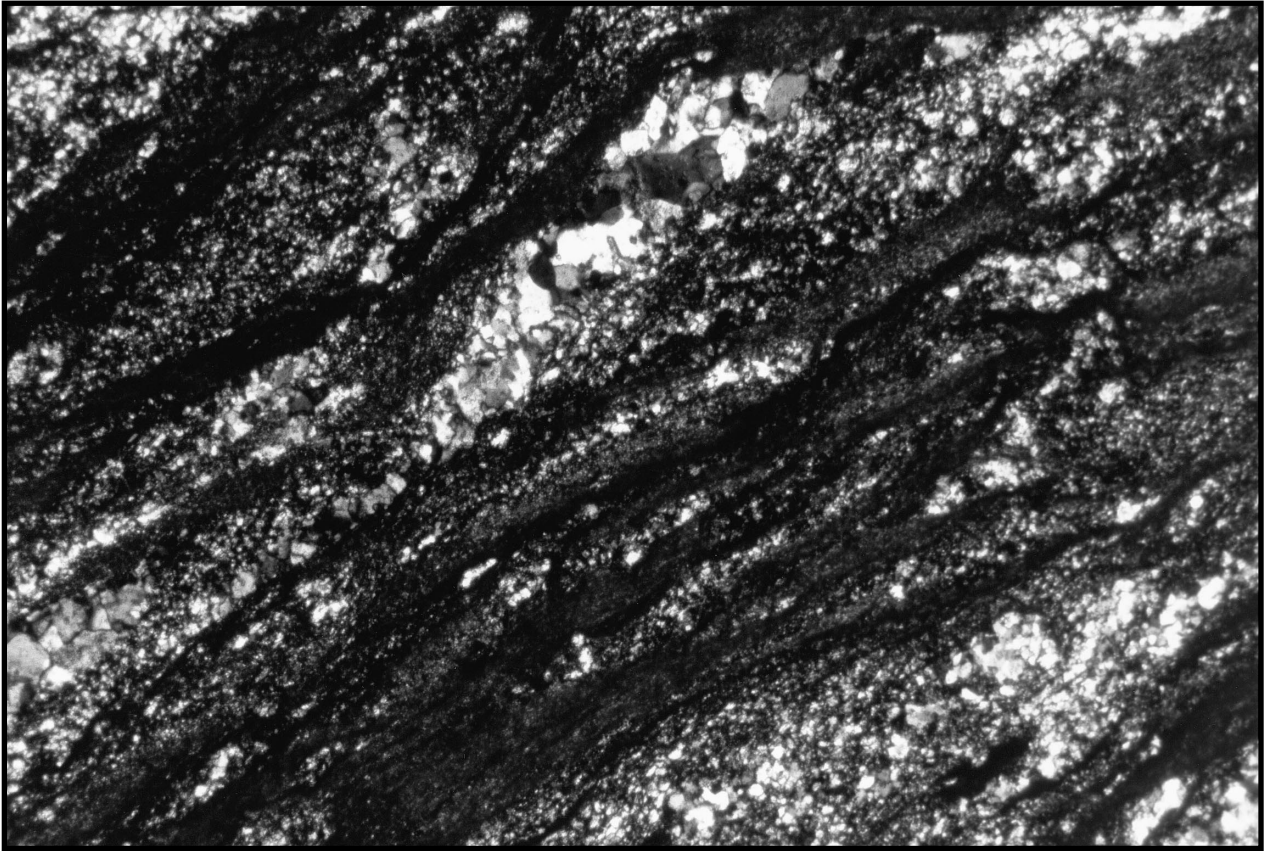


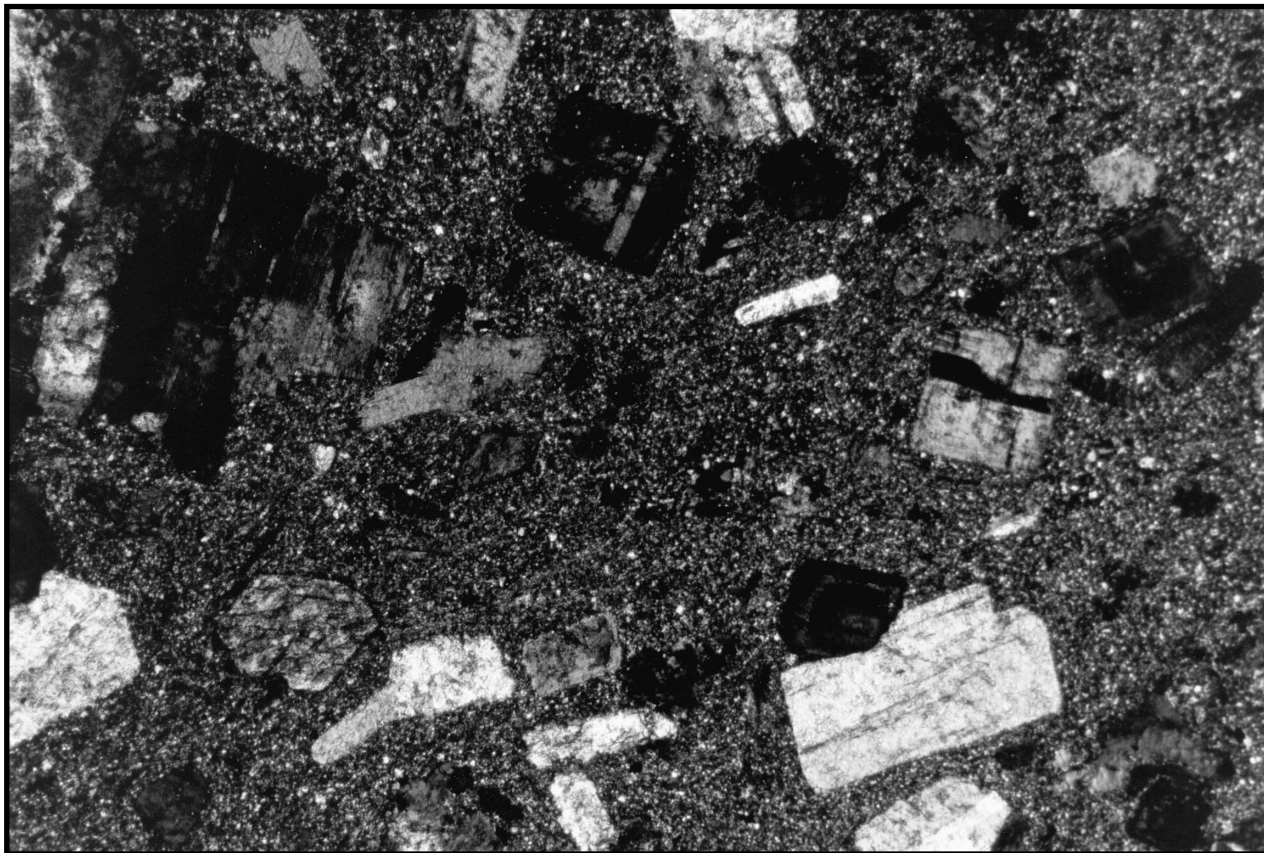
Figure F12 (continued). B. Thin section view of mylonitic quartzo-feldspathic rock, probably originally a granite (crossed polarizers; interval 180-1108B-3R-CC, 16-20 cm).

B



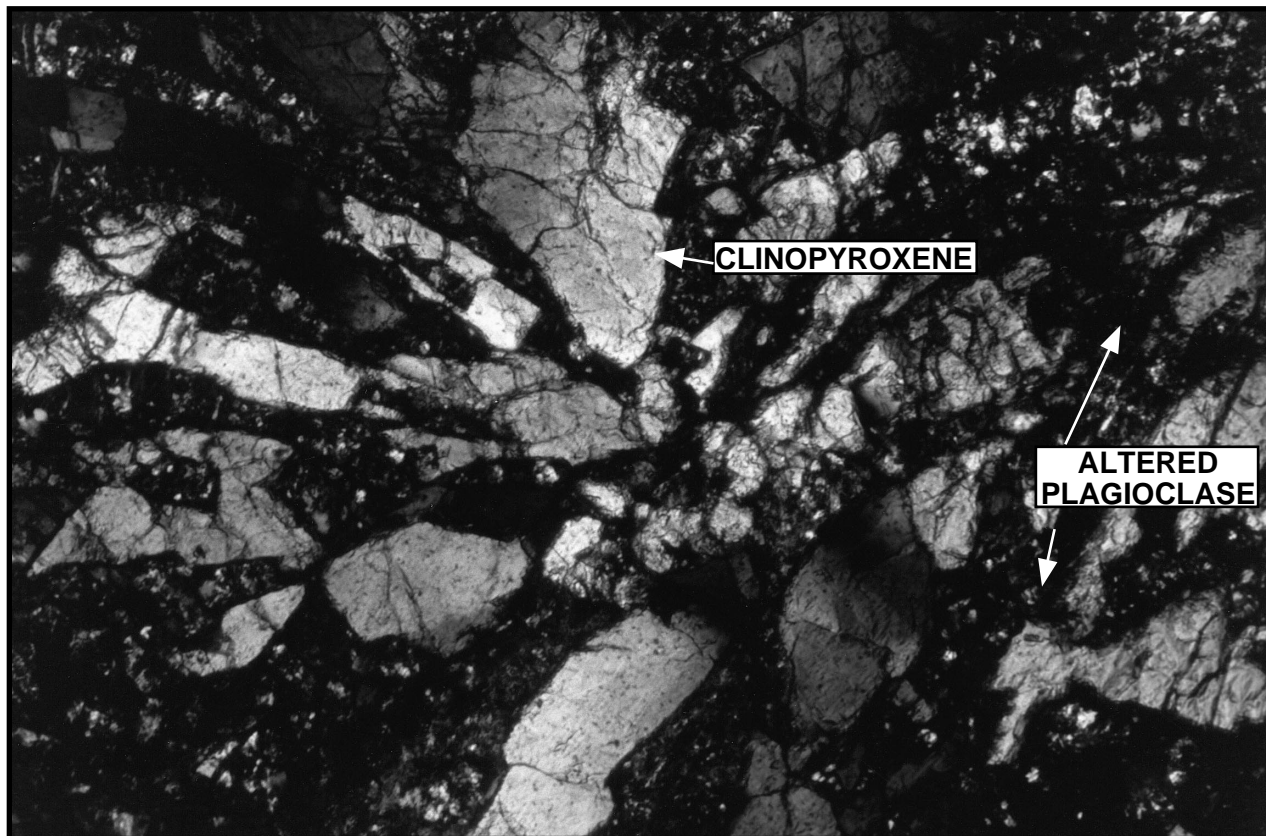
1 mm

Figure F13. Feldspar porphyry with phenocrysts of plagioclase, alkali feldspar, and hornblende (e.g., in lower left of picture) in a quartzo-feldspathic matrix (crossed polarizers; interval 180-1108B-13R- CC, 0-5 cm).



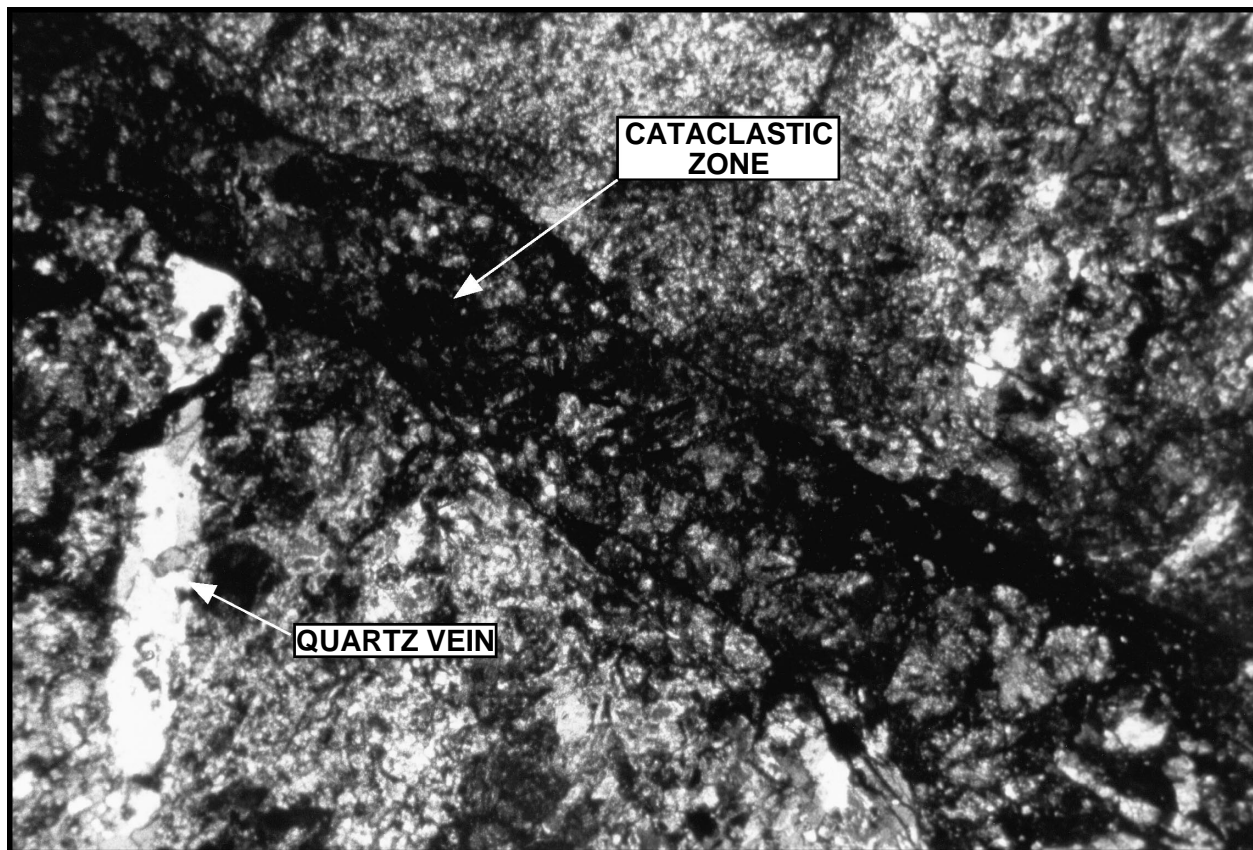
1 mm

Figure F14. Metadolerite—the original ophitic texture—as seen in some fresh examples from Site 1114. It is well preserved because the clinopyroxenes are fresh, whereas feldspars are broken down to altered plagioclase (interval 180-1114A-35R-1, 45-50 cm).



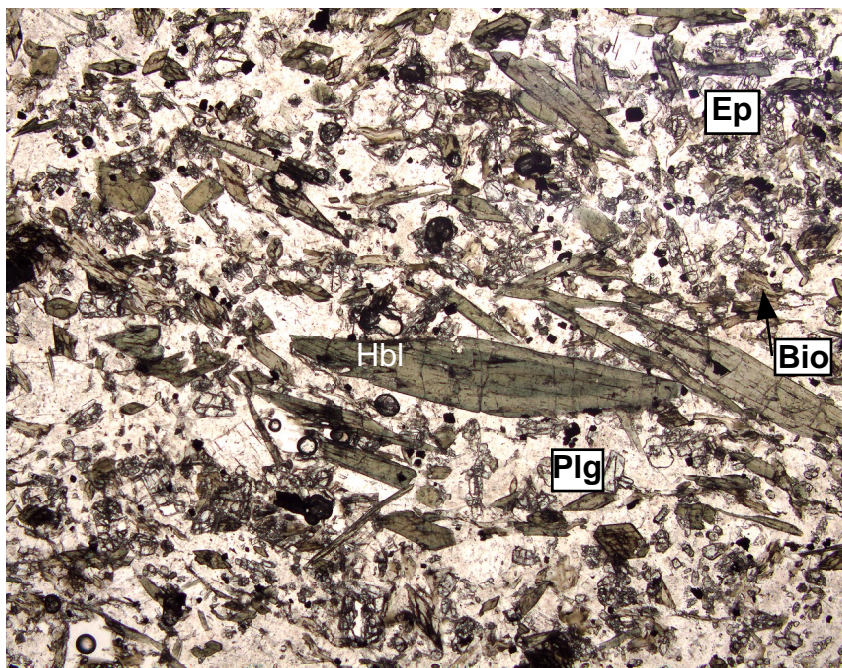
0.25 mm

Figure F15. Cataclastic zone cutting metadolerite and displacing an earlier generation of quartz veins cross-cutting the dolerite (interval 180-1112B-3R-1, 8-10 cm).



1 mm

Figure F16. Rock consisting largely of prismatic green hornblende (Hbl) and intermediate plagioclase (Plg), epidote (Ep), and biotite (Bio) (interval 180-1110D-1W-1, 5-6 cm).



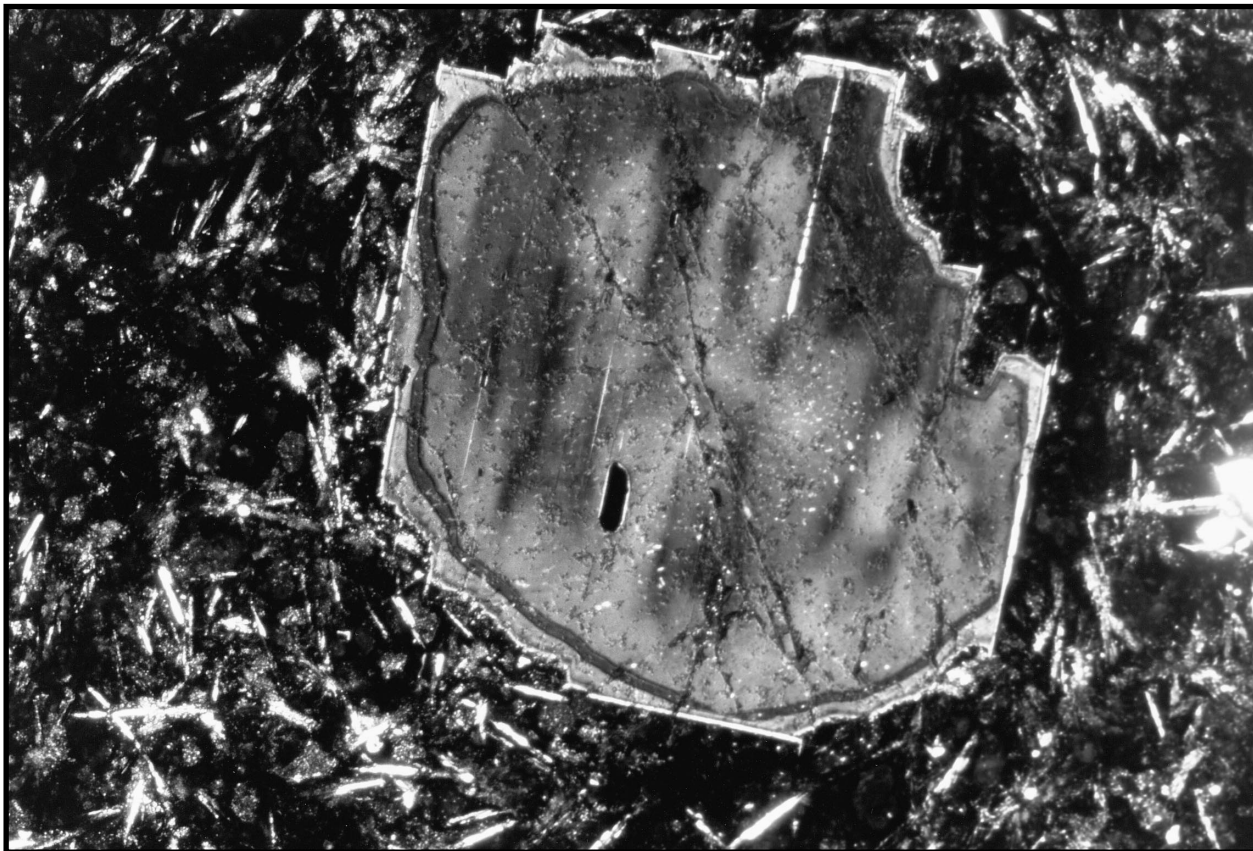
2 mm

Figure F17. Swallowtail of quench plagioclase microlite in a glassy, partly devitrified, basalt (plane-polarized light; interval 180-1108B-26R-1, 0-2 cm).



0.1 mm

Figure F18. Large plagioclase xenocryst in glassy basalt pebble. The core of the plagioclase is overlain by successive thin zones of first more anorthosite-rich material and subsequently an albite-rich mantle, with one further thin compositional reversal (crossed polarizers; interval 180-1108B-3R-CC, 6-7 cm).



1 mm

Figure F19. Oscillatory zoning common in feldspars of calc-alkaline lavas in plagioclase clast in volcaniclastic sandstone. This is associated with lithic fragments that are thought to be largely basalts and andesites (crossed polarizers; interval 180-1108B-47R-CC, 5-7 cm).



0.25 mm

Figure F20. Planktonic foraminifer and calcareous nannofossil zones from Holes 1110A, 1110B, 1111A, 1112A, and 1112B. Cores from Hole 1113A have no sediments. Dashed lines indicate the true zonal boundary may be above or below this level.

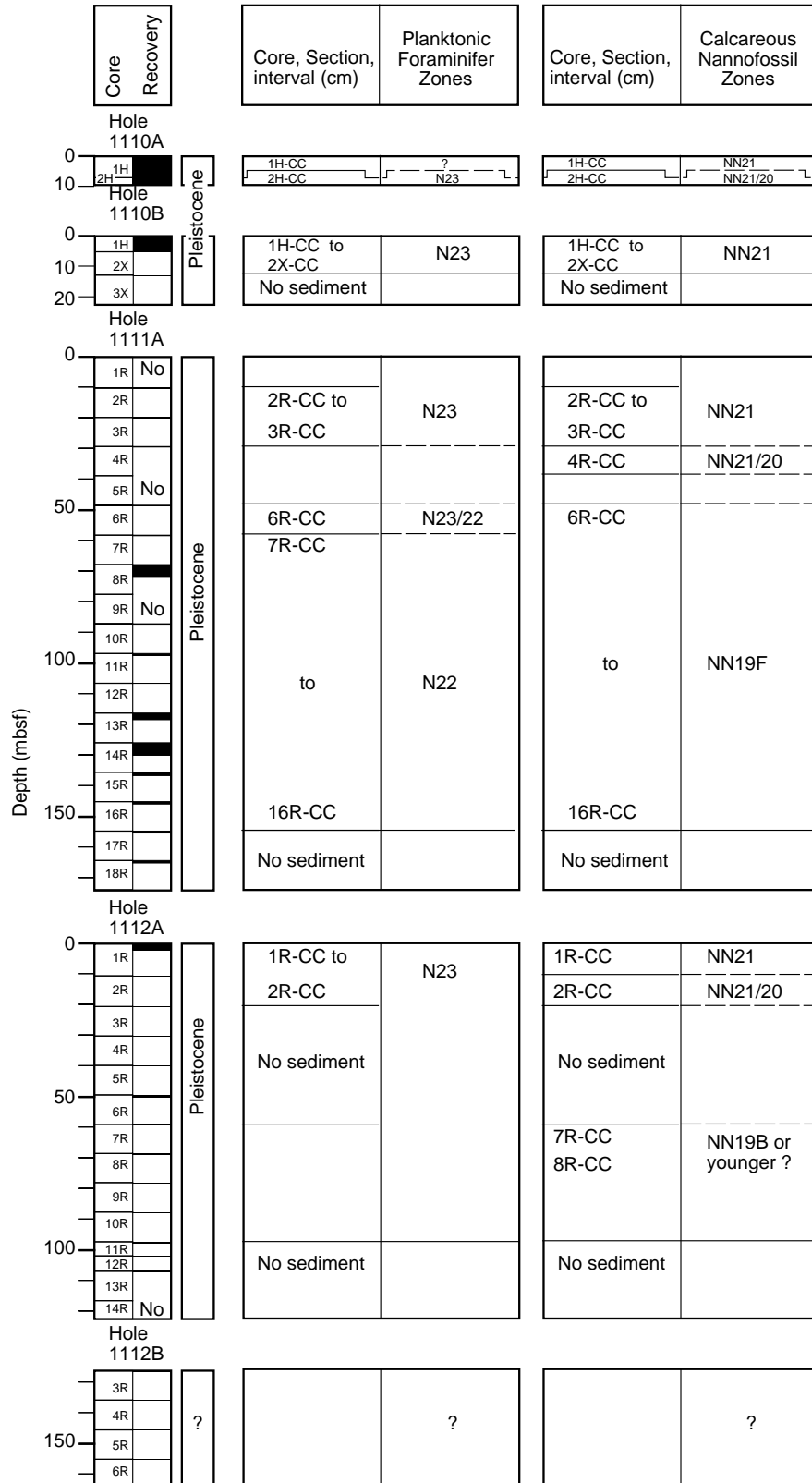


Figure F21. Susceptibility data (uncorrected for volume) from MST and AMST measurements for Sites 1110, 1111, and 1112. A. Holes 1110A, 1110B, and 1112A. (Continued on next page.)

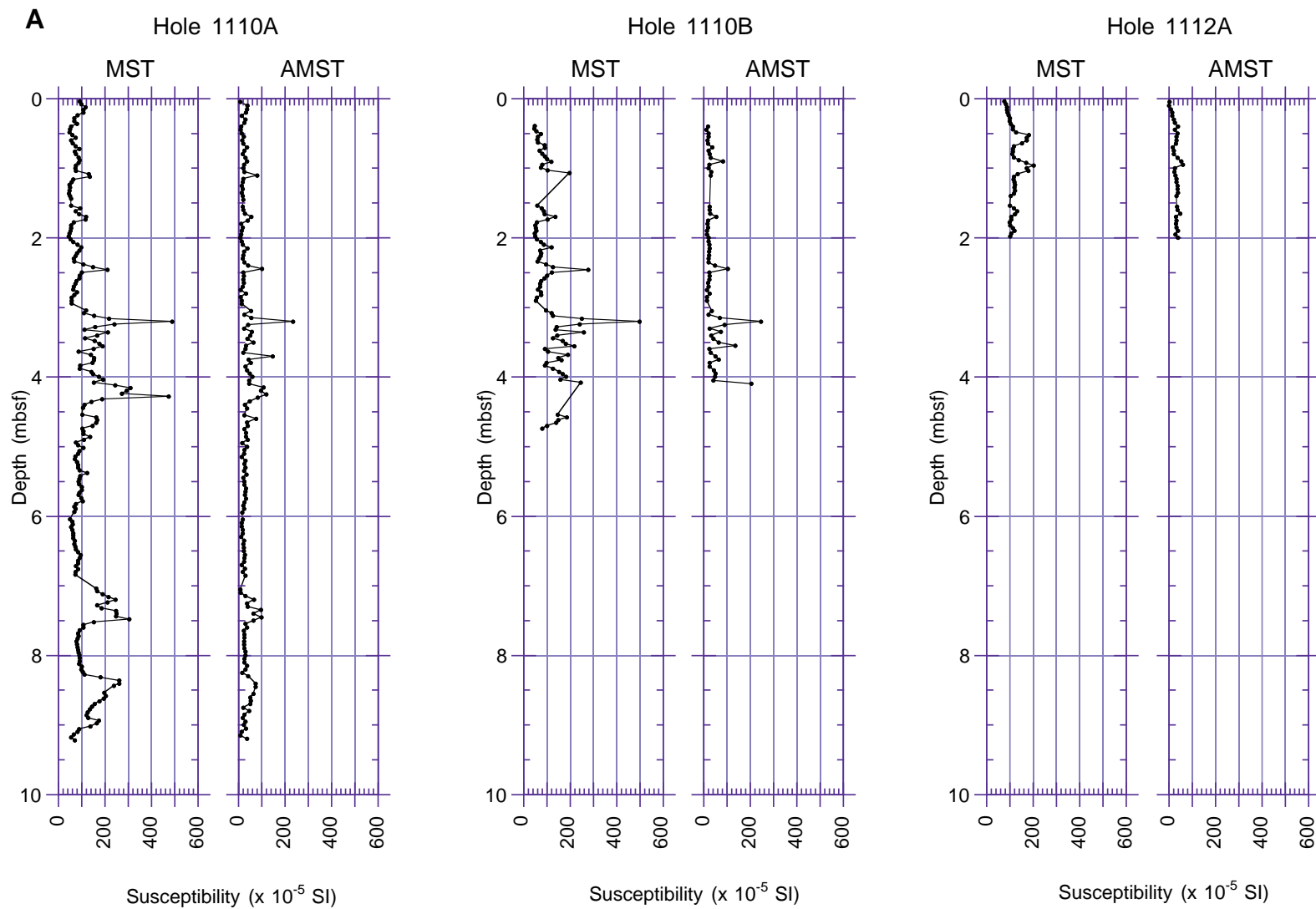


Figure F21 (continued). B. Susceptibility data (uncorrected for volume), Hole 1111A.

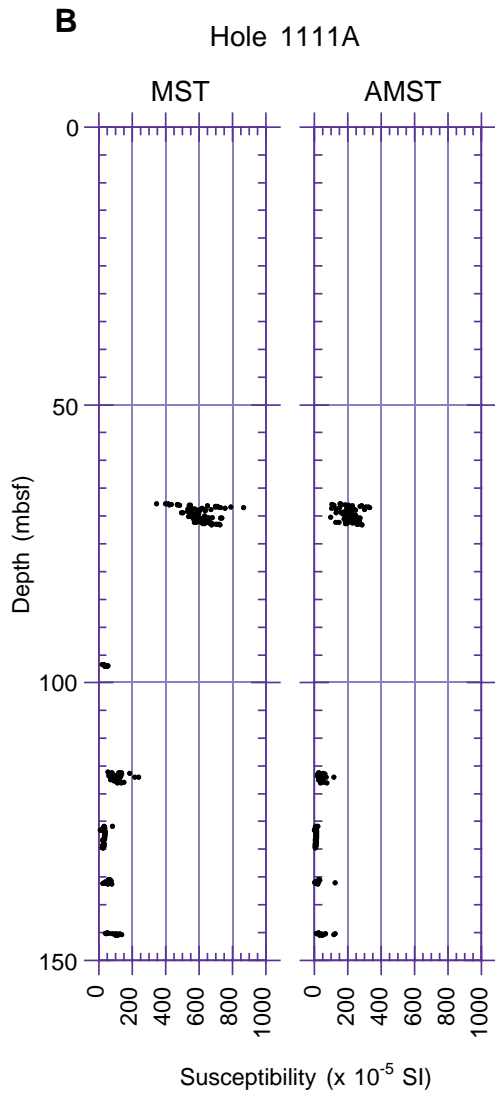


Figure F22. Downhole plots of declination, inclination, and intensity. (Data from long cores after AF demagnetization at 25 mT shown as filled circles; data from discrete samples after AF demagnetization at 25 mT shown as open squares.) Magnetostratigraphic interpretation and paleontologic zonation shown for Hole 1110A only. A. Hole 1110A. Shading represents possible excursion. Polarity: black = normal; white = reversed. Chrons: C1n = Brunhes (0.0–0.78 Ma; Berggren et al., 1995); ? = excursion, possibly the Blake event (~0.128 Ma; Harland et al., 1990). For paleontologic zonations, see “[Biostratigraphy](#),” p. 17. (Continued on next three pages.)

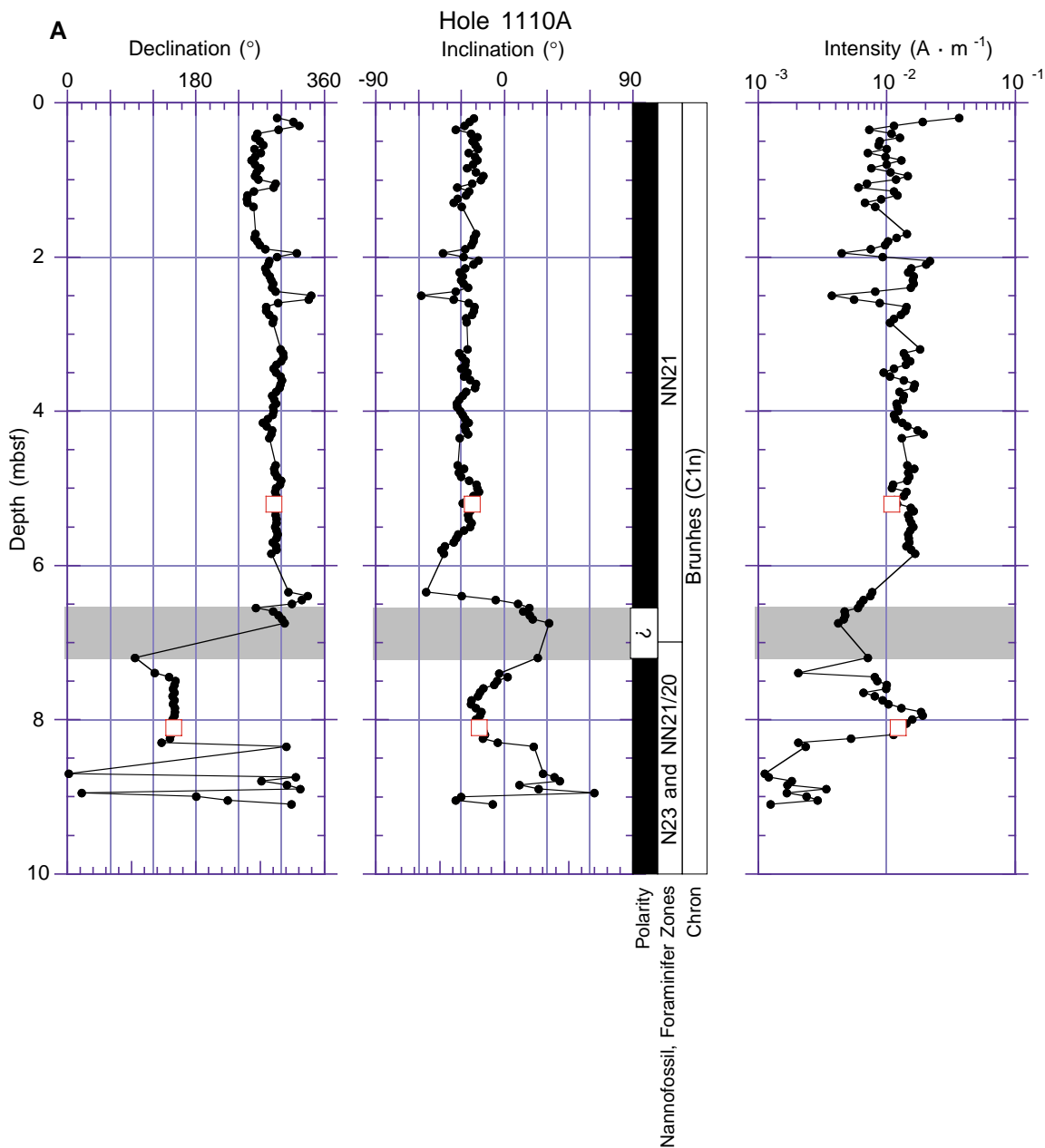


Figure F22 (continued). B. Downhole plots of declination, inclination, and intensity, Hole 1110B.

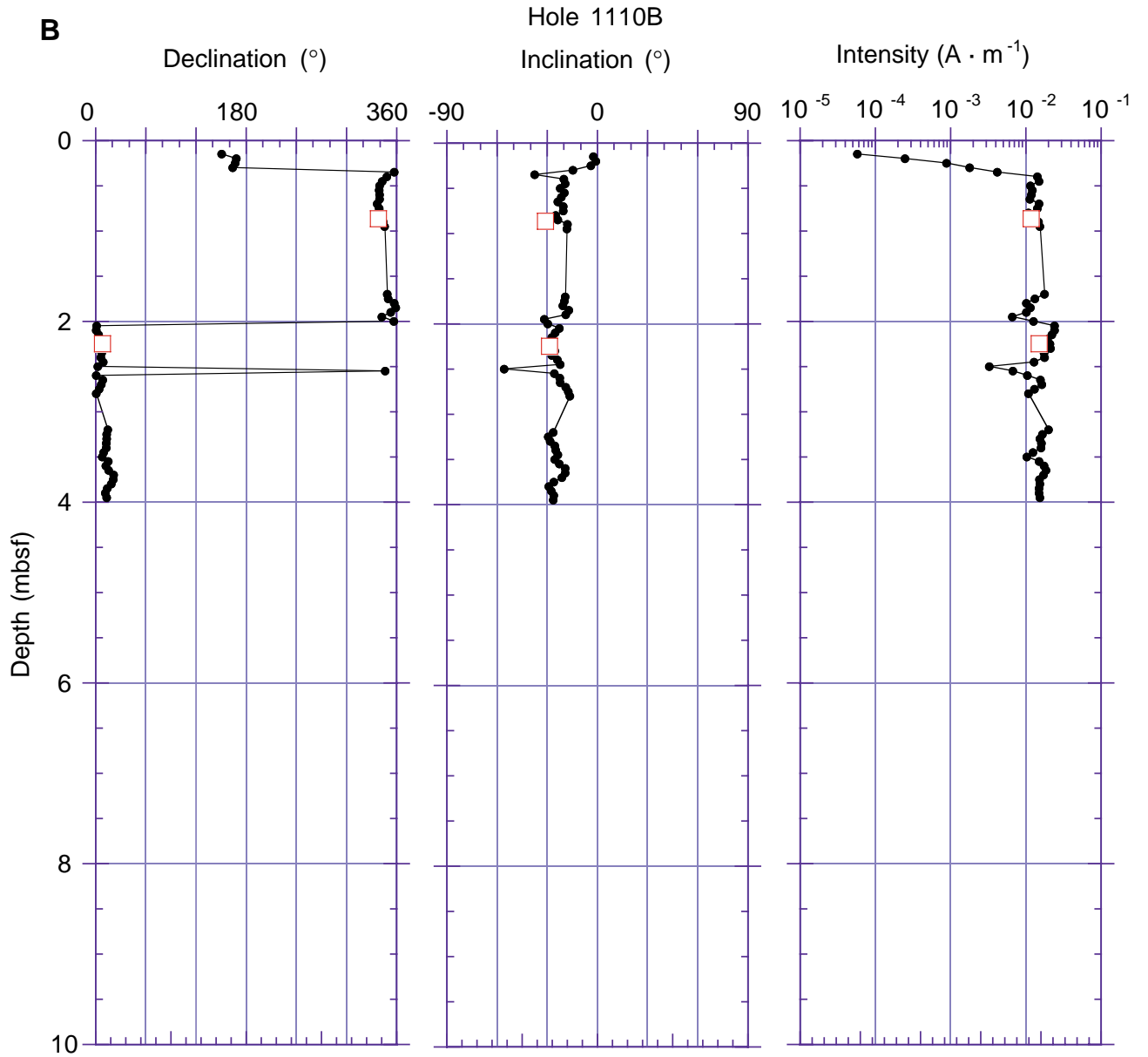


Figure F22 (continued). C. Downhole plots of declination, inclination, and intensity, Hole 1111A.

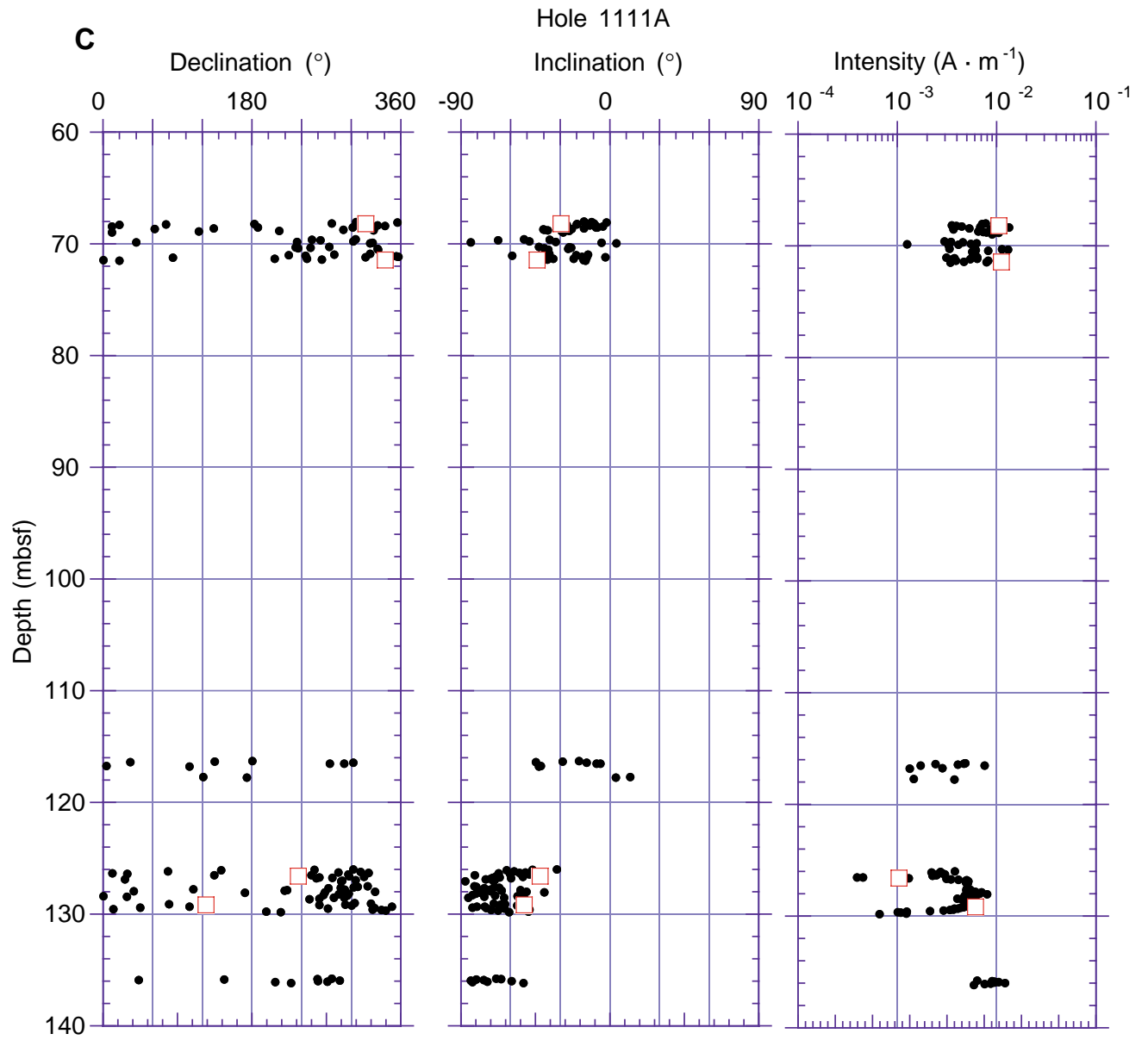


Figure F22 (continued). D. Downhole plots of declination, inclination, and intensity, Hole 1112A.

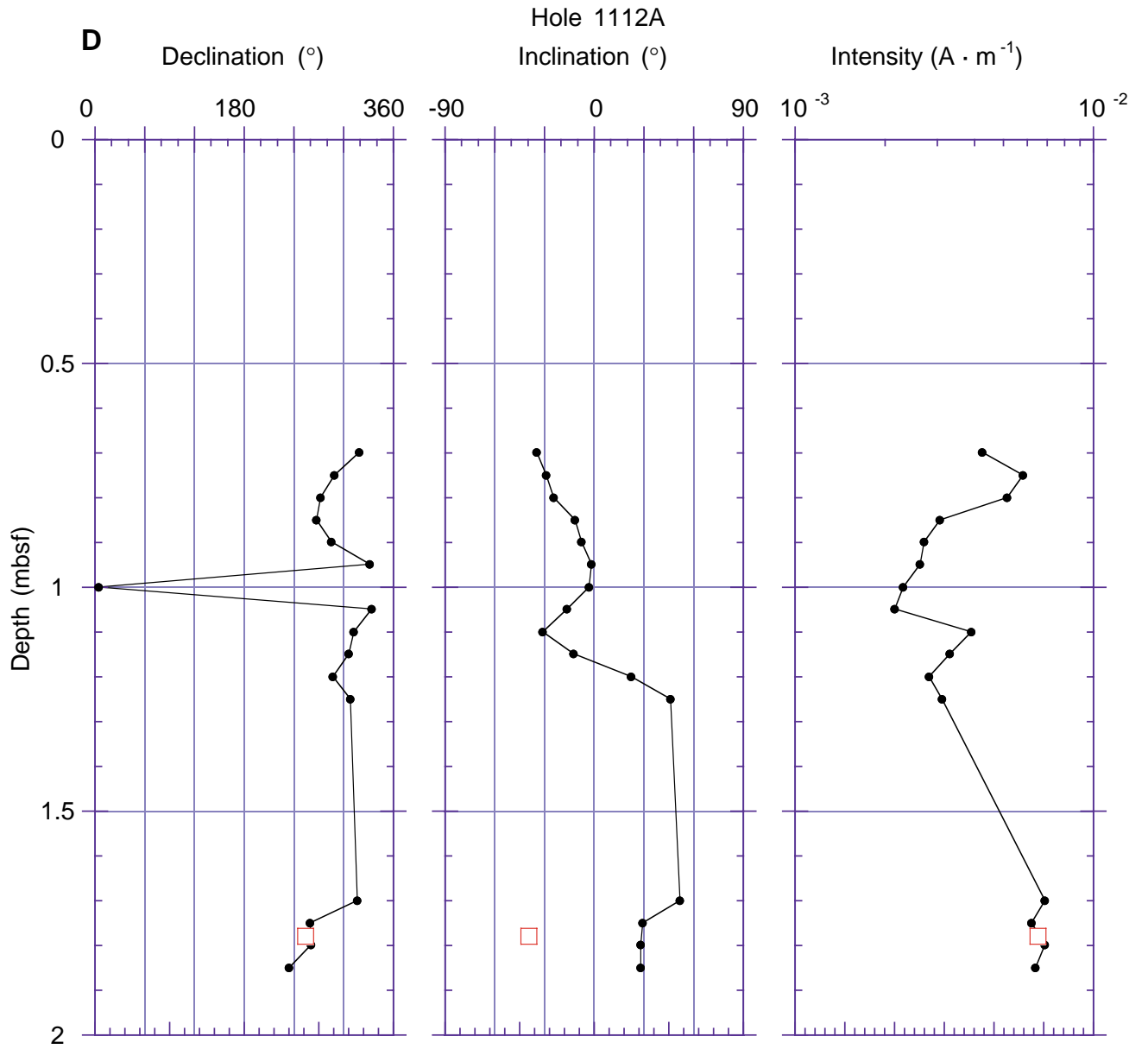


Figure F23. Demagnetization behavior of discrete samples from working halves of core sections. A. Hole 1110A. B. Hole 1110B. C. Hole 1111A. D. Hole 1111A. E. Hole 1112A. Vector plots: horizontal component = filled circles, vertical component = open circles. Stereonet plots: lower hemisphere = filled circles, upper hemisphere = open circles. NRM = natural remanent magnetization; Div. = division; Jo = NRM intensity.

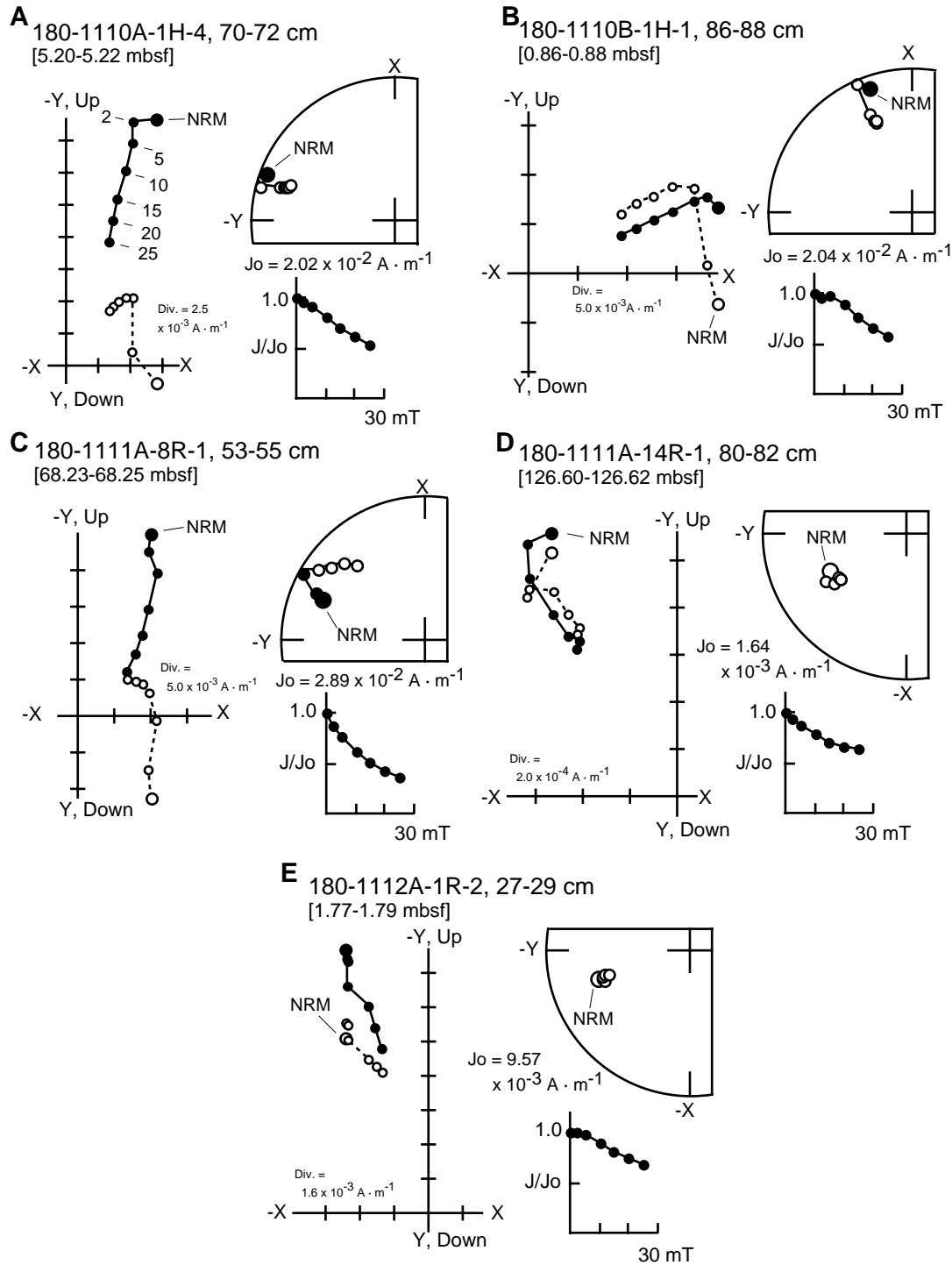


Figure F24. C_1 downhole profiles for Sites 1110, 1111, and 1112.

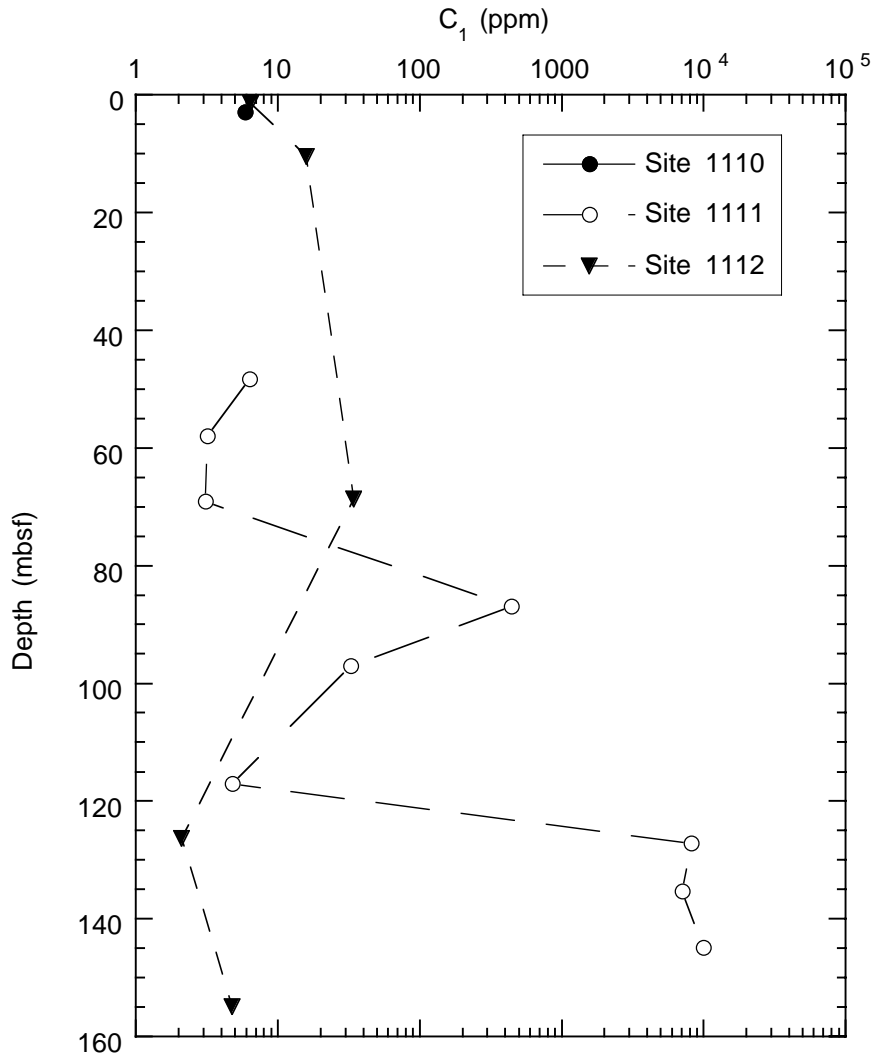


Figure F25. Depth distributions of total bacterial populations (filled symbols) and dividing and divided cells (open symbols) in samples from Sites 1110 (triangles), 1111 (circles), and 1112 (squares). The solid curve represents a general regression line of bacterial numbers vs. depth in deep-sea sediments (Parkes et al., 1994), with 95% upper and lower prediction limits shown by dashed curves.

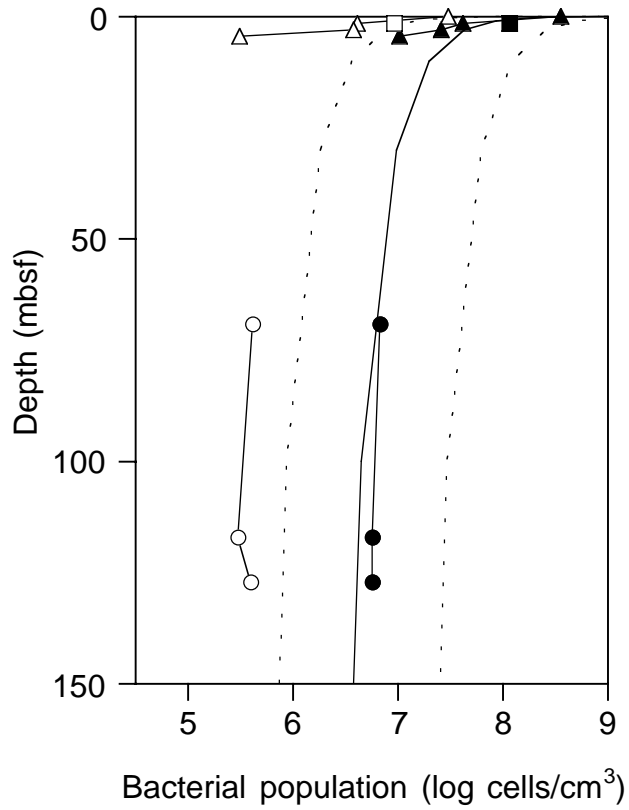


Figure F26. Site 1110 (A) bulk density derived from GRAPE and index properties measurements, (B) grain density, and (C) porosity.

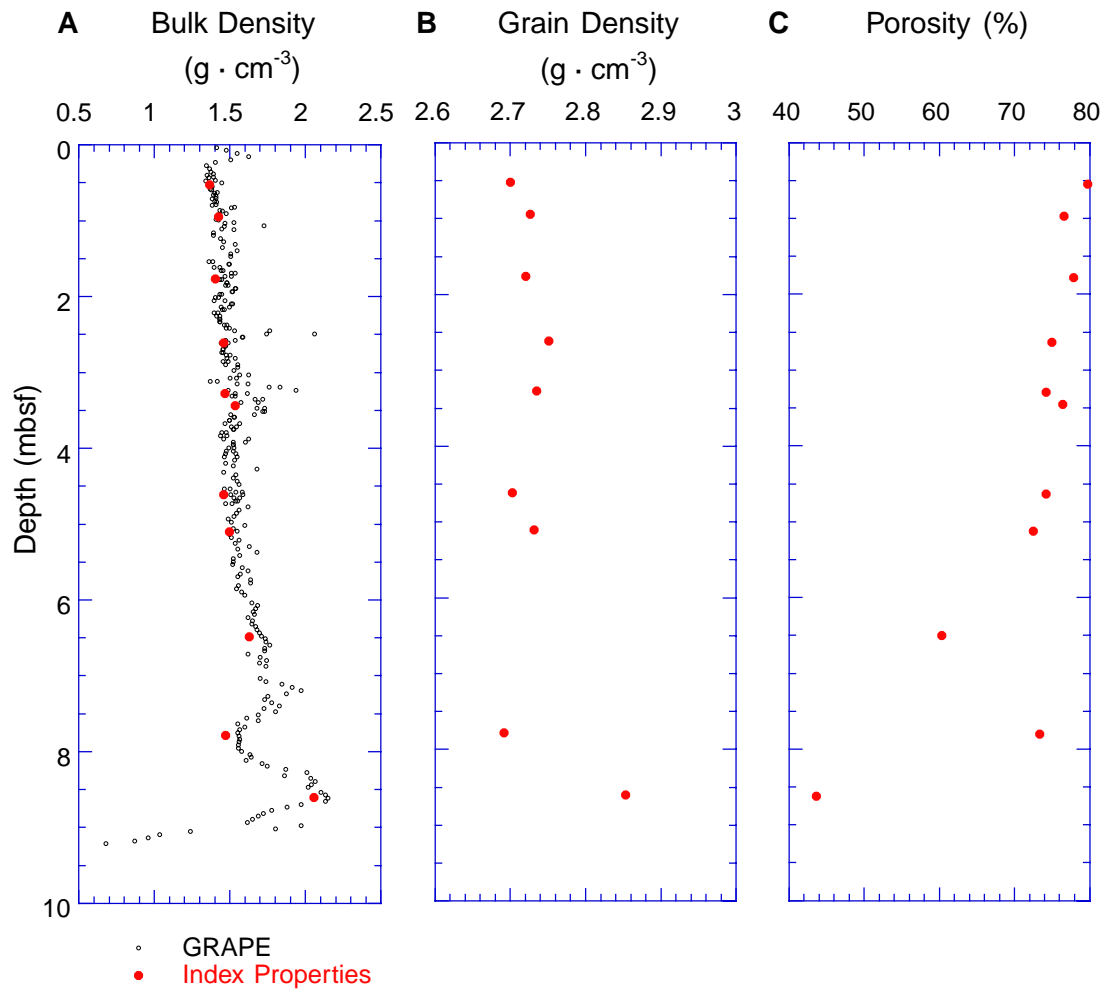


Figure F27. Site 1111 (A) bulk density derived from GRAPE and index properties measurements, (B) grain density, and (C) porosity.

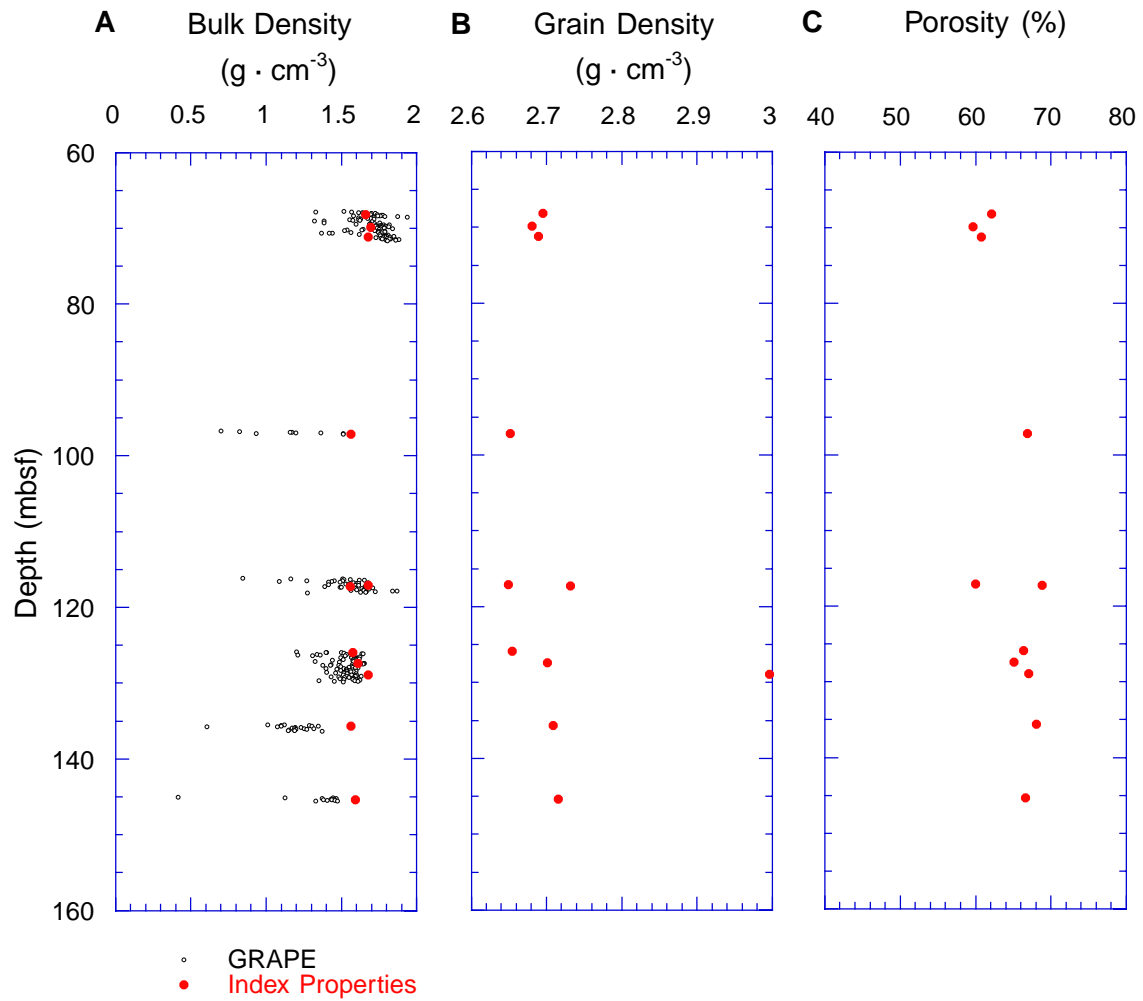


Figure F28. Undrained shear strength and unconfined compressive strength, Sites 1110 and 1111.

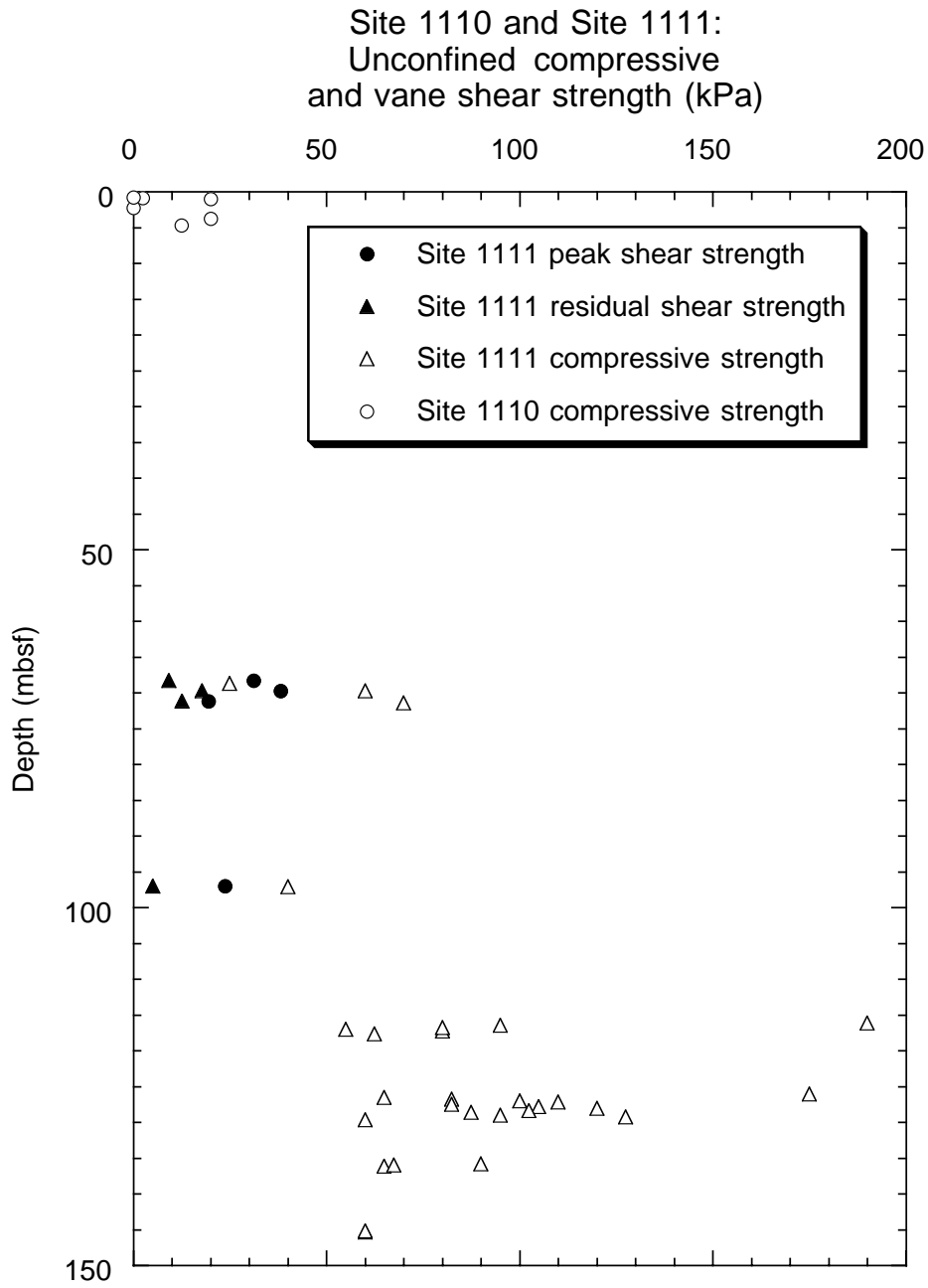


Figure F29. (A) Bulk magnetic susceptibility and (B) natural gamma ray for Holes 1110A and 1110B. Pink/intermediate gray and yellow/light gray stipple identifies nannofossil ooze from volcanoclastic sediments, respectively. Orange/dark gray stipple represents a major silt layer.

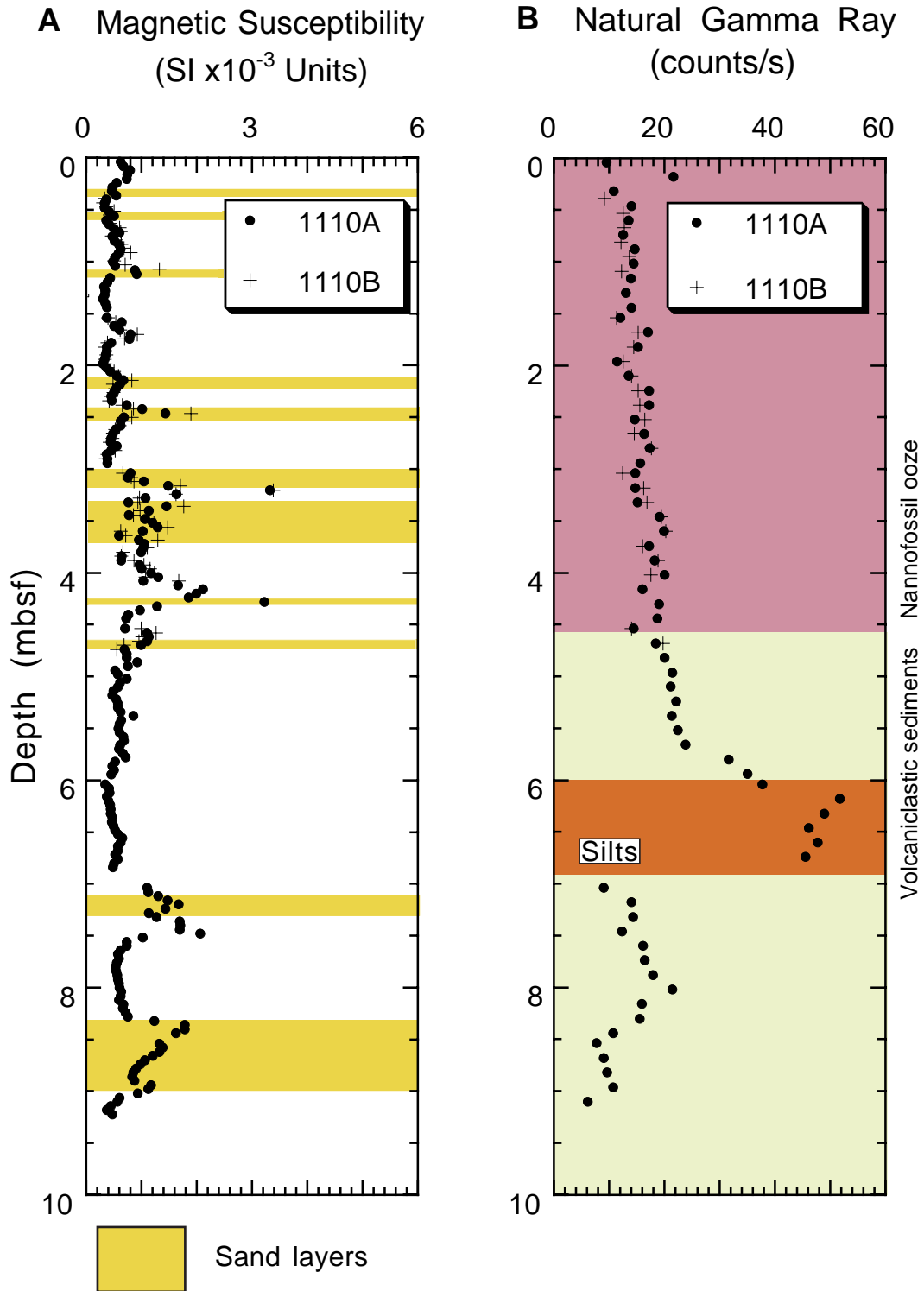


Figure F30. A. Temperature vs. $\ln[t/(t-s)]$ for the open-hole DVTP measurement in Hole 1111A at 94 mbsf. B. Temperature as a function of time for the DVTP penetration at 117.2 mbsf. C. Temperature as a function of time for the DVTP penetration at 136.5 mbsf. Mudline temperature is marked by a solid line, whereas extrapolated equilibrium temperatures are marked by dashed lines.

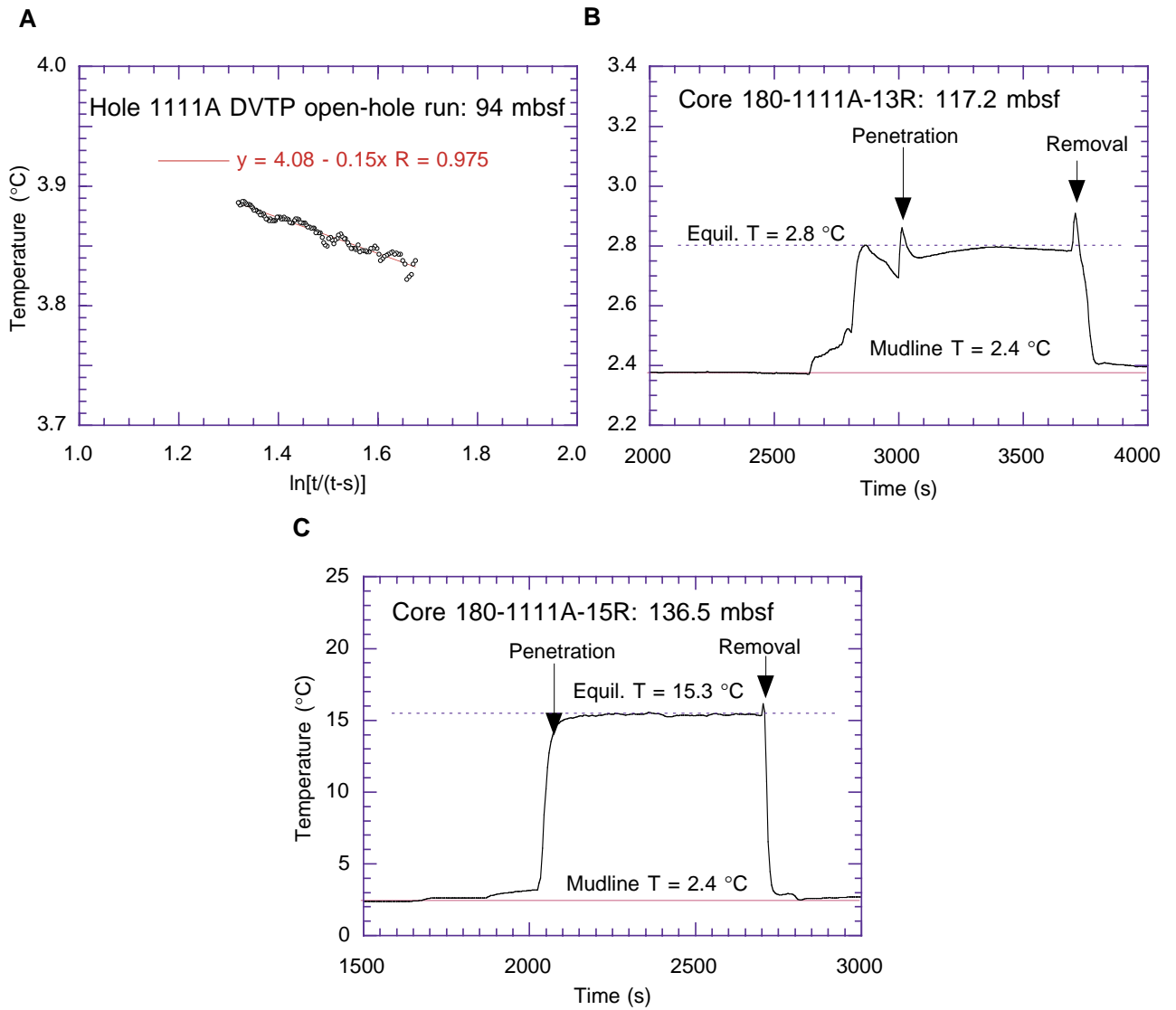


Figure F31. Estimated temperatures as a function of depth and thermal gradient computed from temperatures at mudline and at 136.5 mbsf.

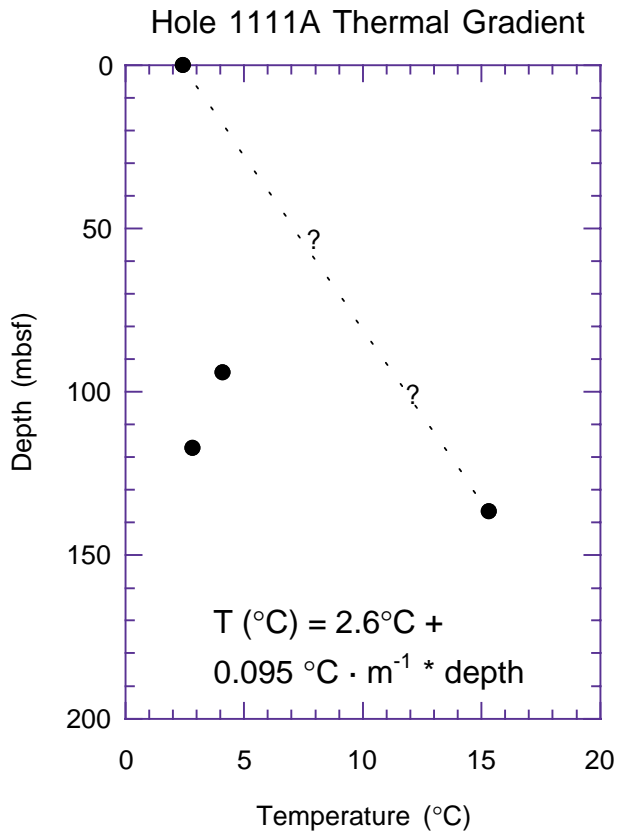


Figure F32. Magnetic susceptibility in Cores 180-1110A-1H and 180-1110B-1H and the correlation between holes. Thin solid lines and stippled areas indicate correlations based on magnetic susceptibility peaks and key beds, respectively.

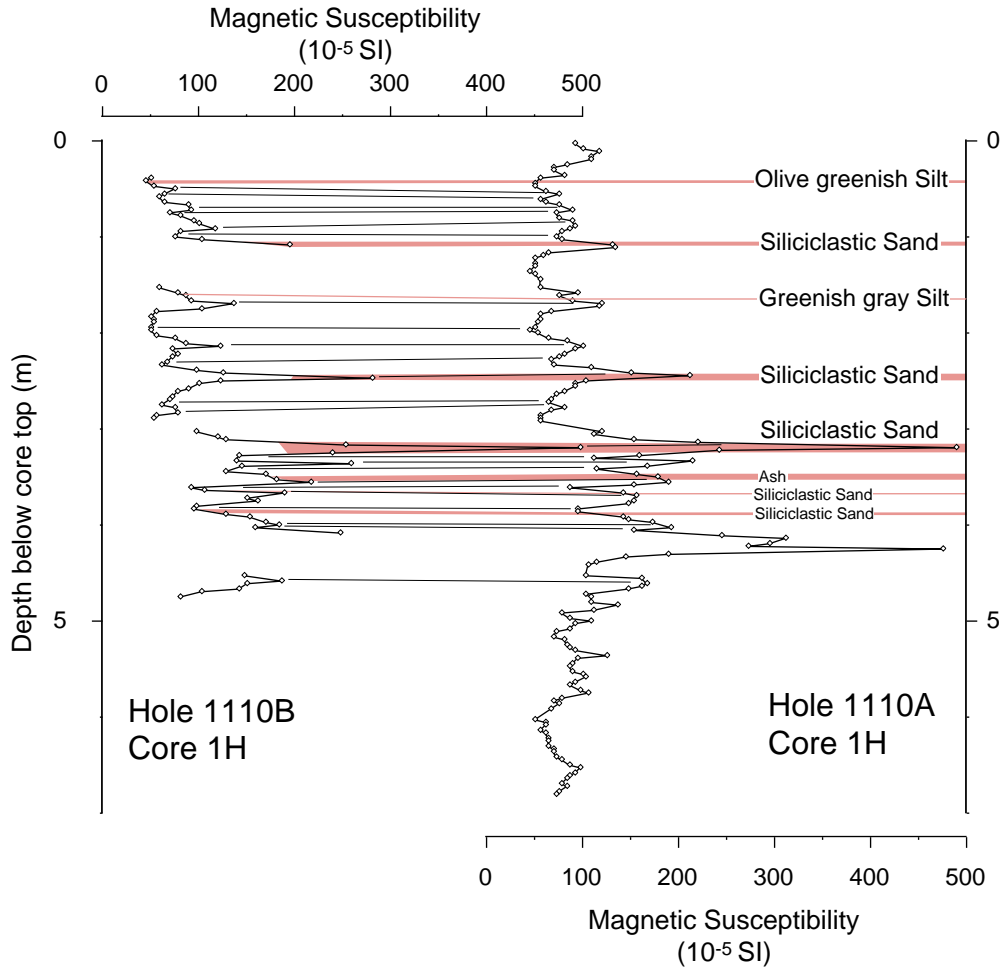


Table T1. Sites 1110, 1111, 1112, and 1113 coring summaries. (Continued on next three pages.)

Hole 1110A

Latitude: 9°43.599'S
 Longitude: 151°34.511'E
 Seafloor (drill-pipe measurement from rig floor, mbrf): 3257.5
 Distance between rig floor and sea level (m): 11.1
 Water depth (drill-pipe measurement from sea level, m): 3246.4
 Total depth (from rig floor, mbrf): 3267.00
 Penetration (mbsf): 9.50
 Total number of cores: 2
 Total length of cored section (m): 9.50
 Total core recovered (m): 9.50
 Core recovery (%): 100

Core	Date (July 1998)	Time (UTC +10 hr)	Depth (mbsf)	Length cored (m)	Length recovered (m)	Recovery (%)
180-1110A-1H	4	1000	0.0-7.0	7.0	7.03	100.4
2H	4	1055	7.0-9.5	2.5	2.47	98.8
Totals:				9.5	9.50	100.0

Hole 1110B

Latitude: 9°43.609'S
 Longitude: 151°34.509'E
 Seafloor (drill-pipe measurement from rig floor, mbrf): 3257.4
 Distance between rig floor and sea level (m): 11.1
 Water depth (drill-pipe measurement from sea level, m): 3246.3
 Total depth (from rig floor, mbrf): 3279.70
 Penetration (mbsf): 22.30
 Total number of cores: 3
 Total length of cored section (m): 22.30
 Total core recovered (m): 5.37
 Core recovery (%): 24

Core	Date (July 1998)	Time (UTC +10 hr)	Depth (mbsf)	Length cored (m)	Length recovered (m)	Recovery (%)
180-1110B-1H	4	1200	0.0-5.1	5.1	5.08	99.6
2X	4	1345	5.1-12.7	7.6	0.09	1.2
3X	4	1700	12.7-22.3	9.6	0.20	2.1
Totals:				22.3	5.37	24.1

Hole 1110C

Latitude: 9°43.599'S
 Longitude: 151°34.498'E
 Seafloor (drill-pipe measurement from rig floor, mbrf): 3257.0
 Distance between rig floor and sea level (m): 11.2
 Water depth (drill-pipe measurement from sea level, m): 3245.8
 Total depth (from rig floor, mbrf): 3272.0
 Penetration (mbsf): 15.00
 Total number of cores: 0

Core	Date (July 1998)	Time (UTC +10 hr)	Depth (mbsf)	Length cored (m)	Length recovered (m)	Recovery (%)
180-1110C-						
*****Drilled from 0.0-15.0 mbsf*****						

Table T1 (continued).

Hole 1110D

Latitude: 9°43.588'S
 Longitude: 151°34.526'E
 Seafloor (drill-pipe measurement from rig floor, mbrf): 3257.0
 Distance between rig floor and sea level (m): 11.2
 Water depth (drill-pipe measurement from sea level, m): 3245.8
 Total depth (from rig floor, mbrf): 3285.70
 Penetration (mbsf): 28.70
 Total number of cores: 2
 Total length of cored section (m): 6.0
 Total core recovered (m): 0.10
 Core recovery (%): 2

Core	Date (July 1998)	Time (UTC +10 hr)	Depth (mbsf)	Length cored (m)	Length recovered (m)	Recovery (%)
180-1110D-						
*****Drilled with core barrel in place*****						
1W	5	1610	0.0-22.7	22.7*	0.06*	0.3*
2R	5	1940	22.7-28.7	6.0	0.10	1.7
Totals:				6.0	0.10	1.7

Hole 1111A

Latitude: 9°43.059'S
 Longitude: 151°34.533'E
 Seafloor (drill-pipe measurement from rig floor, mbrf): 3212.0
 Distance between rig floor and sea level (m): 11.3
 Water depth (drill-pipe measurement from sea level, m): 3200.7
 Total depth (from rig floor, mbrf): 3385.7
 Penetration (mbsf): 173.7
 Total number of cores: 18
 Total length of cored section (m): 173.7
 Total core recovered (m): 15.19
 Core recovery (%): 9

Core	Date (July 1998)	Time (UTC +10 hr)	Depth (mbsf)	Length cored (m)	Length recovered (m)	Recovery (%)
180-1111A-						
1R	5	2300	0.0-10.1	10.1	0.00	0.0
2R	6	0050	10.1-19.7	9.6	0.07	0.7
3R	6	0220	19.7-29.2	9.5	0.15	1.6
4R	6	0345	29.2-38.7	9.5	0.11	1.2
5R	6	0500	38.7-48.4	9.7	0.00	0.0
6R	6	0620	48.4-58.1	9.7	0.09	0.9
7R	6	0740	58.1-67.7	9.6	0.18	1.9
8R	6	0900	67.7-77.4	9.7	4.17	43.0
9R	6	1010	77.4-87.0	9.6	0.00	0.0
10R	6	1120	87.0-96.7	9.7	0.14	1.4
11R	6	1350	96.7-106.4	9.7	0.66	6.8
12R	6	1500	106.4-116.1	9.7	0.02	0.2
13R	6	1715	116.1-125.8	9.7	2.19	22.6
14R	6	1815	125.8-135.4	9.6	4.09	42.6
15R	6	2015	135.4-145.0	9.6	1.10	11.5
16R	6	2115	145.0-154.6	9.6	0.79	8.2
17R	6	2255	154.6-164.2	9.6	0.62	6.5
18R	7	0200	164.2-173.7	9.5	0.81	8.5
Totals:				173.7	15.19	8.7

Table T1 (continued).

Hole 1112A

Latitude: 9°44.749'S
 Longitude: 151°36.721'E
 Seafloor (drill-pipe measurement from rig floor, mbrf): 3058.0
 Distance between rig floor and sea level (m): 11.3
 Water depth (drill-pipe measurement from sea level, m): 3046.7
 Total depth (from rig floor, mbrf): 3180.4
 Penetration (mbsf): 122.4
 Total number of cores: 14
 Total length of cored section (m): 122.4
 Total core recovered (m): 5.85
 Core recovery (%): 5

Core	Date (July 1998)	Time (UTC +10 hr)	Depth (mbsf)	Length cored (m)	Length recovered (m)	Recovery (%)
180-1112A-						
1R	7	1015	0.0-10.5	10.5	2.16	20.60
2R	7	1125	10.5-20.5	10.0	0.28	2.80
3R	7	1250	20.5-30.1	9.6	0.26	2.70
4R	7	1525	30.1-39.7	9.6	0.28	2.90
5R	7	1645	39.7-49.3	9.6	0.22	2.30
6R	7	1810	49.3-58.9	9.6	0.70	7.30
7R	7	1955	58.9-68.4	9.5	0.14	1.50
8R	7	2230	68.4-77.9	9.5	0.33	3.50
9R	8	0225	77.9-87.5	9.6	0.26	2.70
10R	8	0515	87.5-97.2	9.7	0.26	2.70
11R	8	0745	97.2-101.8	4.6	0.40	8.70
12R	8	1125	101.8-106.8	5.0	0.19	3.80
13R	8	1400	106.8-116.4	9.6	0.37	3.90
14R	8	2230	116.4-122.4	6.0	0.00	0.00
Totals:				122.4	5.85	4.80

Hole 1112B

Latitude: 9°44.746'S
 Longitude: 151°36.714'E
 Seafloor (drill-pipe measurement from rig floor, mbrf): 3058.0
 Distance between rig floor and sea level (m): 11.4
 Water Depth (drill-pipe measurement from sea level, m): 3046.6
 Total Depth (from rig floor, mbrf): 3222.6
 Penetration (mbsf): 164.6
 Total number of cores: 6 (including two wash cores)
 Total length of cored section (m): 38.5 (excluding two wash cores)
 Total core recovered (m): 1.19(excluding two wash cores)
 Core recovery (%): 3

Core	Date (July 1998)	Time (UTC +10 hr)	Depth (mbsf)	Length cored (m)	Length recovered (m)	Recovery (%)
180-1112B-						
1W	9	2200	0.0-87.0	87*	0.3*	0.3*
2W	9	0820	87.0-126.1	39.1*	0.00*	0.00*
3R	10	1210	126.1-135.7	9.6	0.57	5.90
4R	10	1500	135.7-145.4	9.7	0.22	2.30
5R	10	1930	145.4-155.0	9.6	0.23	2.40
6R	11	0720	155.0-164.6	9.6	0.17	1.80
Totals:				38.5	1.19	3.10

Table T1 (continued).

Hole 1113A

Latitude: 9°45.449'S
 Longitude: 151°36.737'E
 Seafloor (drill-pipe measurement from rig floor, mbrf): 2927.0
 Distance between rig floor and sea level (m): 11.4
 Water depth (drill-pipe measurement from sea level, m): 2915.6
 Total depth (from rig floor, mbrf): 2952.2
 Penetration (mbsf): 25.2
 Total number of cores: 3
 Total length of cored section (m): 25.2
 Total core recovered (m): 0.44 (excluding two wash cores)
 Core recovery (%): 2

Core	Date (July 1998)	Time (UTC +10 hr)	Depth (mbsf)	Length cored (m)	Length recovered (m)	Recovery (%)
180-1113A-						
1R	12	0000	0.0-10.1	10.10	0.08	0.80
2R	12	0500	10.1-20.2	10.10	0.10	1.00
3R	12	1330	20.2-25.2	5.00	0.26	5.20
Totals:				25.20	0.44	1.70

Notes: UTC = Universal Time Coordinated. * = wash core values not included in totals.

Table T2. Site 1110 coring summary by section.

Core	Date (July 1998)	Time (UTC +10 hr)	Core depth (mbsf)		Length (m)		Recovery (%)	Section	Length (m)		Section depth (mbsf)		Catwalk samples	Comment
			Top	Bottom	Cored	Recovered			Liner	Curated	Top	Bottom		
180-1110A-1H	4	1000	0.0	7.0	7.0	7.03	100.4							
								1	1.50	1.50	0.00	1.50		
								2	1.50	1.50	1.50	3.00		
								3	1.50	1.50	3.00	4.50		
								4	1.50	1.50	4.50	6.00		
								5	0.89	0.89	6.00	6.89		
								CC	0.14	0.14	6.89	7.03	PAL	
									7.03	7.03				
2H	4	1055	7.0	9.5	2.5	2.47	98.8							
								1	1.50	1.50	7.00	8.50		
								2	0.77	0.77	8.50	9.27	PAL	
								CC	0.20	0.20	9.27	9.47		
									2.47	2.47				
				Totals:	9.5	9.50	100.0							
180-1110B-1H	4	1200	0.0	5.1	5.1	5.08	99.6							
								1	1.50	1.50	0.00	1.50	IW, IW, WRMB, WRMB	
								2	1.50	1.50	1.50	3.00	IW, WEL	
								3	1.50	1.50	3.00	4.50	IW, WRMB, WROG, WEL	
								4	0.28	0.28	4.50	4.78	WEL	
								CC	0.30	0.30	4.78	5.08	PAL	
									5.08	5.08				
2X	4	1345	5.1	12.7	7.6	0.09	1.2							
								CC	0.09	0.09	5.10	5.19	PAL	
									0.09	0.09				
3X	4	1700	12.7	22.3	9.6	0.20	2.1							
								1	0.20	0.00				
								CC	0.00	0.00				
									0.20	0.00				
				Totals:	22.3	5.37	24.1							
180-1110C- ***Drilled from 0.0-15.0 mbsf***														
				Totals:	0.0	0.00	0.0							
180-1110D-1W	5	1610	0.0	22.7	22.7*	0.06*	0.3*							
								1	0.06	0.06				
									0.06	0.06				
2R	5	0940	22.7	28.7	6.0	0.10	1.7							
								1	0.10	0.10				
									0.10	0.10				
				Totals:	6.0	0.10	1.7							

Notes: PAL = paleontology; IW = interstitial water; WRMB = whole-round microbiology; WEL = Wellsbury microbiology; WROG = whole-round organic geochemistry; * = wash cores not included in totals. Drilled with core barrel in place.

Table T3. Site 1111 coring summary by section. (Continued on next page.)

Core	Date (July 1998)	Time (UTC + 10 hr)	Core depth (mbsf)		Length (m)		Recovery (%)	Section	Length (m)		Section depth (mbsf)			Comment
			Top	Bottom	Cored	Recovered			Liner	Curated	Top	Bottom	Catwalk samples	
180-1111A- 1R	5	2300	0.0	10.1	10.1	0.00	0.0	1	0.00	0.00				
2R	5	0050	10.1	19.7	9.6	0.07	0.7	CC	0.07	0.07	10.10	10.17	PAL other	
3R	6	0220	19.7	29.2	9.5	0.15	1.6	CC	0.15	0.30	19.70	20.00	PAL other	
4R	6	0345	29.2	38.7	9.5	0.11	1.2	CC	0.11	0.19	29.20	29.39	PAL	
5R	6	0500	38.7	48.4	9.7	0.00	0.0	1	0.00	0.00				
6R	6	0620	48.4	58.1	9.7	0.09	0.9	CC	0.09	0.09	48.40	48.49	PAL other	
7R	6	0740	58.1	67.7	9.6	0.18	1.9	CC	0.18	0.18	58.10	58.28	PAL, HS	
8R	6	0900	67.7	77.4	9.7	4.17	43.0	1	1.50	1.50	67.70	69.20	IW	
								2	1.50	1.50	69.20	70.70	HS, WEL	
								3	0.97	0.97	70.70	71.67		
								CC	0.20	0.20	71.67	71.87	PAL	
									4.17	4.17				
9R	6	1010	77.4	87.0	9.6	0.00	0.0	1	0.00	0.00				
10R	6	1120	87.0	96.7	9.7	0.14	1.4	CC	0.14	0.14	87.00	87.14	PAL, HS other	
11R	6	1350	96.7	106.4	9.7	0.66	6.8	1	0.47	0.47	96.70	97.17	HS	
								CC	0.19	0.19	97.17	97.36	PAL	
									0.66	0.66				
12R	6	1500	106.4	116.1	9.7	0.02	0.2	CC	0.02	0.02	106.40	106.42	PAL	
									0.02	0.02				
13R	6	1715	116.1	125.8	9.7	2.19	22.6							
								1	1.06	1.06	116.10	117.16	PAL, IW other	
								2	0.95	0.95	117.16	118.11	HS, WEL	

Material caught up in the DVTP tool was sampled for Paleo as 13R-1, 0-2 cm. It is being stored in a bag in the working half of 13R-1. Recovery for the DVTP sample is 2 cm but has not been recorded as "official" recovery.

Table T3 (continued).

Core	Date (July 1998)	Time (UTC + 10 hr)	Core depth (mbsf)		Length (m)		Recovery (%)	Section	Length (m)		Section depth (mbsf)		Catwalk samples	Comment	
			Top	Bottom	Cored	Recovered			Liner	Curated	Top	Bottom			
14R	6	1815	125.8	135.4	9.6	4.09	42.6	CC	0.18	0.18	118.11	118.29	PAL		
									2.19	2.19					
								1	1.50	1.50	125.80	127.30	IW		
								2	1.50	1.50	127.30	128.80	HS, WEL		
15R	6	2015	135.4	145.0	9.6	1.10	11.5	3	1.01	1.01	128.80	129.81			
								CC	0.08	0.08	129.81	129.89	PAL		
									4.09	4.09					
								1	0.96	0.96	135.40	136.36	HS		
16R	6	2115	145.0	154.6	9.6	0.79	8.2	CC	0.14	0.14	136.36	136.50	PAL		
									1.10	1.10					
								1	0.58	0.58	145.00	145.58	HS, PAL		
17R	6	2255	154.6	164.2	9.6	0.62	6.5	CC	0.21	0.21	145.58	145.79			
									0.79	0.79					
18R	7	0200	164.2	173.7	9.5	0.81	8.5	1	0.62	0.62	154.60	155.45			
									0.62	0.62					
								1	0.81	1.20	164.20	165.40			
									0.81	1.20					
Totals:					173.7	15.19	8.7								

Note: PAL = paleontology; HS = headspace; IW = interstitial water; WEL = Wellsbury microbiology.

Table T4. Site 1112 coring summary by section. (Continued on next page.)

Core	Date (July 1998)	Time (UTC + 10hr)	Core depth (mbsf)		Length (m)		Recovery (%)	Section	Length (m)		Section depth (mbsf)		Catwalk samples	Comment
			Top	Bottom	Cored	Recovered			Liner	Curated	Top	Bottom		
180-1112A- 1R	7	1015	0.0	10.5	10.5	2.16	20.6							
								1	1.50	1.50	0.00	1.50	IW	
								2	0.54	0.54	1.50	2.04	HS, WEL	
								CC	0.12	0.12	2.04	2.16	PAL	
									2.16	2.16				
2R	7	1125	10.5	20.5	10.0	0.28	2.8							
								CC	0.28	0.28	10.50	10.78	PAL, HS	
									0.28	0.28				
3R	7	1250	20.5	30.1	9.6	0.26	2.7							
								1	0.26	0.00				
									0.26	0.00				
4R	7	1525	30.1	39.7	9.6	0.28	2.9							
								1	0.28	0.38	30.10	30.48		
									0.28	0.38				
5R	7	1645	39.7	49.3	9.6	0.22	2.3							
								1	0.22	0.38	39.70	40.08		
									0.22	0.38				
6R	7	1810	49.3	58.9	9.6	0.70	7.3							
								1	0.70	1.13	49.30	50.43		
									0.70	1.13				
7R	7	1955	58.9	68.4	9.5	0.14	1.5							
								1	0.14	0.19	58.90	59.09		
									0.14	0.19				
8R	7	2230	68.4	77.9	9.5	0.33	3.5							
								CC	0.33	0.42	68.40	68.82	PAL, HS	
									0.33	0.42				
9R	7	0225	77.9	87.5	9.6	0.26	2.7							
								CC	0.26	0.36	77.90	78.26	PAL	Trace to Paleo
									0.26	0.36				
10R	7	0515	87.5	97.2	9.7	0.26	2.7							
								CC	0.26	0.35	87.50	87.85	PAL	Trace to Paleo
									0.26	0.35				
11R	7	0745	97.2	101.8	4.6	0.40	8.7							
								CC	0.40	0.45	97.20	97.65		No Paleo sample
									0.40	0.45				
12R	8	1125	101.8	106.8	5.0	0.19	3.8							
								CC	0.19	0.29	101.80	102.09		No Paleo sample
									0.19	0.29				

Table T4 (continued).

Core	Date (July 1998)	Time (UTC + 10hr)	Core depth (mbsf)		Length (m)			Recovery (%)	Section	Length (m)		Section depth (mbsf)		Catwalk samples	Comment
			Top	Bottom	Cored	Recovered	Liner			Curated	Top	Bottom			
13R	8	1400	106.8	116.4	9.6	0.37	3.9								
								1		0.37	0.45	106.80	107.25		
										0.37	0.45				
14R	8	2230	116.4	122.4	6.0	0.00	0.0								
Total:					122.4	5.85	4.8								
180-1112B- 1W	9	2200	0.0	87.0	87.0	0.30	0.3								Wash core, drilled with core barrel in place
								1		0.30	0.47				
										0.30	0.47				
2W	9	0820	87.0	126.1	39.1	0.00	0.0								Washed interval, drilled with core barrel in place
								1		0.00	0.00				
										0.00	0.00				
3R	10	1210	126.1	135.7	9.6	0.57	5.9								
								1		0.57	0.57	126.10	126.67	PAL, HS	
										0.57	0.57				
4R	10	1500	135.7	145.4	9.7	0.22	2.3								
								1		0.22	0.22	135.70	135.92	PAL	
										0.22	0.22				
5R	10	1930	145.4	155.0	9.6	0.23	2.4								
								CC		0.23	0.42	145.40	145.82	PAL, PAL	
										0.23	0.42				
6R	10	0720	155.0	164.6	9.6	0.17	1.8								
								CC		0.17	0.23	155.00	155.23	PAL, HS	Trace to Paleo
										0.17	0.23				
Washed:					126.1										
Cored total:					38.5	1.19	3.0								
Total:					164.6										

Note: IW = interstitial water; HS = headspace; WEL = Wellsbury microbiology; PAL = paleontology.

Table T5. Site 1113 coring summary by section.

Core	Date (July 1998)	Time (UTC + 10 hr)	Core depth (mbsf)		Length (m)			Section	Length (m)		Section depth (mbsf)		Catwalk samples	Comment
			Top	Bottom	Cored	Recovered	Recovery (%)		Liner	Curated	Top	Bottom		
180-1113A- 1R	11	0000	0.0	10.1	10.1	0.08	0.8	CC	0.08 0.08	0.08	0.00	0.08		
2R	11	0500	10.1	20.2	10.1	0.10	1.0	CC	0.10 0.13	0.13	10.10	10.23		
3R	11	1330	20.2	25.2	5.0	0.26	5.2	1	0.26 0.28	0.28	20.20	20.48		
Totals:					25.2	0.44	1.7							

Table T6. Composition of representative whole-rock samples analyzed by XRD.

Core, section, interval (cm)	Depth (mbsf)	Description	XRD identification: major (minor) minerals
1110A-			
1H-3, 23-24	3.23	Siliciclastic sandstone	Quartz, calcite (chlorite, illite, plagioclase)
1H-4, 34-35	4.84	Nannofossil-rich silty clay	Calcite, quartz (plagioclase, chlorite, amphibole)
2H-1, 7-8	7.07	Sand	Calcite, quartz, plagioclase, chlorite (amphibole, pyroxene, illite)
2H-1, 135-136	8.35	Sand	Plagioclase, quartz, calcite, chlorite, amphibole (illite)
1110B-			
1H-2, 100.5-102	2.51	Silty clay	Calcite, quartz (chlorite, plagioclase, amphibole)
1111A-			
8R-2, 113-114	70.33	Nannofossil-rich silty clay	Plagioclase, quartz, calcite (chlorite, illite, smectite?)
11R-CC, 9-10	97.26	Silty clay nannofossil ooze	Calcite (plagioclase)
13R-1, 63-64	116.73	Calcareous silty clay	Calcite (aragonite)
14R-2, 49-50	127.79	Calcareous silty clay	Calcite (aragonite)
15R-1, 61-62	136.01	Calcareous silty clay	Calcite (aragonite)
16R-1, 17-18	145.17	Silty clay	Calcite (quartz, plagioclase, chlorite)

Table T7. “Lamprophyre” (composition and comparisons) and miscellaneous samples, Moresby Seamount talus.

Core, section, interval (cm)	Sample	SiO ₂	Average	TiO ₂	Average	Al ₂ O ₃	Average	Fe ₂ O ₃	Average	MnO	Average	MgO	Average
180-1111A- 4R-CC, 3-5	1a	53.50		0.88		13.33		9.65		0.19		8.69	
	1b	52.38	52.94	0.86	0.87	13.08	13.21	9.54	9.60	0.19	0.19	8.66	8.68
180-1109	2		51.24		1.37		14.91		12.27		0.19		6.86
	3		53.73		0.96		17.95		8.06		0.10		6.37
	4		50.87		1.87		13.80		7.81		0.12		8.30
180-1112B- 1W-1, 12-18	5a	62.86		0.54		14.02		4.74		0.07		5.77	
	5b	63.25	63.05	0.54	0.54	14.13	14.07	4.77	4.75	0.07	0.07	5.87	5.82
180-1111A- 16R-CC, 16-20	6a	69.06		0.26		16.85		1.62		0.06		0.00	
	6b	68.78	68.05	0.26	0.26	16.78	16.81	1.63	1.63	0.06	0.06	0.00	0.00

Notes: LOI = loss on ignition. Major element values are in weight percent. Trace elements are in parts per million. a and b = duplicate analyses of the same sample; 1 = lamprophyre; 2 = average analysis of dolerite in Hole 1109D (Table T4, p. 248, in the “Site 1109” chapter); 3 = from Woodlark Island (table 4 of Ashley and Flood, 1981); 4 = average of three analyses of Madilogo Volcano, Papua (Blake, 1976); 5 = “andesite”; 6 = one of four recovered during Leg 180. ND = not determined.

Table T7 (continued).

Sample	CaO	Average	Na ₂ O	Average	K ₂ O	Average	P ₂ O ₅	Average	Total	Average	LOI	Average	Rock type
1a	7.91		1.64		5.06		0.63		101.48		3.05		Lamprophyre
1b	7.80	7.86	1.73	1.69	4.96	5.01	0.62	0.63	99.82	100.70	3.05	3.05	
2		12.45		1.71		0.11		0.11		101.21		1.79	Dolerite Porphyritic clinopyroxene shoshonite
3		7.93		3.06		2.92		0.52		99.67		1.02	
4		6.90		1.83		5.45		1.12		98.07		ND	
5a	4.64		3.74		3.51		0.17		100.07		1.78		“Andesite”
5b	4.68	4.66	3.69	3.67	3.52	3.51	0.18	0.17	100.72	100.40	1.78	1.78	
6a	2.02		5.13		5.51		0.11		100.26		2.05		Granite porphyry
6b	2.01	2.01	5.26	5.19	5.49	5.50	0.11	0.11	100.02	100.19	2.05	2.05	

Table T8. Trace element composition of “Lamprophyre” and miscellaneous samples, Moresby Seamount talus.

Core, section, interval (cm)	Sample	Nb	Zr	Y	Sr	Rb	Zn	Cu	Ni	Cr	V	Ce	Ba	Rock type
180-1111A- 4R-CC, 3-5	1	3	114	31	1099	137	77	86	90	372	225	43	1584	Lamprophyre
180-1109	2	4	71	22	137	2	83	140	94	363	302	10	7	Dolerite
	3	ND	151	24	1109	54	37	66	47	168	228	ND	1375	Porphyritic clinopyroxene shoshonite
180-1112B- 1W-1, 12-18	5	4	169	13	909	61	58	22	191	364	121	65	1203	“Andesite”
180-1111A- 16R-CC, 16-20	6	6	173	13	1162	111	45	6	8	0	41	49	1242	Granite porphyry

Table T9. Data from discrete sample measurement of susceptibility and its anisotropy, Sites 1110, 1111 and 1112.

Core, section, interval (cm)	Depth (mbsf)	Mean volume susceptibility ($\times 10^{-6}$ SI)	P_j	T	Orientation of susceptibility axes ($^\circ$)					
					K_{\max}		K_{int}		K_{\min}	
					Dec	Inc	Dec	Inc	Dec	Inc
180-1110A-										
1H-4, 70-72	5.20-5.20	439.1	1.029	0.487	28	39	263	35	148	31
1H-5, 60-62	6.60-6.62	440.5	1.020	-0.460	19	7	109	3	225	82
2H-1, 110-112	8.10-8.12	463.0	1.018	0.391	281	8	42	75	189	13
180-1110B-										
1H-1, 86-88	0.86-0.88	546.5	1.031	0.362	70	71	264	19	173	4
1H-2, 74-76	2.24-2.26	448.5	1.024	0.169	286	35	99	55	194	4
180-1111A-										
8R-1, 53-55	68.23-68.25	4410	1.077	0.210	239	10	331	9	102	77
8R-3, 77-79	71.47-71.49	3874	1.075	0.495	248	6	339	11	131	77
14R-1, 80-82	126.60-126.62	90.67	1.049	0.839	105	40	349	27	235	37
14R-3, 40-42	129.20-129.20	204.9	1.036	0.203	270	19	7	20	141	62
180-1112A-										
1R-2, 27-29	1.77-1.79	400.7	1.026	0.412	257	27	72	63	166	2

Notes: Degree of anisotropy (P_j) and the shape parameter (T) calculated according to Jelinek (1981). K_{\max} , K_{int} , and K_{\min} are the maximum, intermediate, and minimum axes, respectively, of the susceptibility ellipsoid. Dec = declination, Inc = inclination.

Table T10. Data from discrete sample measurement of remanent magnetization after 25-mT AF demagnetization, Sites 1110, 1111, and 1112.

Core, section, interval (cm)	Depth (mbsf)	Declination (°)	Inclination (°)	Intensity (A·m ⁻¹)	Demagnetization behavior
180-1110A-					
1H-4, 70	5.21	288.94	-22.720	1.09000 E-05	Stable
1H-5, 60	6.61	295.81	-25.050	3.07000 E-06	No stable end-point
2H-1, 110	8.11	148.71	-17.780	1.22000 E-05	Stable
180-1110B-					
1H-1, 86	0.87	337.67	-31.050	1.17000 E-05	Stable
1H-2, 74	2.25	7.70	-28.840	1.48000 E-05	Stable
180-1111A-					
8R-1, 53	68.24	317.49	-29.800	1.05000 E-05	Curved trajectory; no stable end-point
8R-3, 77	71.48	341.23	-44.070	1.11000 E-05	No stable end-point
14R-1, 80	126.61	236.04	-42.350	1.04000 E-06	Stable
14R-3, 40	129.21	124.33	-51.840	6.13000 E-06	Stable
180-1112A-					
1R-2, 27	1.78	253.96	-39.570	6.52000 E-06	Stable

Notes: Demagnetization behavior: stable = colinear decay toward origin on vector plots or consistent direction on stereonet plots between 15 and 25 mT; no stable end-point = directions do not trend toward origin on vector plot and directions are not stable on stereonet plot; curved trajectory = overlapping coercivity spectra.

Table T11. Interstitial water geochemistry, Sites 1110, 1111, and 1112.

Core, section, interval (cm)	Depth (mbsf)	pH	Alkalinity (mM)	Salinity	Cl (T) (mM)	Cl (IC) (mM)	SO ₄ (mM)	Na (mM)	K (mM)	Mg (mM)	Ca (mM)	Ca/Mg	Li (μM)	SiO ₂ (μM)
180-1110B-														
1H-1, 30-35	0.30	7.81	3.389	34	558	563	28.6	473	11.5	50.5	10.2	0.20	20	336
1H-1, 145-150	1.45	7.86	4.499	34	559	562	28.2	472	11.7	49.9	9.9	0.20	16	531
1H-2, 145-150	2.95	7.78	5.471	34	558	565	27.6	473	10.8	50.6	10.0	0.20	15	460
1H-3, 145-150	4.45	7.92	5.340	34	561	566	27.6	474	11.4	49.0	9.4	0.19	16	476
180-1111A-														
8R-1, 145-150	69.15	7.95	15.529	34	570	576	16.0	481	11.0	50.4	4.2	0.08	12	584
13R-1, 101-106	117.11	7.86	23.229	34	574	577	5.0	467	11.2	39.8	2.9	0.07	19	758
14R-1, 143-150	127.23	8.05	26.905	33	563	574	1.5	470	11.4	37.8	2.6	0.07	13	744
180-1112A-														
1R-1, 145-150	1.45	7.88	3.633	35	558	564	29.0	469	11.2	47.2	10.3	0.22	41	376

Note: Cl (T) = chloride by titration, Cl (IC) = chloride by ion chromatography.

Table T12. Composition of headspace gas in sediments, Sites 1110, 1111, and 1112.

Core, section, interval (cm)	Depth (mbsf)	C ₁
180-1110B- 1H-3, 0-5	3.00	6
180-1111A- 6R-CC, 0-1	48.40	6
7R-CC, 0-1	58.10	3
8R-2, 0-2	69.20	3
10R-CC, 0-1	87.00	442
11R-1, 46-47	97.16	33
13R-2, 0-2	117.16	5
14R-2, 0-5	127.30	8192
15R-1, 0-2	135.40	7111
16R-1, 0-2	145.00	9932
180-1112A- 1R-2, 0-2	1.50	7
2R-CC, 0-1	10.50	16
8R-CC, 28-29	68.68	35
180-1112B- 3R-1, 23-24	126.33	2
6R-CC, 0-1	155.00	5

Note: All concentrations are reported in parts per million by volume.

Table T13. Calcium carbonate, carbon, nitrogen, and sulfur contents in sediments, Sites 1110, 1111, and 1112.

Core, section, interval (cm)	Depth (mbsf)	Inorganic carbon (wt%)	CaCO ₃ (wt%)	Organic carbon (wt%)	Total nitrogen (wt%)	Total sulfur (wt%)
180-1110A-						
2H-1, 7-8	7.07	1.99	16.56			
2H-1, 55-56	7.55	4.25	35.38	0.42		
2H-1, 135-136	8.35	1.10	9.19	0.09		
180-1110B-						
1H-1, 36-37	0.36	4.37	36.37	0.19		
1H-2, 100.5-102	2.51	3.27	27.24			
1H-3, 61-62	3.61	4.92	41.02	0.36		
180-1111A-						
8R-2, 114-115	70.34	0.94	7.81	0.39		
11R-CC, 10-11	97.27	6.24	51.97	0.26		
13R-1, 64-65	116.74	7.53	62.76	0.47		
14R-2, 49-50	127.79	6.40	53.33	0.39		
15R-1, 60-61	136.00	6.49	54.08	0.45		
16R-1, 17-18	145.17	4.56	38.03	0.62		
180-1112A-						
1R-2, 33-34	1.83	3.70	30.84	0.35		

Note: Blanks indicate values below detection limit.

Table T14. Total bacterial populations and numbers of dividing and divided cells in sediments, Sites 1110, 1111, and 1112.

Hole	Depth (mbsf)	Total bacterial population (log cells/cm ³)	Dividing and divided cells (log cells/cm ³)
1110B	0.00	8.561	7.483
	1.50	7.624	6.617
	3.00	7.416	6.581
	4.50	7.022	5.497
1111A	69.20	6.830	5.619
	117.16	6.760	5.475
	127.30	6.758	5.600
1112A	1.50	8.068	6.971

Table T15. Index properties measured in cores, Sites 1110, 1111, and 1112.

Leg	Site	Hole	Core	Type	Section	Top (cm)	Bottom (cm)	Depth (mbsf)	Water content (bulk)	Water content (dry)	Bulk density (g-cm ⁻³)	Dry density (g-cm ⁻³)	Grain density (g-cm ⁻³)	Porosity (%)	Void ratio
180	1110	A	1	H	1	94.0	96.0	0.94	55.1	122.7	1.423	0.639	2.726	76.6	3.27
180	1110	A	1	H	2	111.0	113.0	2.61	52.7	111.2	1.457	0.690	2.751	74.9	2.99
180	1110	A	1	H	3	43.0	45.0	3.43	51.1	104.6	1.530	0.748	3.167	76.4	3.23
180	1110	A	1	H	4	60.0	62.0	5.10	49.7	98.8	1.494	0.752	2.731	72.5	2.63
180	1110	A	1	H	5	48.0	50.0	6.48	38.0	61.2	1.626	1.009	2.541	60.3	1.52
180	1110	A	2	H	1	78.5	80.5	7.78	51.1	104.6	1.469	0.718	2.695	73.4	2.75
180	1110	A	2	H	2	10.5	12.5	8.60	21.7	27.7	2.057	1.611	2.853	43.5	0.77
180	1110	B	1	H	1	52.0	54.0	0.52	59.9	149.3	1.363	0.547	2.700	79.7	3.94
180	1110	B	1	H	2	26.0	28.0	1.76	56.9	131.9	1.401	0.604	2.720	77.8	3.50
180	1110	B	1	H	3	27.0	29.0	3.27	51.8	107.5	1.466	0.707	2.735	74.2	2.87
180	1110	B	1	H	4	11.0	13.0	4.61	52.1	108.8	1.458	0.698	2.702	74.2	2.87
180	1111	A	8	R	1	42.5	44.5	68.13	38.4	62.2	1.658	1.022	2.695	62.1	1.64
180	1111	A	8	R	2	66.0	68.0	69.86	36.0	56.3	1.694	1.083	2.680	59.6	1.47
180	1111	A	8	R	3	45.0	47.0	71.15	37.1	58.9	1.678	1.056	2.689	60.7	1.55
180	1111	A	11	R	1	41.5	43.5	97.11	43.8	77.9	1.563	0.879	2.651	66.9	2.02
180	1111	A	13	R	1	94.0	96.0	117.04	36.6	57.8	1.675	1.061	2.649	59.9	1.50
180	1111	A	13	R	2	8.0	10.0	117.24	45.2	82.5	1.557	0.853	2.731	68.8	2.20
180	1111	A	14	R	1	8.0	10.0	125.88	43.2	76.1	1.573	0.893	2.654	66.3	1.97
180	1111	A	14	R	2	8.0	10.0	127.38	41.4	70.8	1.609	0.942	2.701	65.1	1.87
180	1111	A	14	R	3	8.0	10.0	128.88	40.9	69.3	1.675	0.989	2.996	67.0	2.03
180	1111	A	15	R	1	21.0	23.0	135.61	44.6	80.4	1.563	0.866	2.708	68.0	2.13
180	1111	A	16	R	1	31.0	33.0	145.31	42.9	75.2	1.589	0.907	2.715	66.6	1.99
180	1112	A	1	R	1	72.0	74.0	0.72	49.2	96.8	1.505	0.765	2.760	72.3	2.61
180	1112	A	1	R	2	38.0	40.0	1.88	46.8	87.9	1.546	0.823	2.800	70.6	2.40

Notes: This table is also available in ASCII format in the [TABLES](#) directory. No index properties were measured for Site 1113.

Table T16. Longitudinal (z) and transverse (x and y) velocities for cores, Sites 1110 and 1111.

Leg	Site	Hole	Core	Type	Section	Top (cm)	Bottom (cm)	Depth (mbsf)	x-velocity (m·s ⁻¹)	y-velocity (m·s ⁻¹)	z-velocity (m·s ⁻¹)
180	1110	A	1	H	1	91.7	91.7	0.92		1512.6	1510.4
180	1110	A	1	H	2	110.4	110.4	2.60		1507.6	1540.5
180	1110	A	1	H	3	45.5	45.5	3.46		1511.2	1511.7
180	1110	A	1	H	4	56.9	56.9	5.07		1516.5	1509.8
180	1110	A	1	H	5	45.9	45.9	6.46		1582.9	1593.8
180	1110	A	2	H	1	89.0	89.0	7.89	1565.6	1520.5	1527.5
180	1110	B	1	H	1	66.9	66.9	0.67		1512.6	1510.4
180	1110	B	1	H	2	122.4	122.4	2.72		1495.7	1500.0
180	1110	B	1	H	3	58.3	58.3	3.58	1551.3	1504.7	1507.8
180	1110	B	1	H	4	18.4	18.4	4.68	1558.3	1503.4	1514.4
180	1111	A	8	R	1	41.8	41.8	68.12		1450.1	1509.7
180	1111	A	8	R	2	68.4	68.4	69.88		1570.4	1566.5
180	1111	A	8	R	3	46.1	46.1	71.16		1277.7	1512.1
180	1111	A	11	R	1	39.6	39.6	97.10	1549.2		
180	1111	A	13	R	1	38.0	38.0	116.48	1597.7		
180	1111	A	13	R	2	55.3	55.3	117.71	1604.6		
180	1111	A	14	R	1	90.3	90.3	126.70	1537.2		
180	1111	A	14	R	2	105.0	105.0	128.35	1547.9		
180	1111	A	14	R	3	70.6	70.6	129.51	1549.9		
180	1111	A	15	R	1	67.5	67.5	136.08	1560.2		
180	1111	A	16	R	1	35.0	35.0	145.35	1537.9		

Notes: This table is also available in ASCII format in the [TABLES](#) directory. No velocity data were collected from Sites 1112 and 1113.

Table T17. Thermal conductivity in cores, Sites 1110, 1111 and 1112.

Leg	Site	Hole	Core	Type	Section	Top interval (cm)	Bottom interval (cm)	Depth (mbsf)	Thermal conductivity (W·m ⁻¹ ·°C ⁻¹)	Thermal conductivity average (W·m ⁻¹ ·°C ⁻¹)
180	1110	A	1	H	1	75.0	75.0	0.75	0.872	
180	1110	A	1	H	1	75.0	75.0	0.75	0.881	
180	1110	A	1	H	1	75.0	75.0	0.75	0.885	0.879
180	1110	A	1	H	3	75.0	75.0	3.75	0.961	
180	1110	A	1	H	3	75.0	75.0	3.75	0.966	
180	1110	A	1	H	3	75.0	75.0	3.75	0.976	0.968
180	1110	A	1	H	5	45.0	45.0	6.45	0.867	
180	1110	A	1	H	5	45.0	45.0	6.45	0.874	
180	1110	A	1	H	5	45.0	45.0	6.45	0.887	0.876
180	1110	A	2	H	1	75.0	75.0	7.75	1.000	
180	1110	A	2	H	1	75.0	75.0	7.75	1.000	
180	1110	A	2	H	1	75.0	75.0	7.75	1.013	1.004
180	1110	B	1	H	1	76.0	76.0	0.76	0.828	
180	1110	B	1	H	1	76.0	76.0	0.76	0.876	
180	1110	B	1	H	1	76.0	76.0	0.76	0.869	0.858
180	1110	B	1	H	3	57.0	57.0	3.57	0.939	
180	1110	B	1	H	3	57.0	57.0	3.57	0.944	
180	1110	B	1	H	3	57.0	57.0	3.57	0.949	0.944
180	1111	A	8	R	1	72.0	72.0	68.42	0.821	
180	1111	A	8	R	1	72.0	72.0	68.42	0.816	
180	1111	A	8	R	1	72.0	72.0	68.42	0.810	0.816
180	1111	A	8	R	3	62.0	62.0	71.32	0.925	
180	1111	A	8	R	3	62.0	62.0	71.32	0.898	
180	1111	A	8	R	3	62.0	62.0	71.32	0.893	0.905
180	1111	A	11	R	1	38.0	38.0	97.08	0.475	
180	1111	A	11	R	1	38.0	38.0	97.08	0.470	
180	1111	A	11	R	1	38.0	38.0	97.08	0.462	0.469
180	1111	A	13	R	1	66.0	66.0	116.76	0.871	
180	1111	A	13	R	1	66.0	66.0	116.76	0.870	
180	1111	A	13	R	1	66.0	66.0	116.76	0.865	0.869
180	1111	A	14	R	1	57.0	57.0	126.37	0.775	
180	1111	A	14	R	1	57.0	57.0	126.37	0.751	
180	1111	A	14	R	1	57.0	57.0	126.37	0.771	0.766
180	1111	A	14	R	3	51.0	51.0	129.31	0.436	
180	1111	A	14	R	3	51.0	51.0	129.31	0.421	
180	1111	A	14	R	3	51.0	51.0	129.31	0.462	0.440
180	1111	A	15	R	1	48.0	48.0	135.88	0.555	
180	1111	A	15	R	1	48.0	48.0	135.88	0.531	
180	1111	A	15	R	1	48.0	48.0	135.88	0.539	0.542
180	1111	A	16	R	1	29.0	29.0	145.29	0.557	
180	1111	A	16	R	1	29.0	29.0	145.29	0.485	
180	1111	A	16	R	1	29.0	29.0	145.29	0.529	0.524
180	1112	A	1	R	1	75.0	75.0	0.75	0.923	
180	1112	A	1	R	1	75.0	75.0	0.75	0.926	
180	1112	A	1	R	1	75.0	75.0	0.75	0.936	0.928

Notes: This table is also available in ASCII format in the [TABLES](#) directory. No thermal conductivity measurements collected for Site 1113.

Table T18. Shear and compressive strength data, Sites 1110 and 1111.

Leg	Site	Hole	Core	Type	Section	Top interval (cm)	Bottom interval (cm)	Depth (mbsf)	Peak vane shear strength (kPa)	Residual vane shear strength	Unconfined compressive (kPa)
180	1110	A	1	H	1	92.5	92.5	0.93	—	—	2.5
180	1110	A	1	H	1	106.0	106.0	1.06	—	—	20.0
180	1110	B	1	H	1	80.0	80.0	0.80	—	—	0.0
180	1110	B	1	H	2	80.0	80.0	2.30	—	—	0.0
180	1110	B	1	H	3	80.0	80.0	3.80	—	—	20.0
180	1110	B	1	H	4	22.0	22.0	4.72	—	—	12.5
180	1111	A	8	R	1	60.0	60.0	68.30	31.24	9.27	—
180	1111	A	8	R	2	58.5	58.5	69.79	38.21	17.83	—
180	1111	A	8	R	3	56.0	56.0	71.26	19.49	12.60	—
180	1111	A	8	R	1	101.5	101.5	68.72	—	—	25.0
180	1111	A	8	R	2	58.0	58.0	69.78	—	—	60.0
180	1111	A	8	R	3	73.5	73.5	71.44	—	—	70.0
180	1111	A	11	R	1	39.5	39.5	97.10	23.73	5.14	—
180	1111	A	11	R	1	44.0	44.0	97.14	—	—	40.0
180	1111	A	13	R	1	10.0	10.0	116.20	—	—	190.0
180	1111	A	13	R	1	40.0	40.0	116.50	—	—	95.0
180	1111	A	13	R	1	70.0	70.0	116.80	—	—	80.0
180	1111	A	13	R	1	90.0	90.0	117.00	—	—	55.0
180	1111	A	13	R	2	15.0	15.0	117.30	—	—	80.0
180	1111	A	13	R	2	55.0	55.0	117.70	—	—	62.5
180	1111	A	14	R	1	80.0	80.0	126.60	—	—	65.0
180	1111	A	14	R	1	25.0	25.0	126.10	—	—	175.0
180	1111	A	14	R	1	100.0	100.0	126.80	—	—	82.5
180	1111	A	14	R	1	130.0	130.0	127.10	—	—	100.0
180	1111	A	14	R	1	140.0	140.0	127.20	—	—	110.0
180	1111	A	14	R	2	20.0	20.0	127.50	—	—	82.5
180	1111	A	14	R	2	50.0	50.0	127.80	—	—	105.0
180	1111	A	14	R	2	80.0	80.0	128.10	—	—	120.0
180	1111	A	14	R	2	110.0	110.0	128.40	—	—	102.5
180	1111	A	14	R	2	140.0	140.0	128.70	—	—	87.5
180	1111	A	14	R	3	20.0	20.0	129.00	—	—	95.0
180	1111	A	14	R	3	50.0	50.0	129.30	—	—	127.5
180	1111	A	14	R	3	90.0	90.0	129.70	—	—	60.0
180	1111	A	15	R	1	40.0	40.0	135.80	—	—	90.0
180	1111	A	15	R	1	60.0	60.0	136.00	—	—	67.5
180	1111	A	15	R	1	80.0	80.0	136.20	—	—	65.0
180	1111	A	16	R	1	20.0	20.0	145.20	—	—	60.0
180	1111	A	16	R	1	40.0	40.0	145.40	—	—	60.0

Notes: This table is also available in ASCII format in the [TABLES](#) directory. No strength data were collected from Sites 1112 and 1113.

Table T19. The depths of the correlative peaks of magnetic susceptibility.

Key bed lithology	Section	Interval (cm)	Distance from core top (m)	Depth below core top (m)	Section	Interval (cm)	Distance from core top (m)	Depth below core top (m)	Depth (mcd)
	Core 180-1110A-1H				Core 180-1110B-1H				
Olive greenish silt	1	56	0.56	0.56	1	51	0.51	0.51	0.56
	1	60	0.60	0.60	1	59	0.59	0.59	0.62
	1	72	0.72	0.72	1	71	0.71	0.71	0.74
	1	76	0.76	0.76	1	75	0.75	0.75	0.78
	1	88	0.88	0.88	1	91	0.91	0.91	0.92
Siliciclastic sand; greenish gray silt	1	100	1.00	1.00	1	99	0.99	0.99	1.02
	2	20	1.70	1.69	2	20	1.70	1.70	1.72
	2	48	1.98	1.97	2	44	1.94	1.94	1.98
	2	64	2.14	2.13	2	64	2.14	2.14	2.16
	2	80	2.30	2.29	2	84	2.34	2.34	2.34
Siliciclastic sand	2	96	2.46	2.45	2	96	2.46	2.46	2.48
	2	136	2.86	2.85	2	124	2.74	2.74	2.82
	2	140	2.90	2.89	2	132	2.82	2.82	2.88
Siliciclastic sand	3	20	3.20	3.19	3	20	3.20	3.20	3.22
	3	32	3.32	3.31	3	32	3.32	3.32	3.34
	3	36	3.36	3.35	3	36	3.36	3.36	3.38
Ash	3	44	3.44	3.43	3	44	3.44	3.44	3.46
	3	56	3.56	3.54	3	56	3.56	3.56	3.58
Siliciclastic sand	3	64	3.64	3.62	3	60	3.60	3.60	3.64
	3	72	3.72	3.70	3	68	3.68	3.68	3.72
Siliciclastic sand	3	88	3.88	3.86	3	84	3.84	3.84	3.88
	3	104	4.04	4.02	3	100	4.00	4.00	4.04
	3	108	4.08	4.06	3	104	4.04	4.04	4.08
	4	12	4.62	4.60	4	8	4.58	4.58	4.61

Note: Thin solid line and areas surrounded by thin solid line indicate horizons of key beds.